POLITECNICO
MILANO 1863

SCUOLA DI INGEGNERIA INDUSTRIALE
E DELL'INFORMAZIONE

Holter analysis of electro-mechanical activity and circadian rhythm through ECG and inertial sensors: a novel approach

MASTER THESIS IN BIOMEDICAL ENGINEERING

Author: **Federica Mozzini**

Student ID:	946400
Advisor:	Prof. Enrico Gianluca Caiani
Co-advisor:	Ing. Sarah Solbiati
Academic Year:	2021-22

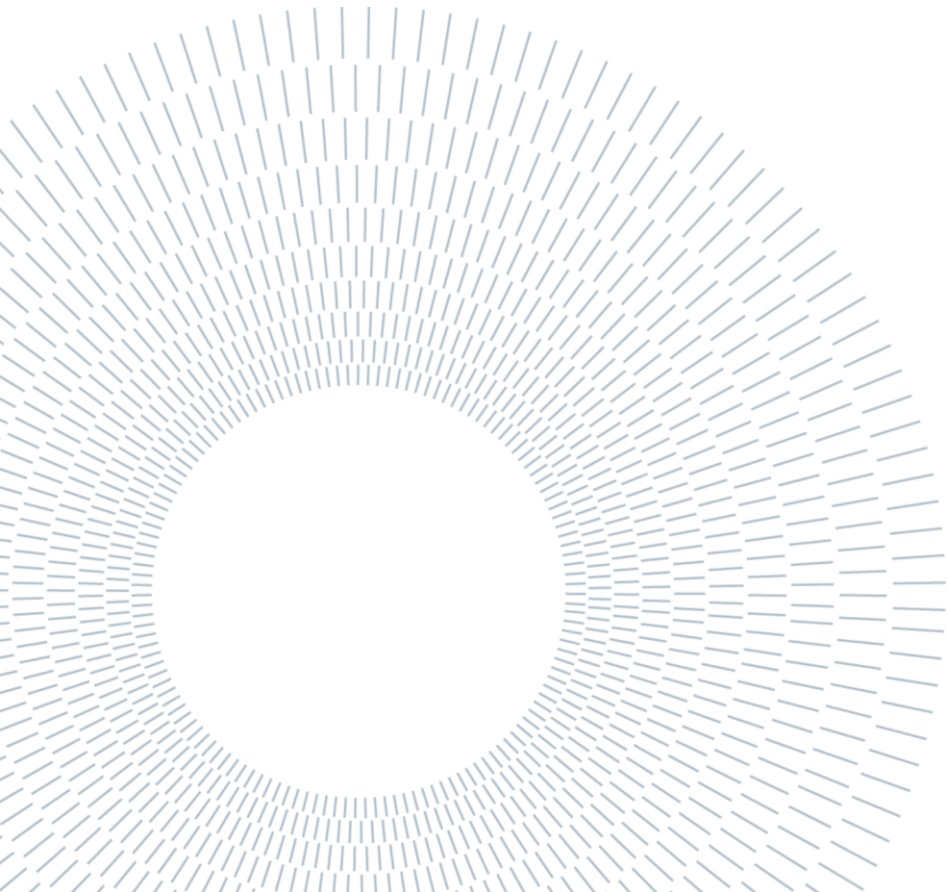

A mio nonno…

Ovunque tu sia, spero tu sia fiero di me

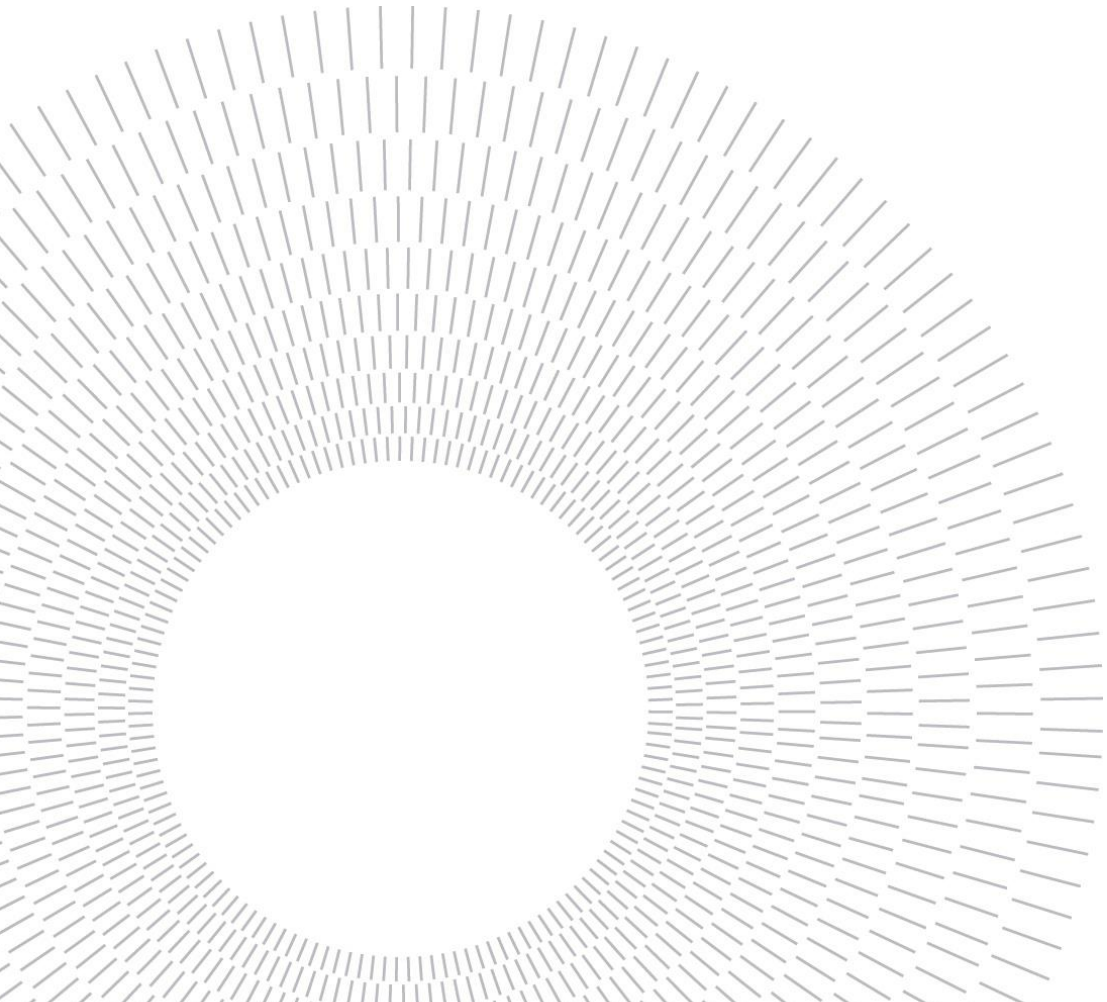

Abstract

Seismocardiography (SCG) records the precordial micro-vibration produced at every heartbeat by the cardiac contraction, valve opening and closing and by blood ejection into the vascular tree. Novel wearable technologies incorporating both ECG and SCG sensors could allow Holter real-time acquisitions, thus opening new possibilities to study the circadianity of cardiac electro-mechanical activity.
The aim of this study was to determine feasibility of such approach and to propose a novel method for beat-by-beat detection of cardiac mechanical events and relevant circadian rhythms, to determine normality ranges for future comparisons.
24-hour synchronized ECG and SCG signals were acquired from 22 healthy volunteers using the Movisens EcgMove4 device. SCG heartbeats were identified and, using the ECG as a reference, several fiducial points were detected: mitral valve closure (MC), isovolumetric contraction (IVC), aortic valve opening (AO), rapid ejection of blood in the vascular tree (RE) and aortic valve closure (AC). For each beat, new temporal and morphological biomarkers were then computed.
For each parameter, day-night differences were verified (Wilcoxon Signed Rank test, $p < 0.05$), and the Cosinor analysis was applied to test for circadianity.
Results showed good feasibility for using SCG signal for beat-detection, with 82.5 % of usable beats at night and 51.8 % during the day. All the computed electro-mechanical parameters showed a significant difference between day and night and presence of circadianity. The acrophases for the total of the morphological parameters occurred between 15:00 and 16:00, while for almost all temporal parameters occurred between 05:00 and 06:00.
The study suggests that new electro-mechanical biomarkers and their circadianity can be derived from long-term SCG and ECG registrations, which normality curves could be used in the context of comparing results from pathological subjects to better understand the effects of disease-related changes.

Key-words: Circadian rhythm, Electrocardiogram, Electro-mechanical cardiac parameters, Holter, Seismocardiogram

Abstract in lingua italiana

La sismocardiografia (SCG) registra la microvibrazione prodotta, ad ogni battito cardiaco, dalla contrazione cardiaca, dall'apertura e chiusura delle valvole e dall'eiezione di sangue nell'albero vascolare. L'impiego di nuovi dispositivi indossabili che incorporino sia sensori ECG che SCG potrebbero consentire acquisizioni in tempo reale tramite Holter, aprendo così nuove frontiere per lo studio della circadianità dell'attività elettromeccanica del cuore. Lo scopo di questo studio è determinare la fattibilità di tale approccio e sviluppare un nuovo metodo per la rilevazione battito-battito di eventi meccanici cardiaci e ritmi circadiani rilevanti, al fine di individuare intervalli di normalità per confronti futuri.
Nello studio sono stati arruolati 22 volontari non patologici e, tramite l'utilizzo del dispositivo Movisens EcgMove4, sono stati acquisiti segnali ECG e SCG sincronizzati nell'arco di 24 ore. Sono stati identificati i battiti cardiaci nel segnale SCG e, utilizzando l'ECG come riferimento, sono stati identificati diversi punti fiduciali: chiusura della valvola mitrale (MC), contrazione isovolumetrica (IVC), apertura della valvola aortica (AO), rapida eiezione di sangue nell'albero vascolare (RE) e chiusura della valvola aortica (AC). Per ogni battito sono stati quindi calcolati nuovi biomarcatori temporali e morfologici. Per ciascun parametro sono state indagate le differenze tra giorno e notte (Wilcoxon Signed Rank test, $p < 0,05$), ed è stata applicata l'analisi Cosinor per analizzare la circadianità.
I risultati hanno mostrato una buona fattibilità per l'utilizzo del segnale SCG per il rilevamento dei battiti, ottenendo valori dell'82.5% di notte e del 51.8% durante il giorno. Tutti i parametri elettromeccanici calcolati hanno mostrato una differenza significativa tra giorno e notte e presenza di circadianità. Le acrofasi per il totale dei parametri morfologici si sono verificate tra le 15:00 e le 16:00, mentre per la quasi totalità dei parametri temporali si sono verificate tra le 05:00 e le 06:00.
Lo studio suggerisce che nuovi biomarcatori elettromeccanici e la loro circadianità possano essere derivati da registrazioni SCG ed ECG di lunga durata, le cui curve di normalità potrebbero essere utilizzate nella comparazione dei risultati di soggetti patologici per comprendere meglio gli effetti dei cambiamenti correlati alla malattia.

Parole chiave: Elettrocardiogramma, Holter, Parametri elettro-meccanici cardiaci, Ritmo Circadiano, Seismocardiogramma

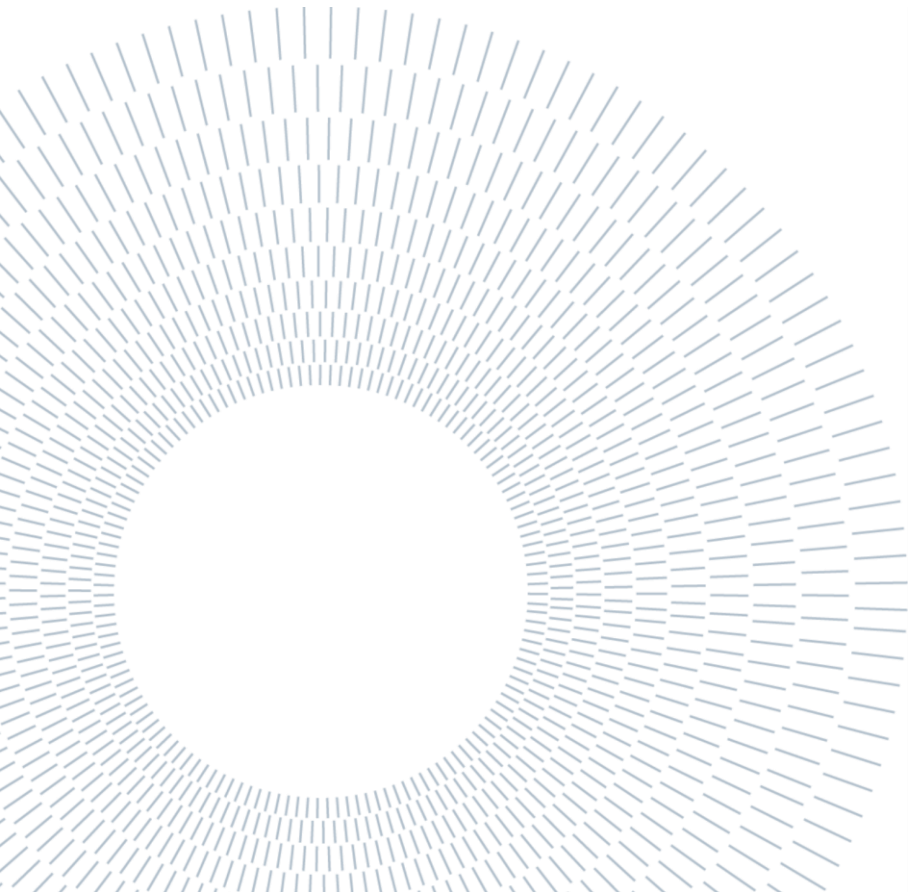

1. Contents

Acronyms and Abbreviations

AC	Closure of the aortic valve
AO	Opening of the aortic valve
AO_iAO_{i+1}	Time delay between two consecutive AO peaks
AV	Atrioventricular
CV	Cardiovascular
ECG	Electrocardiogram
HF	High frequency
HR	Heart rate
HRV	Heart rate variability
IVC	Isovolumetric contraction
LF	Low frequency
LVET	Left ventricular ejection time
MC	Closure of the mitral valve
MO	Opening of the mitral valve
QS2	Electromechanical systole
QT	Time delay between Q and T
QTc	QT interval corrected (Bazett's correction)
PEP	Pre-ejection period
PT	Pan Tompkins
RE	Rapid ejection of blood
R_iR_{i+1}	Time delay between two consecutive R peaks
SA	Sinoatrial
SC	Systolic complex
SCG	Seismocardiogram
SLOPE(IVC-AO)	Slope between IVC and AO
SLOPE(minAC-AC)	Slope between the minimum point before AC and AC
SLOPE(minAORE-RE)	Slope between the minimum point between AO and RE and RE
ΔA(AO-AC)	Amplitude difference between AO and AC

ΔA(AO-minAORE)	Amplitude difference between AO and the minimum point between AO and RE
ΔA(AO-RE)	Amplitude difference between AO and RE
ΔA(AC-minAC)	Amplitude difference between AC and the minimum point before AC
ΔA(IVC-AO)	Amplitude difference between IVC and AO
ΔA(IVC-MC)	Amplitude difference between IVC and MC
ΔA(RE-minAORE)	Amplitude difference between RE and the minimum point between AO and RE
ΔT(AO-AC)	Time delay between AO and AC
ΔT(AO-minAORE)	Time delay between AO and the minimum point between AO and RE
ΔT(AO-RE)	Time delay between AO and RE
ΔT(IVC-AO)	Time delay between IVC and AO
ΔT(AC-minAC)	Time delay between AC and the minimum point before AC
ΔT(IVC-MC)	Time delay between IVC and MC
ΔT(R-AO)	Time delay between R and AO
ΔT(R-AC)	Time delay between R and AC
ΔT(R-MC)	Time delay between R and MC

1. Introduction

1.1 Cardiovascular System

The CV system consists of the heart, blood vessels and blood. It is a hydraulic system composed by a pump (heart) and conductors (blood vessels) with the purpose of circulating the blood reaching every portion of the body and allowing the blood to carry out its transport functions [1].

The circulatory system is further divided into two major circuits: the pulmonary circulatory system and the systematic circulatory system (*Figure 1.1*).

The pulmonary circulation is the portion of the CV system in which oxygen-depleted blood is pumped away by the right heart, via the pulmonary artery, to the lungs and returned, oxygenated, to the left heart via the pulmonary vein.

Systemic circulation is the portion of the CV system that transports oxygenated blood away from the heart through the aorta from the left ventricle, where the blood has been previously flown from pulmonary circulation to the rest of the body and returns oxygen-depleted blood back to the right heart. Its primary function is to transport nutrients and oxygen-rich blood to organs, tissues, and cells [2].

The human circulatory system is closed, i.e. the blood is contained within the vascular network and venous and arterial blood never come into contact.

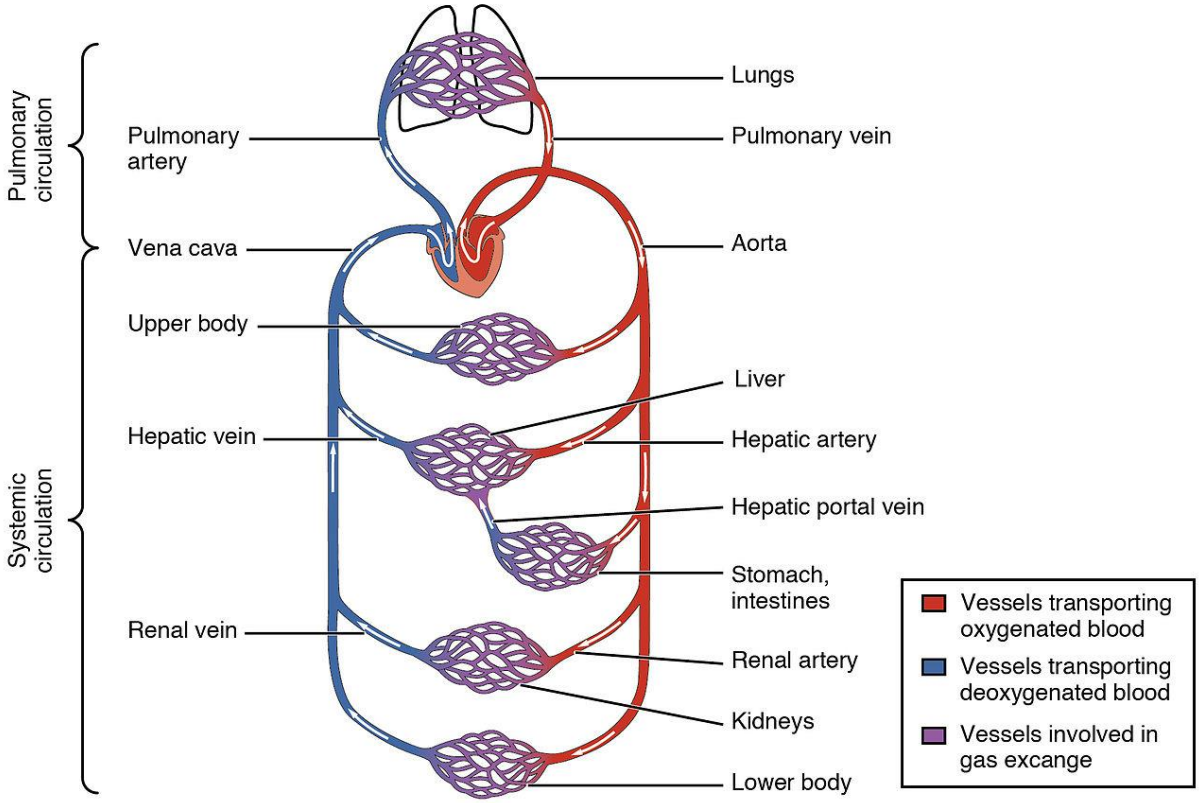

Figure 1.1: Cardiovascular system, systemic circulation, and pulmonary circulation [3]

The blood is pumped around the body through a network of blood vessels (*Figure 1.2*) [4]:

- Arteries: deliver oxygen-rich blood from the heart to the tissues of the body. The largest artery is the aorta;
- Arterioles: small-diameter blood vessels which form part of the microcirculation that extends from an artery and leads to capillaries. Arterioles have muscular walls and are the primary site of vascular resistance, which reduces the pressure and velocity of flow for gas and nutrient exchange within the capillaries;
- Capillaries: connect arterioles and venules and enable the exchange of water, oxygen, carbon dioxide, and many other nutrients and waste substances between blood and surrounding tissues. The thin wall of the capillary allows for gas and lipophilic molecules to pass through without the need for special transport mechanisms and allows bidirectional diffusion;
- Venules: small blood vessel in the microcirculation that allows deoxygenated blood to return from capillary bed to veins. Venules are formed when capillaries come together;

- Veins: formed when many venules come together. The main difference between veins and arteries is the direction of blood flow (out of the heart through arteries, returning to the heart through veins). Veins carry blood lacking in oxygen back forward the heart and, as they get nearer it, they get bigger.

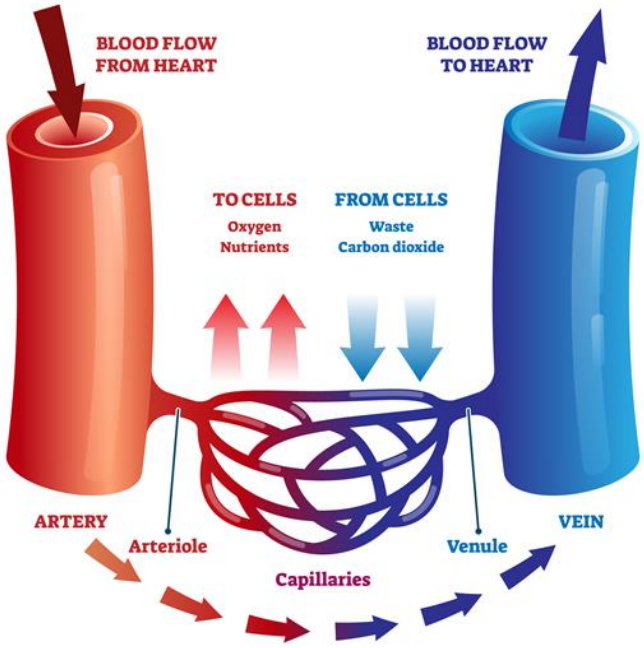

Figure 1.2: Blood vessels – arteries, arterioles, capillaries, venules, and veins [5]

The heart is the primary organ of the circulatory system. It is a four-chambered muscular organ containing an involuntary conduction system that initiates rhythmic contractions to pump blood throughout the body (about 5 liters per minute at rest) [6].

The heart is located in the thoracic cavity between the lungs in the middle of the chest, behind and slightly to the left of the breastbone and protected by the rib cage (*Figure 1.3(a)*). The outer layer of the pericardium surrounds the roots of the heart's major blood vessels and is attached by ligaments mainly to the spinal cord and diaphragm. The inner layer of the pericardium is attached to the heart muscle. A coating of fluid separates the two layers of membrane, letting the heart move as it beats.

The wall of the heart is composed of three layers of tissues (*Figure 1.3(b)*):

- Epicardium
- Myocardium
- Endocardium

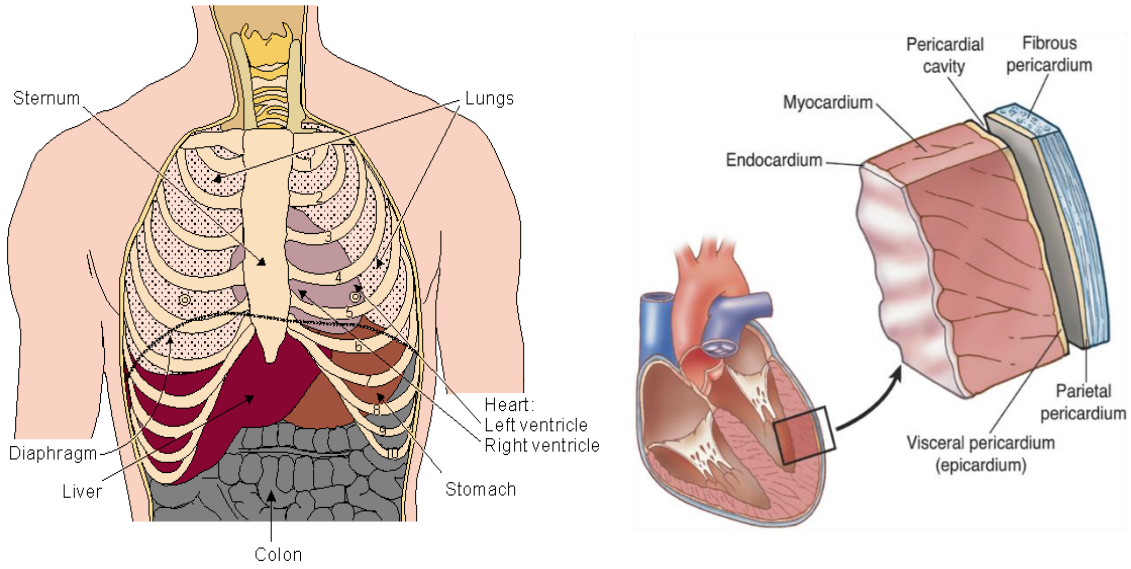

(a) Location of the heart (b) Layers of cardiac tissues

Figure 1.3: (a) Location of the heart in the thoracic cavity between the lungs, behind the sternum and protected by the ribcage; (b) The wall of the heart is composed of three cardiac layers of tissues: endocardium, myocardium and epicardium [7,8]

The right heart deals with pulmonary circulation: it receives blood (i.e. venous blood) that is low in oxygen, it pumps this to the lungs, where it picks up a new supply of oxygen. The blood then returns to the left side of the heart. Instead, the left heart deals with systematic circulation: the blood returns to the left side of the heart (i.e. atrial blood), ready to be pumped back out to the brain and rest of the body. The left and right side of the heart are separated by a wall, called septum (*Figure 1.4*).

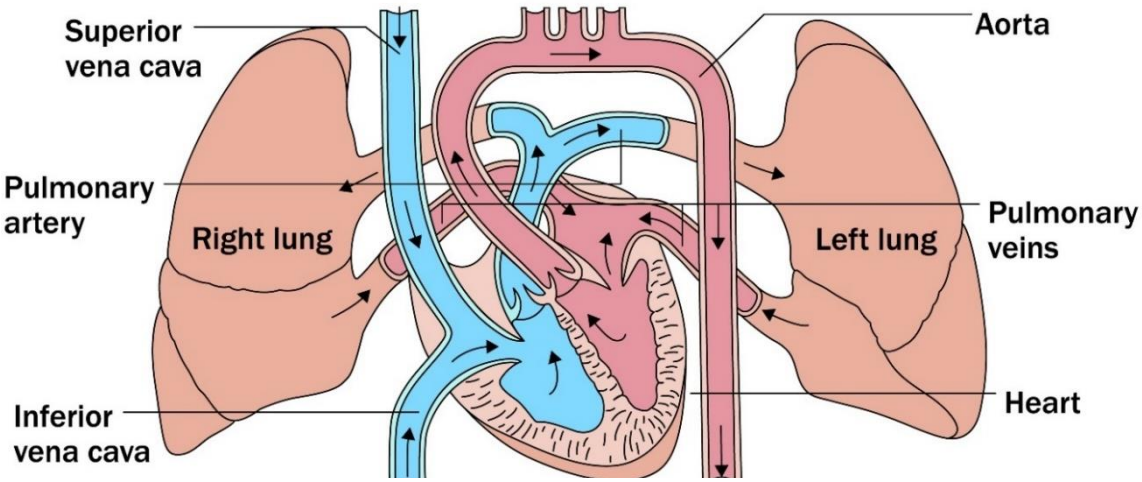

Figure 1.4: *Pulmonary and systematic circulation in the heart [9]*

The heart consists of four chambers separated into two sides, each side contains an atrium and a ventricle. The two small upper chambers are the atria, while the two larger lower chambers are the ventricles (*Figure 1.5(a)*). The atrium receives blood into the heart and flows into a ventricle, which pumps the blood out of the heart. The atria and the ventricle on each side are linked together by valves that prevent backflow of blood.

The four valves are (*Figure 1.5(b)*):

1. Tricuspid valve: separates the right atrium from the right ventricle and prevents the backflow of blood from the right ventricle to the right atrium;
2. Pulmonary valve: separates the right ventricle from the pulmonary artery and prevents the back flow of blood from the pulmonary artery to the ventricle. It opens to allow blood to be pumped from the right ventricle to the lungs (through the pulmonary artery) where it receives oxygen;
3. Mitral valve: separates the left atrium from the left ventricle and prevents the backflow of blood from the left ventricle to the left atrium;
4. Aortic valve: separates the left ventricle from the aorta and prevents the backflow of blood from the aorta to the left ventricle. It opens to allow blood to leave the heart from the left ventricle through the aorta.

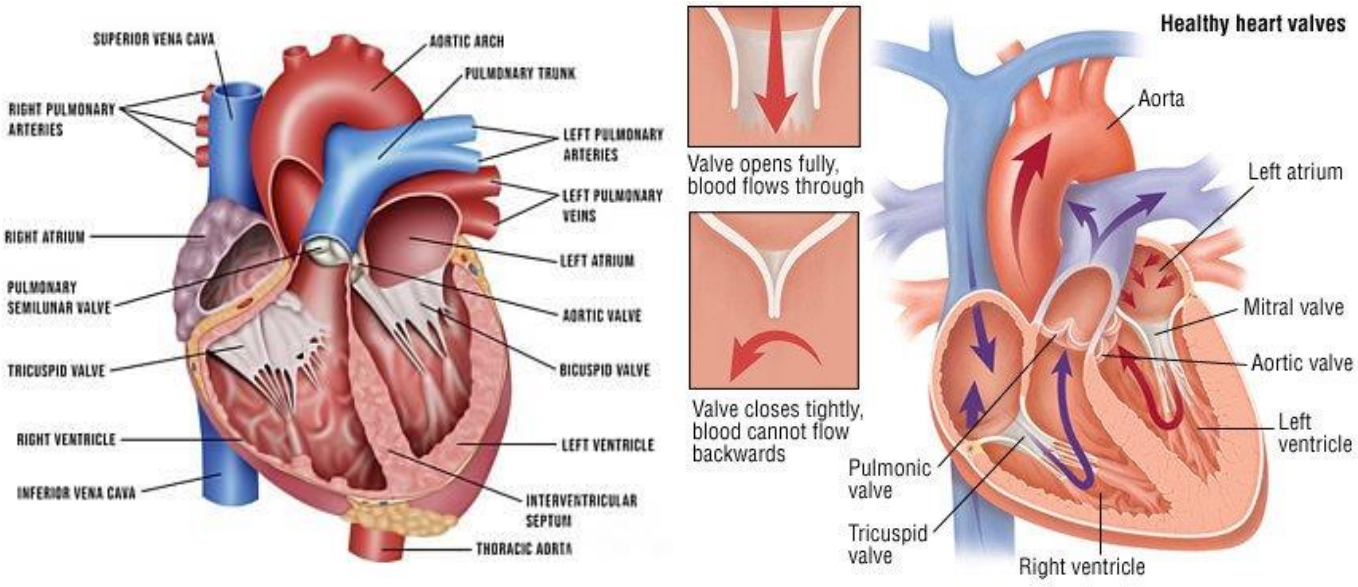

(a) Anatomy of the heart (b) Heart valves

Figure 1.5: (a) Anatomy of the heart: two atria and two ventricle separated by valves and interventricular septum (b) Tricuspid and pulmonary valves allow blood to flow from superior vena cava to pulmonary arteries, while mitral and aortic valves allow blood to flow from left atrium to aorta. [10,11]

1.2 Electrical activity of the heart

For the heart to work efficiently, the atria and the ventricles must be activated rapidly and sequentially. Atria are activated first to fill the ventricles before ventricular contraction begins. To coordinate these processes, the heart has an electrical conduction system composed of specialized myocardial cells [12].

The myocardium is a layer of involuntary striated muscle tissue surrounded by collagen. It acts as cardiac muscle and is made up of two different types of cells:

- Muscle/Conduction cells: the 90% of the heart muscle mass is composed by muscle cells. These cells have virtually no contractile function and form the fiber networks that spread the action potential rapidly and sequentially to contractile myocardium in the atria and ventricles.
- Pacemaker/Contractive myocardial cells: the remaining 10% of the heart muscle mass is composed by pacemaker cells. They are responsible for the actual contraction and for auto-rhythmicity, the ability to initiate a cardiac action potential at a fixed rate.

1.2.1 Cardiac Action Potential

The cardiac muscle (i.e. conduction cells) doesn't activate through a stimulus coming from a motoneuron, but it activates due to a stimulus coming from adjacent cells or from cells of the conductive system. The latter one propagates the stimulus from a specific area of the myocardium, a cluster of contractive myocardial cells, which activates regularly.

The action potential travels towards conduction cells and depolarizes (i.e. activation phase) or repolarizes (i.e. recovery phase) them. The action potential of the common ventricular myocardium ranges between 250 and 350 ms [13]. During each cardiac cycle, specific ions (Na^+, Ca^{2+} and K^+ ions) - which are charged particles - move back and forth across the cardiomyocyte cell membrane, thereby changing the membrane potential. The cardiac potential is subdivided into phases, each one reflecting the major ionic movements that take place (*Figure 1.6*):

1. Phase 4 : Resting membrane potential and diastolic depolarization:
   The resting potential of a cardiac cell is -90 mV due to a constant outward of flow of K^+. Na^+ and Ca^{2+} channels are closed at resting transmembrane potential.

2. Phase 0 : Rapid depolarization:
   As a depolarizing stimulus arrives at the portion of membrane, a few Na^+ channels open, letting Na^+ ions to enter the neuron. The increase in positive ions inside the cell depolarizes the membrane potential and brings it closer to the threshold (-90 mv) at which an action potential is generated. If the depolarization reaches the threshold potential, additional voltage-gated sodium channels opens and the voltage across the membrane reaches 0 mV and slightly above 0 mV for a transient period of time called overshoot. Then, Fast Na^+ channels close and Slow Ca^{2+} channels open.

3. Phase 1 : Early rapid repolarization:
   At the peak of the action potential, many voltage-gated sodium channels begin to close. Simultaneously, many K^+ channels open, allowing positive ions to leave the cell. These processes cause the membrane potential to decrease;

4. Phase 2 : Plateau:
   Many K^+ channels open, allowing positive ions to leave the cell. Simultaneously, Ca^{2+} channels are still open and there is a constant inward of positive Ca^{2+} ions inside the cell. These two countercurrents are electrically balanced, and the transmembrane potential is maintained at a plateau just below 0 mV throughout phase 2;

5. Phase 3 : Final rapid repolarization:
   Ca^{2+} channels are gradually inactivated and continuous outflow of K^+ brings the transmembrane potential back towards resting potential of -90 mV to prepare the cell for a new cycle of depolarization.

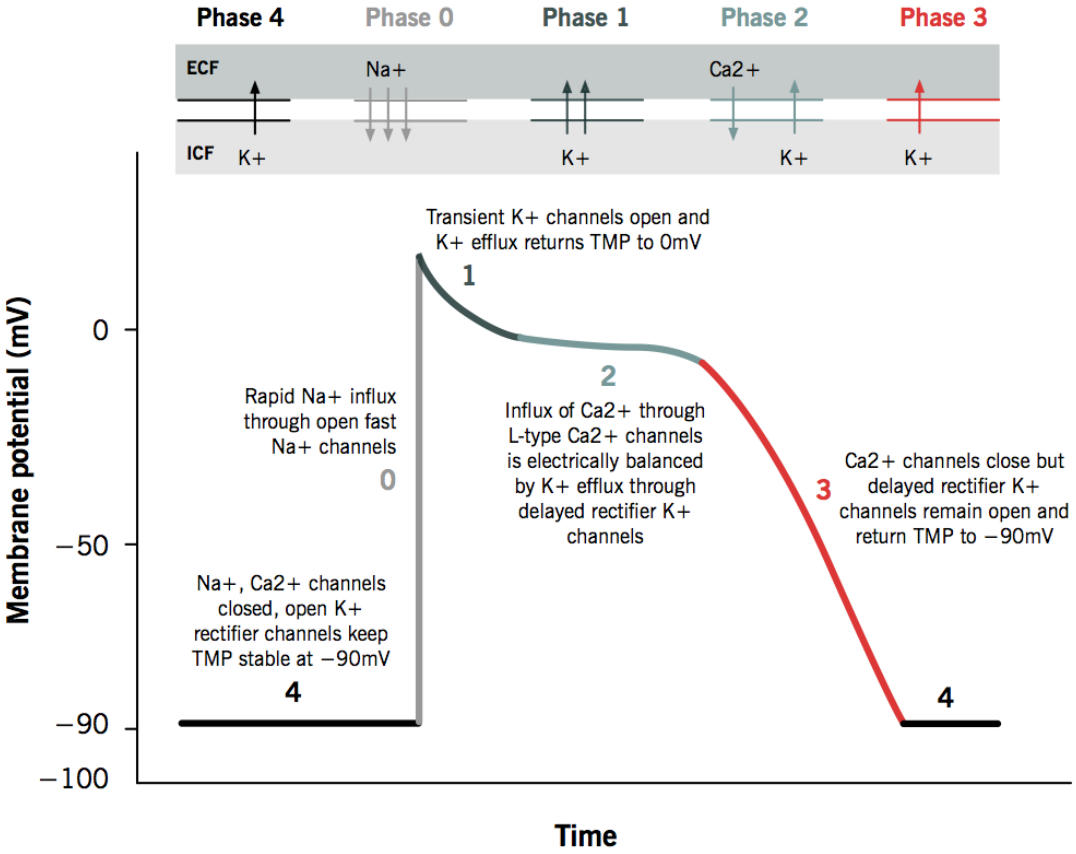

Figure 1.6: Cardiac action potential from phase 0 to phase 4. Relationship between cardiac phase and opening and closure of Na^+, Ca^{2+} and K^+ channels [14]

1.2.2 Cardiac cycle: electrical activity

The components of the cardiac conduction system include the sinoatrial (SA) node, the atrioventricular (AV) node, the atrioventricular bundle, the atrioventricular bundle branches, and the Purkinje cells [15].

The electrical activity of the heart is divided in 5 steps (*Figure 1.7*):

1. An electrical impulse is generated by the SA node, a specialized group of myocardial conducting cells located in the right atria of the heart, in the proximity of the orifice of the superior vena cava. The SA node is known as the pacemaker of the heart and initiates the sinus rhythm (it generates an electrical stimulus regularly, 60 to 100 times per minute under normal conditions [16]) followed by the contraction of the heart. The ability of the sinoatrial node to depolarize spontaneously (discharging an action potential without being stimulated) is referred to as automaticity [17]. The rate of spontaneous depolarization is modified by the automatic nervous system: sympathetic

stimulation increases the rate whereas parasympathetic stimulation lowers the rate.

2. The electrical impulse spreads from the sinoatrial node to the atria, which are activated by the impulse. The propagation of the impulse through the atria is facilitated by the internodal pathway. Then, the atrial impulse reaches the AV node, the only connection between the atria and ventricles. The AV node receives the atrial impulse and delays it before conducting it to the ventricles. The delay is due to the slow conduction through the AV node. The purpose of the slow conduction is to give the atria adequate time to fill the ventricles with blood before ventricular contraction begins.
3. Following the delay, the impulse travels through the atrioventricular bundle (bundle of His), which splits into the right and left bundle branches to stimulate the right and left ventricles. Through the Purkinje fibers – originating from bundle branches – the impulse reaches the papillary muscle. The impulse transmission in the Purkinje fibers is very fast (4 m/s), allowing all ventricular myocardium to be activated almost simultaneously.
4. The impulse spreads to the contractile fibers of the ventricles.
5. Ventricular contraction begins. Each contraction of the ventricles represents one heartbeat.

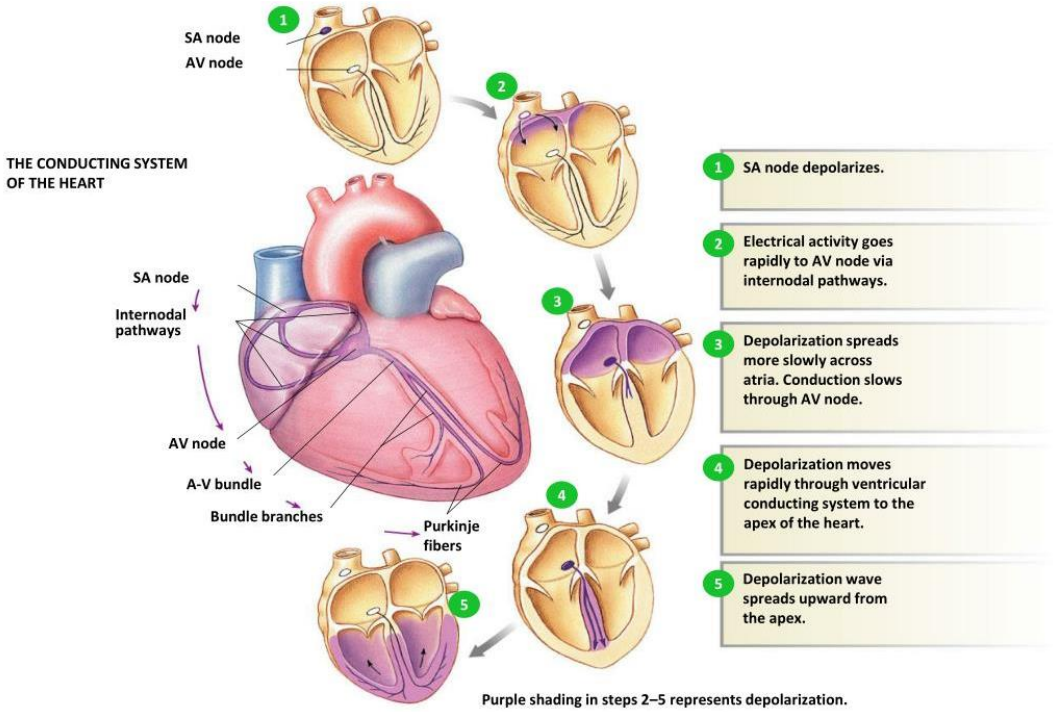

Figure 1.7: Phases of the electrical activity of the heart from the depolarization of SA to ventricular contraction. Purple shading in figure represents depolarization [18]

1.3 Mechanical activity of the heart

The spread of an electrical impulse is directly coupled to a mechanical event. The mechanical activity of the heart consists of a cycling succession of contraction (systole) and relaxation (diastole) called cardiac cycle [19].

Every single heartbeat involves three major mechanical stages: cardiac diastole (ventricular and atrial) when chambers are relaxed and filling passively; atrial systole when the atria contract leading to ventricular filling; ventricular systole when blood is ejected into both the pulmonary artery and aorta (*Figure 1.8*).

- Ventricular systole can subdivided in three phases:
    - Isovolumetric contraction: following the electrical stimulation, during which the ventricles contract with no corresponding volume change. This causes ventricular pressures to rise above atrial pressures, which close tricuspid and mitral valves. The ventricular pressure is still less than the one of the arteries, thus aortic and pulmonary valves remain closed. This phase marks the beginning of systole, and usually lasts about 13% of the cardiac cycle [20].
    - Ventricular rapid ejection: the pressure inside the ventricles rises above pulmonary artery and aorta pressures, thus opening the respective valves. Tricuspid and mitral valves remain closed to prevent the backflow of blood from ventricles to atria. Ventricles pump blood into the lungs through the pulmonary artery and into the brain and the rest of the body through the aorta and all the arteries.
    - Reduced ejection: this phase marks the beginning of ventricular repolarization, a rapid decline in ventricular pressures and hence reduced rate of ejection. This phase usually lasts about 15% of the cardiac cycle [20].

- Ventricular diastole, subdivided in two phases:
    - Isovolumetric relaxation: after the contraction, when the ventricular pressures drop below the diastolic aortic and pulmonary pressures (80 mmHg and 10 mmHg respectively [21,22,23]), the aortic and pulmonary valves close. The ventricles generate negative pressure without changing their volume so that the ventricular pressure becomes lower than the atrial pressure. Then, tricuspid and mitral valves open. This phase marks the beginning of the diastole.
    - Inflow (ventricular filling): as tricuspid and mitral valves open, ventricular filling start, and the heart expands while receiving blood returning from the circulatory system. The ventricular pressure

gradually increases until it equals the atrial pressure and the tricuspid and mitral valves close.
This phase usually lasts about 44% of the cardiac cycle [20].

- Atrial systole:
  Late in the ventricular filling period (end of ventricular diastole) the atria begin to contract (related to the P wave in the ECG) and each atrium pumps blood in the ventricle through tricuspid and mitral valves, respectively for right and left heart, while aortic and pulmonary valves are closed to prevent the backflow of blood from the pulmonary artery and aorta into the ventricles.
  This phase usually lasts about 14% of the cardiac cycle [20].

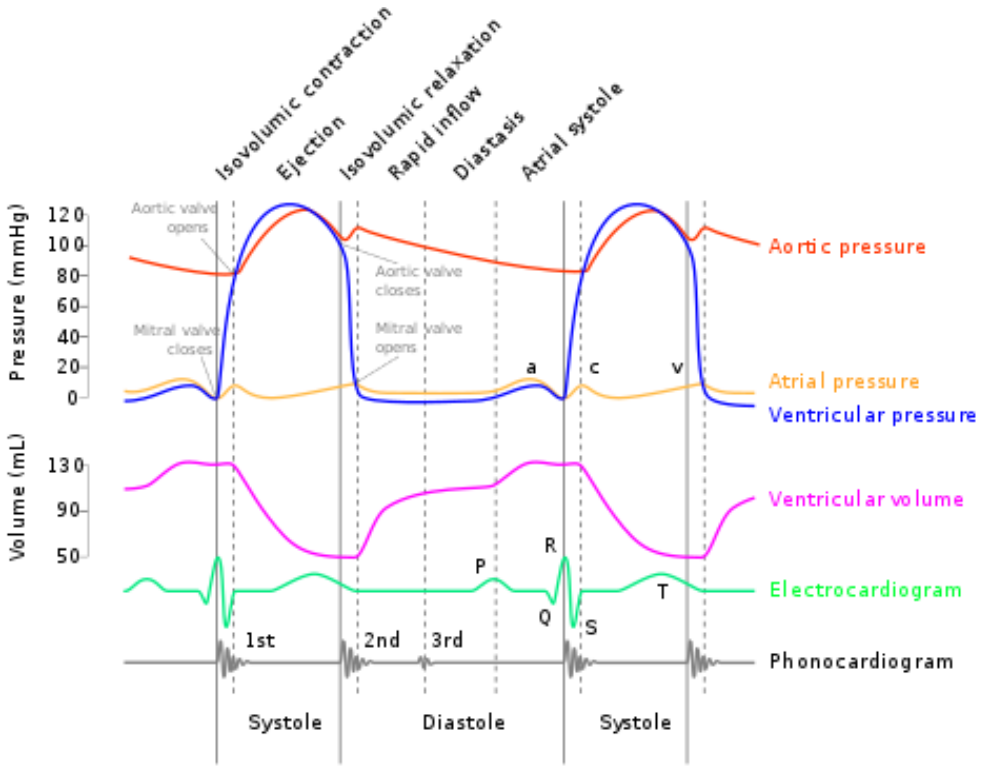

Figure 1.8: *Correlation of electrical and mechanical events of the cardiac cycle [24]*

1.4 Techniques for cardiac activity monitoring

There are several techniques for non-invasive monitoring of the cardiac activity [25].
Phonocardiography (PCG) detects sounds produced by the heart and the blood flow, produced by the vibrations created by the closure of the heart valves: the first sound is produced by the closure of the tricuspid and mitral valves at the beginning of the systole, while the second sound is produced by the closure of the aortic and pulmonary valves at the end of the systole [26]. Sounds are recorded with the help of a specific device called phonocardiograph.
Another non-invasive motoring technique is electrocardiography (ECG). Electrocardiography studies the electrical functioning of the heart and is recorded through electrodes placed on the skin of the patient. ECG produces an electrocardiogram, which is a graph of voltage vs time as a consequence of cardiac muscle depolarization followed by repolarization during each cardiac cycle (heartbeat) [27].
Next, Impedance cardiography (ICG) was proposed to measure the changes in thoracic impedance induced due to changes in the fluid content of the chest. The continuous change in thoracic impedance over time, allows estimating important cardiac functional parameters such as stroke volume, cardiac output, ventricular ejection time and pre-ejection period [28].
Additionally, echocardiography (ECHO) is a cardiac imaging method based on ultrasound to see how blood moves through the heart (by Doppler effect) and how the structure of the heart appears (by B-mode, size and shape of the heart location and extent of any tissue damage, assessment of valves, etc.). ECHO looks for irregularities in the heart's structure [29].
At every heartbeat, the blood travelling along the vascular tree produces changes in the body center of mass and body movements are produced by the recoil forces to maintain the overall momentum [30]. These micro-movements (displacement, velocity, acceleration) can be recorded by inertial sensors (accelerometers, gyroscopes), generating the so called ballistocardiogram (BCG). While BCG measures the overall body displacements at each cardiac beat, seismocardiography (SCG) focuses on the precordial vibrations generated by heart, thus measuring only the local vibrations of the chest wall in response to the heartbeat. As such, it contains information related to the mechanical activity of the heart [31], very similar to those that can be obtained using PCG, but using a different physical principle.
In 2016, gyrocardiography (GCG), a non invasive technique based on SCG was proposed [32]. It assesses the cardiac motion (precordial micro vibrations) using a microelectromechanical gyroscope sensor - a sensor that measures the angular motion – attached to the skin anterior to the sternum.

For the purposes of this project, the ECG and SCG signals are described more in detail in the following sections.

1.4.1 Electrocardiogram – ECG

The electrocardiogram is a graph of voltage vs time which displays the electrical activity of the heart using electrodes placed on the skin [33]. These electrodes detect the small electrical changes that are a consequence of cardiac muscle depolarization and repolarization during each cardiac cycle.
Thus, cells depolarization and repolarization generate electrical currents which are conducted all the way to the skin, because tissues and fluids surrounding the heart act as electrical conductors. By placing electrodes (conductive pads) on the skin it is possible to detect these electrical currents.

The standard 12 leads-ECG is obtained using 10 electrodes attached to the body surface (*Figure 1.9(a)*). Any pair of electrodes can measure the potential difference between two corresponding locations of attachment, the exploring (i.e. positive) electrode and the reference (i.e. negative) electrode. The ECG is constructed such that if an electrical current is travelling towards the exploring electrode, it yields to a positive deflection, while if it is moving towards the reference electrode a negative deflection appears. Twelve leads are created by analysing the electrical potential differences between ten electrodes, resulting in a graphical description of the electrical activity of the heart. At any instant during the cardiac cycle, all ECG leads sense the same electrical events but from different angles.

These 12 leads (i.e. derivations) consist of two sets of ECG leads: chest and limbs. Depending on the position of the reference electrode in each derivation, the electrical activity of the heart can be observed from the horizontal plane or the frontal plane.

The limb leads, of which there are six (I, II, III, aVF, aVR and aVL) detects the electrical activity in the frontal plane, while chest (i.e. precordial) leads (V1, V2, V3, V4, V5 and V6) detects the electrical activity happening in the horizontal plane (*Figure 1.9(b)*).

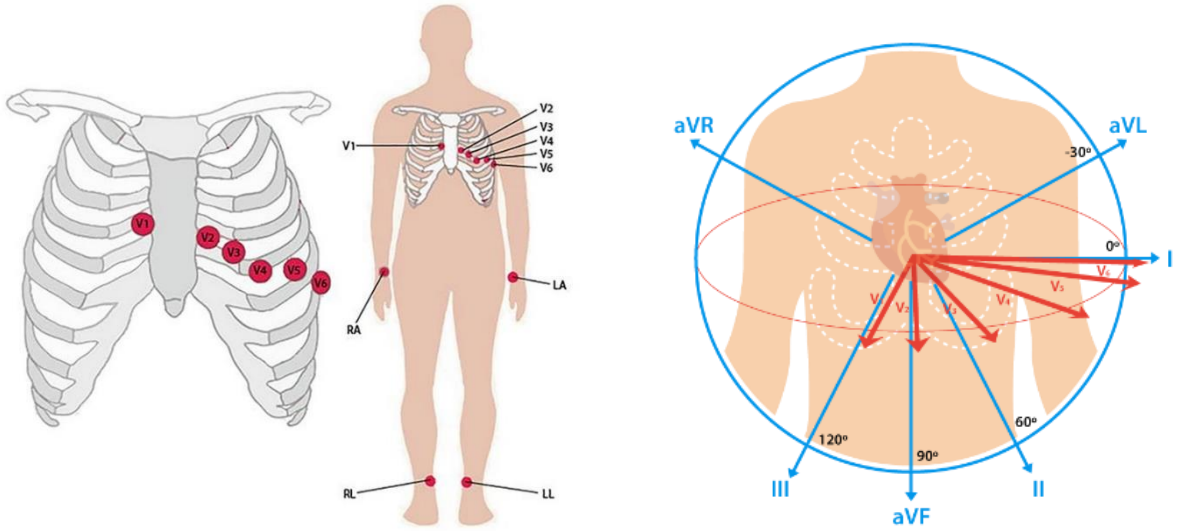

(a) Electrodes positioning (b) ECG derivation

Figure 1.9: (a) Positioning of 10 electrodes in 12 leads-ECG. Six electrodes are placed on the chest (V1,V2,V3,V4,V5,V6), while four electrodes are placed on arms and legs (RA: right arm; LA: left arm; RL: right leg; LL: left leg); (b) 12 derivations obtained measuring the potential difference between 10 electrodes. Red vectors represent chest derivations happening in the horizontal plane, while blue vectors represent limb derivations happening in the frontal plane [34,35].

The axis of the ECG is the major direction of the overall electrical activity of the heart (heart electrical axis). The electrical axis reflects the average direction of ventricular depolarization during ventricular contraction (QRS axis) and in the normal adult ranges between -30° and +90°, which is directed downward and to the left on the frontal plane.
Lead II is angled 60° in the frontal plane, which means that the atrial vector in the frontal plane in always directed towards lead II. This derivation displays wider electrocardiographic waves because, by convention, has the same direction of the heart electrical axis (60°).

Figure 1.10 shows the classical ECG waveforms:

- P wave:
  The first deflection is the P-wave which represents activation (depolarization) of atria. Atria depolarization spreads from SA node towards the AV node and from the right atrium to the left atrium.
  The P wave is a small, positive (always positive in lead II because the vector is directed downwards and to the left in the frontal plane) and smooth wave.
  P wave duration in healthy subject is around 80 ms; if the wave is of unusually long duration, it may represent atrial enlargement.
  The repolarization of atria is usually non-visible because it occurs at the same time as the depolarization of ventricles, which generates larger electrical potentials.

- QRS complex:
  Ventricular depolarization is visible through the QRS complex. The ventricles have a large muscle mass compared to the atria, so the QRS complex usually has a much larger amplitude than the P wave. Since the electrical vector generated by the left ventricle is many times larger than the vector generated by the right ventricle, the QRS complex reflects left ventricular depolarization.
  - Q wave: represents the depolarization of the ventricular septum;
  - R wave: represents the descent depolarization along the walls of the ventricles up their apex;
  - S wave: represents the depolarization of the external areas of ventricles.

  QRS complex duration in healthy subject ranges from 120 to 200 ms; if the QRS complex is wider it suggests disruption of the heart's conduction system.

- T wave:
  T-wave represents the repolarization of ventricles. T wave duration in healthy subject is around 160 ms. The normal T wave is slightly asymmetric, with a steeper downward slope.

- U wave:
  U wave is a positive wave occurring after the T wave. It has a low amplitude or is not always present and it is hypothesized to be caused by the repolarization of the intraventricular septum. It is most frequently seen in leads V2-V4.

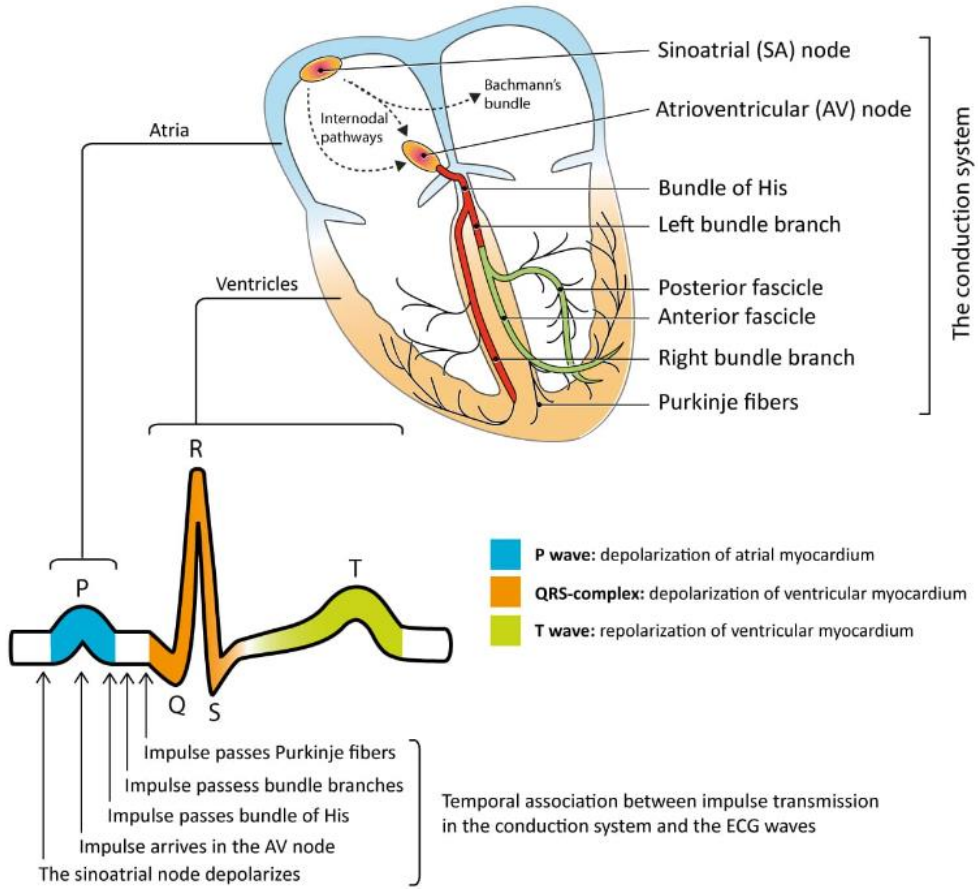

Figure 1.10: Cardiac conduction propagation pattern from the depolarization of SA node to the repolarization of ventricular myocardium. Correlation between signal propagation and the ECG wave [36].

Several clinical parameters are derived from ECG waveform. Three of the most important ones are heart rate (HR), R_iR_{i+1} interval and ventricular repolarization interval (QT).

QT is the time delay between the start of the Q wave and the end of the T wave and represents the time taken for ventricular depolarization and repolarization. It measures the period of ventricular systole from ventricular isovolumetric contraction to isovolumetric relaxation. The QT is inversely proportional to HR and is an important clinical parameter to access pathologies [37]. Thus, an abnormally prolonged QT is associated with an increased risk of ventricular arrhythmias [38]. A corrected measure of QT is often used instead of QT. The corrected QT interval (QTc) estimates the QT interval at a standard HR of 60 bpm and this allows comparison of QT values over time at different HRs.

There are multiple formulas used to estimate QTc:

- Bazett formula: $QT_c^{Baz} = \frac{QT}{\sqrt{RR}}$ (1.1)
- Fridericia formula: $QT_c^{Fri} = \frac{QT}{\sqrt[1/3]{RR}}$ (1.2)
- Framingham formula: $QT_c^{Fra} = QT + 0.154(1 - RR)$ (1.3)
- Hodges formula: $QT_c^{Hod} QT + 1.75(heart\ rate - 60)$ (1.4)

Bazett formula (*Formula 1.1*) is the most commonly used due to its simplicity.

QT_c^{Baz} is considered prolonged if is greater than 450 ms in men or greater than 470 ms in women and is abnormally short if is lower than 350 ms [39].

R_iR_{i+1} interval is the time elapsed between two successive R waves of the QRS signal.

HR is a term used to describe the frequency of the cardiac cycle. Usually, HR is calculated as the number of contractions (heartbeats) of the heart in one minute and expressed as beat per minute (bpm), as the reciprocal of R_iR_{i+1} interval. When resting, the adult normal HR ranges between 60 and 100 bpm [40]. Bradycardia and tachycardia are two forms of irregular rhythm: bradycardia is related to an irregularly slow HR (less than 60 bpm), while tachycardia is related to high HR at rest (more than 100 bpm) [41]. Both are generally caused by an electrical conduction problem within the heart tissue [42].

1.4.2 Seismocardiogram – SCG

Seismocardiography (SCG) is a non-invasive technique that measures the mechanical activity of the heart. It records the precordial vibration produced at every heartbeat by the cardiac contraction and relaxation, relevant valvular opening and closing, and by the blood ejection from the ventricles into the vascular tree.

SCG applies similar principles of BCG, which measures the whole body motion due to ejection of blood. BSG was first observed in 1877 by Gordon with the finding that, as a subject would stand on a weighing scale, the needle would vibrate synchronously to the subject's heartbeat [43]. Sixty years later, in 1940, Starr and colleagues [44] created an instrument to measure the BSG in a repeatable scientific manner but, as the equipment was very complex, it was not possible to use it in everyday life. The SCG was first measured by Bozhenko in 1961 [45] and was first applied in clinical studies 30 years later by Salerno and Zanetti [46]. Then, because of the advent of echocardiography and more advanced monitoring system techniques, BCG and SCG were abandoned by the medical community [47]. Nowadays, technologies advancements and miniaturization of sensors (e.g., micro-electro mechanical systems, MEMS) simplify the measurement and assessment of these signals, thus enabling BSG and SCG measurements in everyday life, outside of clinical settings [48].

In particular, SCG can be recorded by positioning inertial sensors in contact with the chest. If a tri-axial accelerometers is used, SCG components are acquired in the three orthogonal axes (i.e., head-to-foot, dorso-ventral, left-right), each displaying a specific pattern. Each SCG component has its own pattern with a magnitude in the order of few milli-g (where g is the gravity acceleration on Earth, corresponding to 9.8 m/s^2). Most of the time studies on SCG focuses on the dorso-ventral component (i.e. z axis), which is proven to contain more information relevant to heartbeat occurrence [49].

Chest vibrations show two components: at low frequency related to the flow of the blood into the aorta and vascular tree, and at high frequency related to the opening and closure of heart valves [50]. In addition, the modulation due to the respiratory activity is also present.

A typical SCG-beat waveform is characterized by peaks and valleys that have been correlated to specific events in the cardiac cycle. Specifically, considering the dorso-ventral component, some of these peaks and valleys are associated to physiological events [51]:

- Mitral valve closure (MC)
- Isovolumetric contraction (IVC)
- Aortic valve opening (AO)

- Rapid ejection of blood (RE)
- Aortic valve closure (AC)
- Mitral valve opening (MO)
- Rapid filling (RF)

The correspondence between SCG fiducial points and the cardiac events was verified by Crow and colleagues [52], comparing points extracted from SCG with their corresponding systolic and diastolic points extracted from echocardiography.

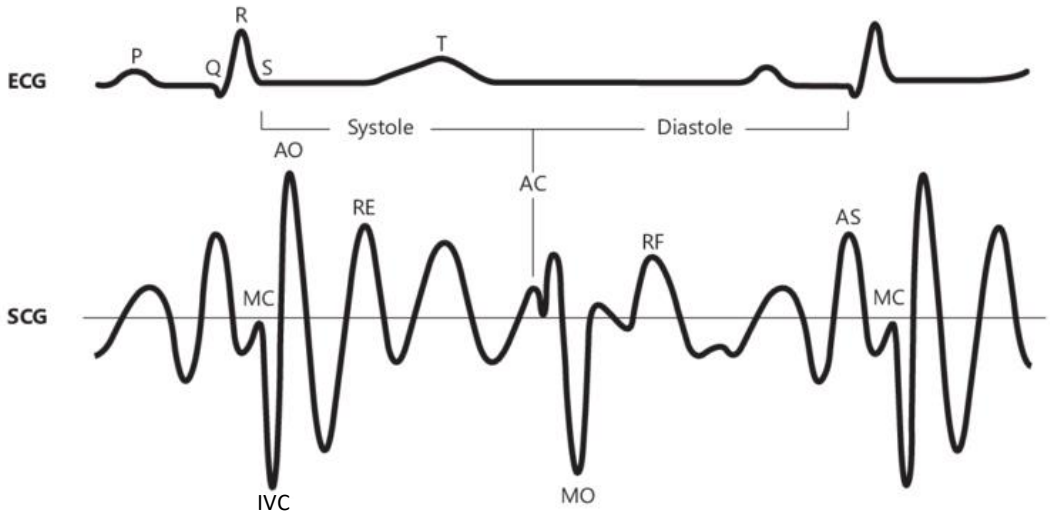

Figure 1.11: Comparison between ECG and SCG. Correspondence between electrical activity peak in ECG and mechanical activity fiducial points in SCG [51]

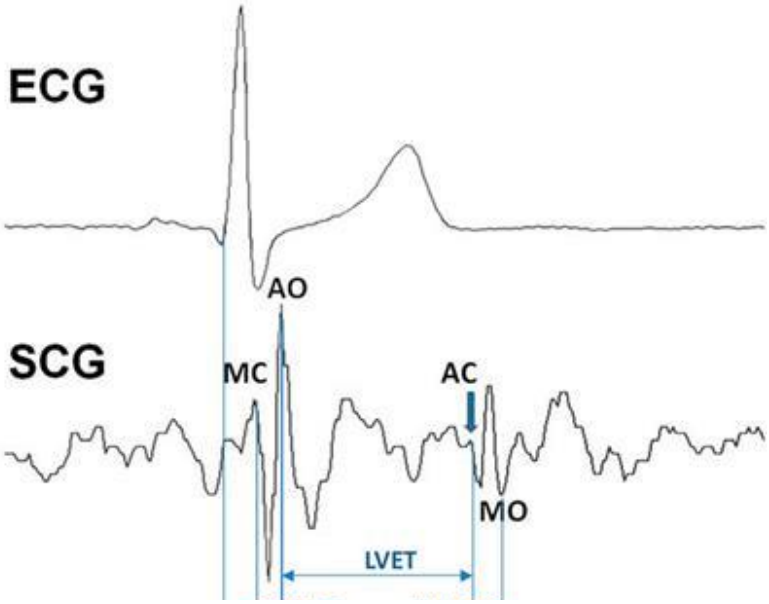

Figure 1.12: Cardiac time intervals computed from fiducial points extracted from SCG [54]

Based on the combined analysis of the fiducial points delineated from the ECG and from the SCG, several temporal parameters with a clinical relevance can be computed.

At the beginning of the systolic phase, the heart begins to contract but no blood is ejected in the vascular tree. This phase is called pre-ejection period (PEP) and is defined as Q-AO delay. PEP is considered as a measure of the contractility of the heart, the lower PEP the higher the contractility of cardiac muscles is [55].

The rest of the systolic phase is defined as the left ventricular ejection time (LVET) and measures the time interval where the aortic valve is opened and the blood is ejected into the vascular tree (AO-AC time delay) [52]. LVET is influenced by preload, afterload, left ventricular geometry and contractility, thus there is a direct relationship between LVET and stroke volume [56]

Electromechanical systole (QS2) is defined as the summation of PEP and LVET [54]. It includes the time interval from the start of the electrical stimulation of the ventricle (corresponding to the onset of ECG Q wave) to the end of the mechanical ventricular contraction. QS2 is an important clinical parameter: it has been suggested that abnormal values of the ratio between QT interval in the ECG and QS2 could be a marker of myocardial failure, so as an excessive lengthening of QS2 with respect to the ventricle relaxation time (RR-QS2) was suggested to be a marker for ventricular dysfunction [56,57].

Furthermore, a relationship in normal individuals between HR and the duration of the phases of left ventricular systole has been proposed [58], where the duration of QS2, LVET and PEP are inversely and linearly related to HR [59].

$$\begin{cases} QS2_{male} &= -0.0021 * HR + 0.546 \\ QS2_{female} &= -0.0020 * HR + 0.549 \end{cases} \quad (1.5)$$

Other important time parameters extracted from SCG are the isovolumic contraction time (IVCT), defined as the time delay between the closure of the mitral valve and the opening of the aortic valve (MC-AO time delay) [60], and the isovolumic relaxation time (IVRT), defined as the time delay between the closure of the aortic valve and the opening of the mitral valve (AC-MO time delay) [61], that has been proposed as a parameter sensitive to diastolic dysfunction [62].

1.5 Circadian rhythm

A circadian rhythm is an oscillation of a physiological process over a 24-hour period.

In the CV system, most physiological parameters (including HR, HR variability, electrocardiogram waveforms, and blood pressure) and pathological events demonstrate a robust circadian rhythm [63]. Also, many cardiovascular diseases vary in prevalence by time of day, including myocardial infarction, supraventricular/ventricular arrhythmias, and sudden cardiac death (SCD) [64].

Dealing with HR, it has been shown that there is a sudden rise around awakening with a peak value between 10 and 12 AM [65]. After that, HR gradually begins to decrease and maintains a lower value during the whole night. The circadian change of HR ensures that the heart adapts to the needs of different activity levels during the day and night by increasing or decreasing cardiac output [65].

ECG parameters also display circadian rhythm: P wave duration and its area, P-R interval, QRS duration and QT interval have been found to show diurnal changes [66,67]. During the daytime, when sympathetic output is enhanced and HR increased, all these indices have been found to decrease, reaching lowest values between 10 AM and 2 PM [66,67]. On the contrary, during night-time, following parasympathetic dominance, there parameters begin to increase, reaching their peaks values between 12 AM and 6 AM [66,67]. Also, QTc interval shows diurnal changes [68]. Duration of PR intervals and QRS complexes additionally exhibit higher values during night, indicating slower conductions of atrioventricular node and His-Purkinje system.

Heart rate variability (HRV) refers to the variation in time between successive heart beats and represents a non-invasive index of the autonomic nervous system. Because the autonomic nervous system regulates HR during sinus rhythm, HRV summarises complex non-linear cardiovascular accommodative responses, which are dictated by the parasympathetic (high frequency component: HF) and sympathetic (low frequency component: LF) nervous systems, to dynamic physiological variations. Also, HRV shows a diurnal rhythm correlated to circadian variations in autonomic nervous system activity. In general, all HRV indices (except for the ratio between LF and HF) increases during the daytime and decreases during the night-time [69,70,71]. In some pathological conditions, such as ischemic cardiac disease and stroke, which impair autonomic nervous function, the amplitude of the circadian rhythm of HRV can be altered or nearly absent [72,73].

Furthermore, some physiological parameters correlated to the mechanical activity of the heart, as stroke volume and cardiac force show a circadian rhythm and decrease while sleeping [74]. Upon awakening, these parameters increase rapidly in association with autonomic nervous system fluctuations (sympathetic and autonomic tone) [75].

1.6 Previous studies on SCG

During the last years many studies focused on evaluating the potential of using SCG signals for monitoring cardiac activity [76,77].

To do so, there is the need to extract reference points from the SCG signal. Due to the high levels of noise, this can be difficult, and so algorithms that use the synchronously acquired ECG signal as a reference were proposed. [78,79,80]. *Tadi et al.* [80] used the Q- and R-peaks of the ECG signal as reference points to automatically annotate the AO and MC peaks in the SCG signal. In [78, 80], the authors used the ECG to segment the SCG for each cardiac cycle. Especially the Aortic Valve Opening (AO) point has been investigated extensively and results are consistent among most studies [81,82]. Accurate determination of events, including AO, could make SCG a diagnostic tool for cardiac disease, comparable with the ECG. Other new methods based on ML algorithm were applied only on SCG data to predict the position of R peaks [83].

All these methods however have in common the fact that they were applied and evaluated on short recordings, from a few seconds to a few minutes, acquired in laboratory conditions. With much longer recordings, it is considerably harder to mitigate the difficulties arising from the variability and noise in the SCG signal.

After the identification of fiducial points, several salient parameters of potential clinical interest can be computed. In [84], a novel method was proposed for measuring PEP and LVET based on the combined analysis of ECG, ICG and SCG in head-to-foot direction; in another study Ramos-Castro et al [85] proved the feasibility of applying short-term HRV analysis on beat-to-beat series obtained from 5 minutes of SCG signals. For ECG-derived HRV analysis, the interest in using very short recordings (<5 minutes, even up to 10 sec) is emerging in the recent years, leading to the extraction of ultrashort variability (USV) indices in the time domain, able to characterize the sympatho-vagal balance in different circumstances, especially when acquisition time is limited [86]. Furthermore, the HRV analysis is an effective measure to access mental stress detection and the potential of using HRV for stress evaluation has been demonstrated [87].

Furthermore, in [88] smartphone-acquired SCG signals (one minute duration) was evaluated for monitoring cardiac deconditioning after prolonged bed rest, showing the potential of using these signals in a portable and non-invasive way.

1.7 Aim of the thesis

The availability of novel technologies incorporating both ECG and SCG sensors and allowing for extended time acquisition (24 hours and more) opens the possibility of noninvasively studying both electrical and mechanical activity of the heart, also evaluating the circadianity of the derived parameters. Accordingly, the main aim of this study was thus to investigate the feasibility of extracting parameters of cardiac electro-mechanical activity from long-duration recordings, to define normal ranges for such parameters, and to study their circadianity.

To do so, 24-hour long acquisitions of both electrical heart activity (ECG) and mechanical heart activity (SCG) were used, and a specific signal processing pipeline was developed to extract the needed fiducial points from which to derive temporal, slope and amplitude beat-by-beat parameters of possible clinical interest from which circadianity was evaluated, together with normal ranges of values.

2. Methods and Materials

Section 2.1 presents the data used for this study and how they were collected. *Section 2.2* shows in the first part the pre-processing of the signals and the algorithm to extract fiducial points, and compute temporal and morphological parameters (*Section 2.2.1*, *Section 2.2.2*, *Section 2.2.3*, *Section 2.2.4* and *Section 2.2.5*). In *Section 2.2.6* and *Section 2.2.7* the description of methods used to perform the circadian analysis of the previously extracted parameters and statistical analysis will be presented.

2.1 Materials

2.1.1 Protocol and Acquisitions

A total of 22 volunteers (15 females and 7 males) were recruited to participate to the following experimental protocol, in agreement with the ethics principles defined in the Helsinki Declaration of 1975, as revised in 2000, and approved by the Ethical Committee of Politecnico of Milano. Each subject provided voluntary written informed consent to participate in the experimental protocol.

The study involved the acquisition of electrocardiogram (ECG) and seismocardiogram (SCG) signals for 24 hours, during which the subject carried out the normal activities of his/her every-day life.

Each volunteer provided, in addition to the cardiac signal acquisitions, other personal data regarding: sex, age, weight, height and information on the activities performed during the 24 hours (sleep period and sleep duration, sport activity, work, etc.).

Age (y)	Weight (Kg)	Height (cm)
30 (25 – 55)	65 (61 – 75)	168 (164 – 177)

Table 2.1: Anthropometric characteristics of the population in terms of age, weight and height, expressed as median (first row) and 25th and 75th percentiles (second row)

2.1.2 Movisens device

The physical activity sensor EcgMove 4 from Movisens Gmbh was used to simultaneously acquire the ECG and SCG signals during the study.

The sensor acquires a single channel ECG signal (1024 Hz) and can be used with a dry electrode chest belt or with disposable electrodes (*Figure 2.1*). In addition, the sensor records the acceleration in three dimensions (64 Hz), the angular rate (gyroscope) (64 Hz) and atmospheric air pressure. Moreover the ambient temperature is also acquired [89].

(a) Electrode chest belt (b) Disposable electrodes

Figure 2.1: Usage possibilities with (a) dry electrode chest belt or (b) disposable electrodes [89]

The axes of the integrated inertial sensor (accelerator and gyroscope) are defined as:

- X axis: longitudinal axis (foot-head);
- Y axis: transverse axis (left-right);
- Z axis: sagittal axis (dorso-ventral).

For this study, the sensor was used with disposable electrodes – the electrodes were attached directly to the sensor and positioned between the 5th and 6th ribs, close to the cardiac apex. As seen in *Section 1.4.2*, the acquired signal reflects the SCG because the sensor is measuring the body vibrations due to the ejection of blood at the level of the chest.

(a) EcgMove4 positioning (b) Axis of the sensor

Figure 2.2: (a) The EcgMove4 is positioned through disposable electrodes on the chest, between the 5th and 6th ribcage. (b) The x-axis is the longitudinal axis; the y-axis is the transverse axis; the z-axis is the sagittal axis [89]

At the end of the 24h duration, the acquisition was stopped and the acquired raw data can be exported either in the unisens format (open data format for multi sensor data) or as .csv file.

2.2 Methods

The entire processing workflow to analyze the acquired 24h ECG and SCG signals is schematized in *Figure 2.3* and described in the next sections. All software was developed using the software Matlab (The MathWorks, USA).

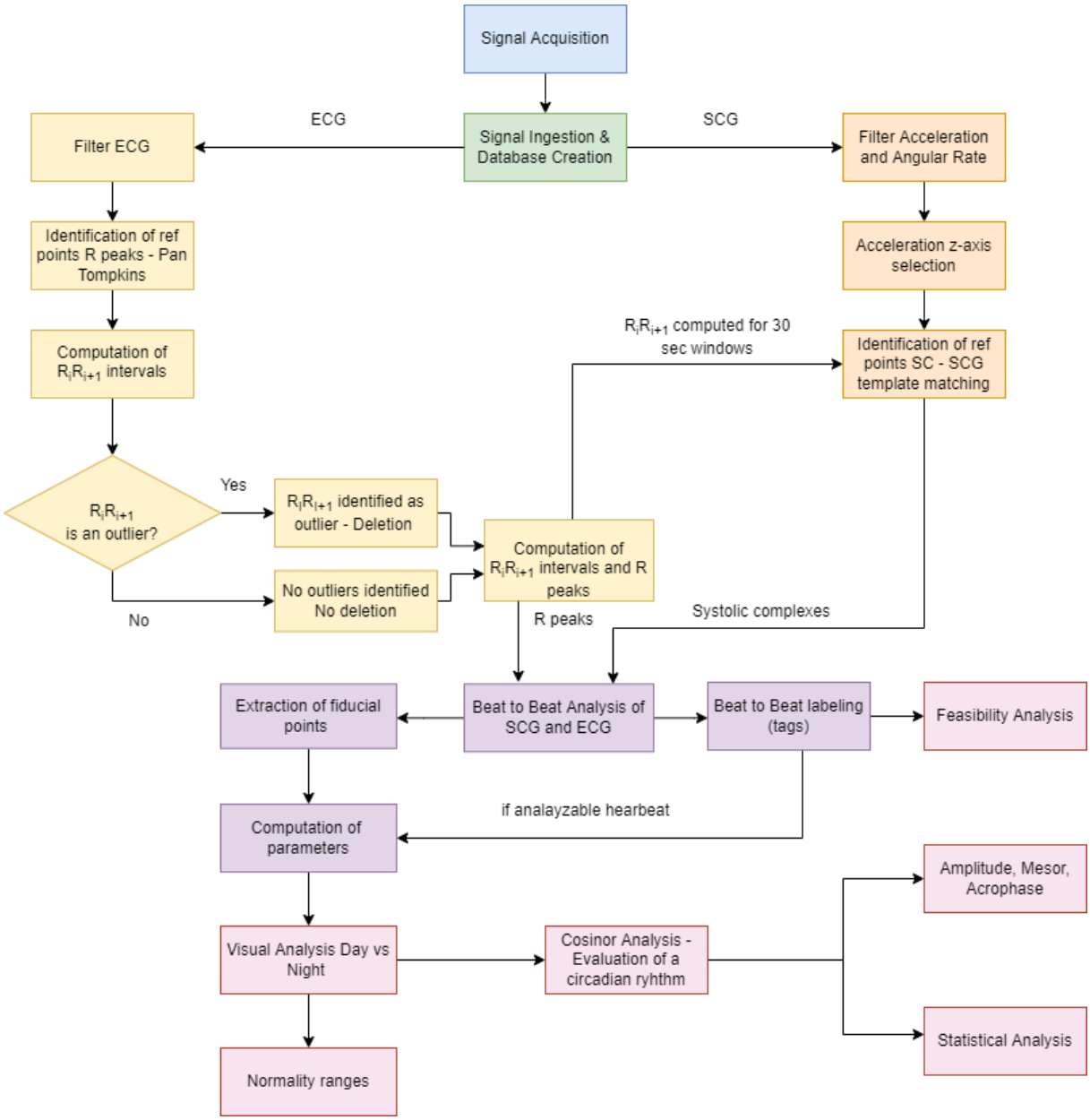

Figure 2.3: Workflow from signal acquisition to circadian and statistical analysis

2.2.1 ECG pre-processing

Several sources of noise can affect the ECG: baseline wander, electromyographic (EMG) noise due to muscle contractions, electrode contact noise and motion artifacts [90]

To try to remove them, ECG was preprocessed with 4° order, zero phase, band-pass Butterworth filter (high- pass filtering followed by low-pass filtering). A high pass-filter with cut-frequency equal to 0.5 Hz was used to reduce baseline wander. Then, the low pass-filtering of ECG was performed with a cut-off frequency equal to 30 Hz to reduce noise [91].

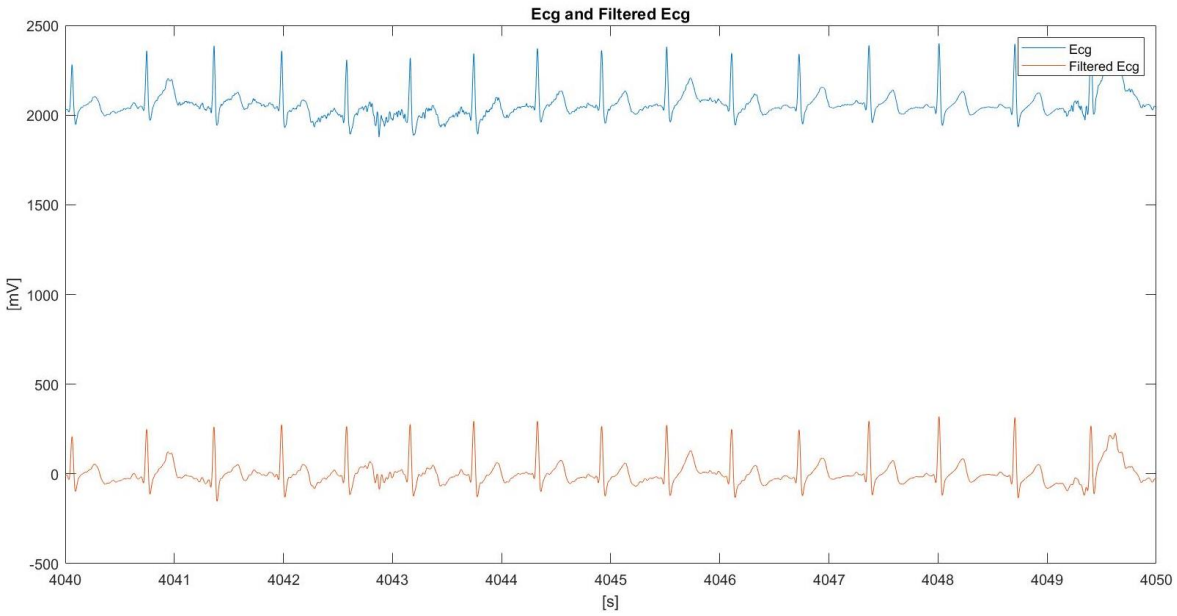

Figure 2.4: Comparison between ECG signal before filtering (blue signal) and ECG after filtering process (red signal)

2.2.2 SCG pre-processing

The SCG signal most of the time is adulterated by motion artifacts, environmental vibrations, and sensor mechano-electronics noise [92].

SCG components were band-pass filtered with 4th order Butterworth filter. Cut-off frequency of 5 and 25 Hz were used for Z (sagittal axis) and X axis (longitudinal axis), while 1 and 30 Hz for Y (frontal axis) axis (*Figure 2.5*) [93].

This step allows to remove out-of-band noise and breathing related motion artifacts.

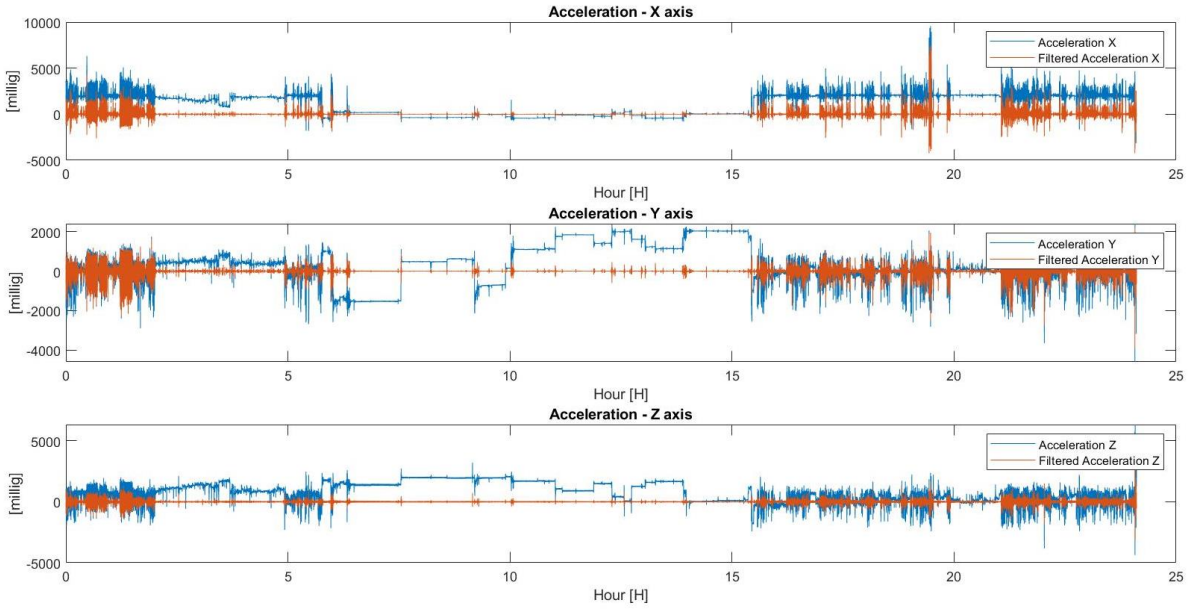

Figure 2.5: Comparison between SCG acceleration components before and after signal filtering along the 24 hours. In filtered SCG, the difference between the sleeping phase (in this example from hours 6 to 15) and the awake phase can be noticed: during sleeping, the signal appears clean and mostly free of artefacts, whereas with more noise elsewhere

The SCG signal includes 6 channels, 3 accelerations acquired with an accelerometer and 3 angular velocities acquired with a tri-axial gyroscope. However, of these 6, in the following analysis the focus was posed only on the dorso-ventral component of the acceleration (z axis), which has been proven to contain more information relevant to heartbeat occurrence [93].

2.2.3 Identification of reference points

The morphology of the SCG signal is not similar to the ECG signal. However, the SCG is capable of yielding similar HRV indices as compared to those extracted from the ECG with high correlation [94].

AO peaks, which temporally occur after the R-peak in an ECG signals, are used as fiduciary points to measure heart activity with the underlying assumption that the AO_iAO_{i+1} intervals in the SCG signals correspond to the R_iR_{i+1} intervals in an ECG signal [95].

2.2.3.a Identification of R peaks - ECG

The Pan-Tompkins (PT) algorithm is commonly used to detect QRS complexes (in particular R peak) in ECG signals [96]. It applies a series of filters (low pass filtering, high pass filtering and derivative filtering) to highlight the frequency content of the rapid depolarization of the heart and remove the background noise. Then, it squares the signal to enhance the QRS complex and reduces the possibility of erroneously recognizing a T wave as an R peak. Then, it applies adaptive thresholding to detect the peaks of the filtered signal (*Figure 2.6*).

Once the QRS complex is successfully recognized, the HR is computed as a function of the distance in seconds between two consecutive R peaks [97]:

$$HR(bpm) = \frac{60}{RR(s)} \qquad (2.1)$$

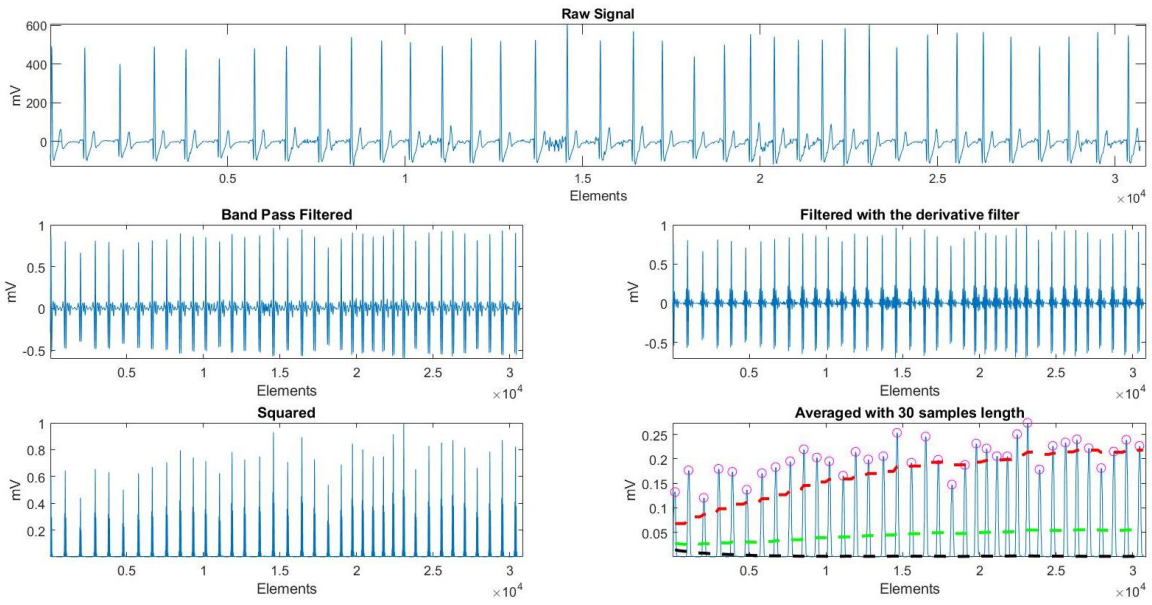

Figure 2.6: *PT steps applied to the raw signal to obtain R peaks [96]*

The 24 h ECG signal was divided into 30 s segments and PT algorithm was applied for each segment.

Each step of PT algorithm introduces a delay [96]: the band pass filtering introduces a delay of 22 samples, the signal differentiation introduces a delay of 2 samples, the squaring and integration introduces a delay of 150 ms, while the moving average filter introduces an initial learning phase delay of 2 seconds. Thus, it is possible to expect the detection of a QRS complex with a minimum delay - given a sampling frequency of 1024 Hz, of 0.02 sec, computed as (*Formula 2.2*):

$$\widetilde{D_{PT}} = \frac{22+2}{fs} \quad (2.2)$$

To prevent an erroneous identification of the QRS complex due to the delays introduced by PT algorithm, the exact Q peak was sought in a neighborhood of the Q peak identified by PT. We identified the exact Q peak as the maximum point inside the searching window, ranging between 0.02 sec before the Q peak (PT) and 0.02 sec after the Q peak (PT).

Another previous step that could introduce a constant delay is based on the FIR filters [98]. FIR filters were applied both on ECG and SCG signals but, due to the low sampling frequencies (*fs*) and the order of the filters (*N*), no significant delays were introduced (*Formula 2.4*).

$$D_{FIR} = \frac{N}{fs} \quad (2.4)$$

To detect possible outliers in the 24 hours resulting from the erroneous detection of R peak by the PT algorithm, R_iR_{i+1} intervals were computed as the temporal distance between two consecutive R peaks. An ECG segment was labelled as outlier if RR_i was longer than 30% of the average between the previous (RR_{i-1}) and next interval (RR_{i+1}) [99,100]. Then, RR_i outliers and R_i peaks were removed (i.e. set to NaN) from further analysis to avoid erroneous results (*Figure 2.7*).

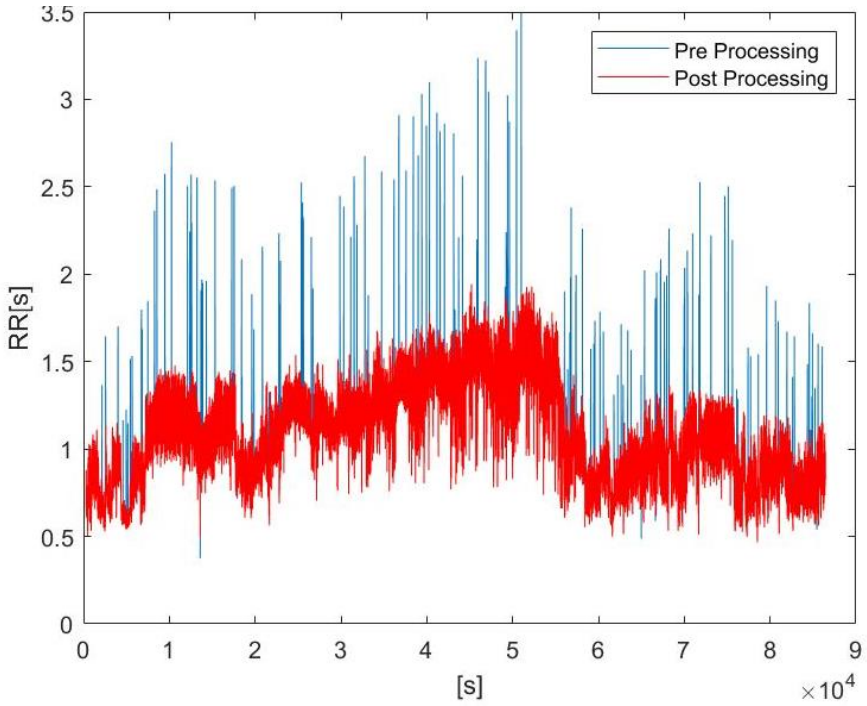

Figure 2.7: Comparison of RR intervals before and after outliers' removal

Then, the mean value of the R_iR_{i+1} intervals for each 30 seconds windows was computed. This parameter is crucial to identify the reference points in the SCG signal.

2.2.3.b Identification of the systolic complex - SCG

To detect AO, an ECG-free algorithm based on template matching technique was first applied [101].

A template of 10 s free of artifacts was initially selected by the operator and extracted during night-time for each subject.

The 24 h SCG signal (z axis) was divided into 30 s segments and cross-correlation was computed between each segment and the previously identified template. The position of maximum values of cross-correlation were used to identify a search window for each heartbeat. The search windows were used to precisely locate each systolic complex (corresponding to the fiducial point AO) as the wave with the maximum absolute amplitude on the z-component of the SCG signal.

Then, beat-to-beat duration AO-AO series were calculated as the distance between two consecutive AOs. The minimum distance allowed between two systolic complexes varies according to the HR: if the mean value of the R_iR_{i+1} intervals for that analyzed 30 sec window was less than or equal to 1 sec, two consecutive SCs must not be less than 0.4 sec apart. Otherwise, 0.5 sec was the minimum distance allowed between two peaks.

2.2.4 Extraction of SCG fiducial points: Algorithm

The heartbeat fiducials point on the SCG signal associated to the sharp cardiac vibration's waves in concomitance to the systolic activity can be detected using a novel ECG-dependent processing algorithm developed in this work, to be able to process 24h duration signals [102].

The first and last five minutes of each recording were excluded to avoid analyzing motion corrupted signals relevant to the experimental protocol attachment and detachment of the wearable device.

2.2.4.a Identification of fiducial points

For each R_i peak of the ECG signal identified in *Section 2.2.3.a*, a window ranging between R_i – 200 ms and R_{i+1} - 200 ms was extracted both from the ECG and SCG signals. The two windows were compared, and the fiducial points-searching algorithm was applied on the SCG signal if three different conditions were met:

1. Two consecutive R_iR_{i+1} intervals were not outliers – two consecutive R peaks were different from NaN;
2. At least one systolic complex (i.e. AO peak) was identified in that SCG segment;
3. At least three peaks were present in that SCG segment (peaks corresponding to aortic valve opening, the rapid ejection of blood and aortic valve closure)

These conditions prevent to analyze the SCG signal for beats in which motion artifacts were completely covering the cardiac mechanical activity. Otherwise, the fiducial points on the SCG corresponding to the AO, IVC, MC and RE were searched using the information from the systolic phase of the ECG. Instead, AC was searched differently, based mainly on the T wave peak on the ECG. In the next paragraphs, the choices implemented for the detection of such fiducial points will be described in detail.

2.2.4.a.1 Aortic valve opening - AO

AO peaks temporally occur after ventricular depolarization, specifically after R peaks.

For each segment, the three maximum peaks on the SCG occurring after the R peak on the ECG were identified, corresponding to the opening of aortic valve (AO), rapid ejection of blood into the vascular tree (RE) and closure of aortic valve (AC). The first occurring maxima was labelled as AO. Then, given the position of AO, other fiducial points were extracted (*Figure 2.8*).

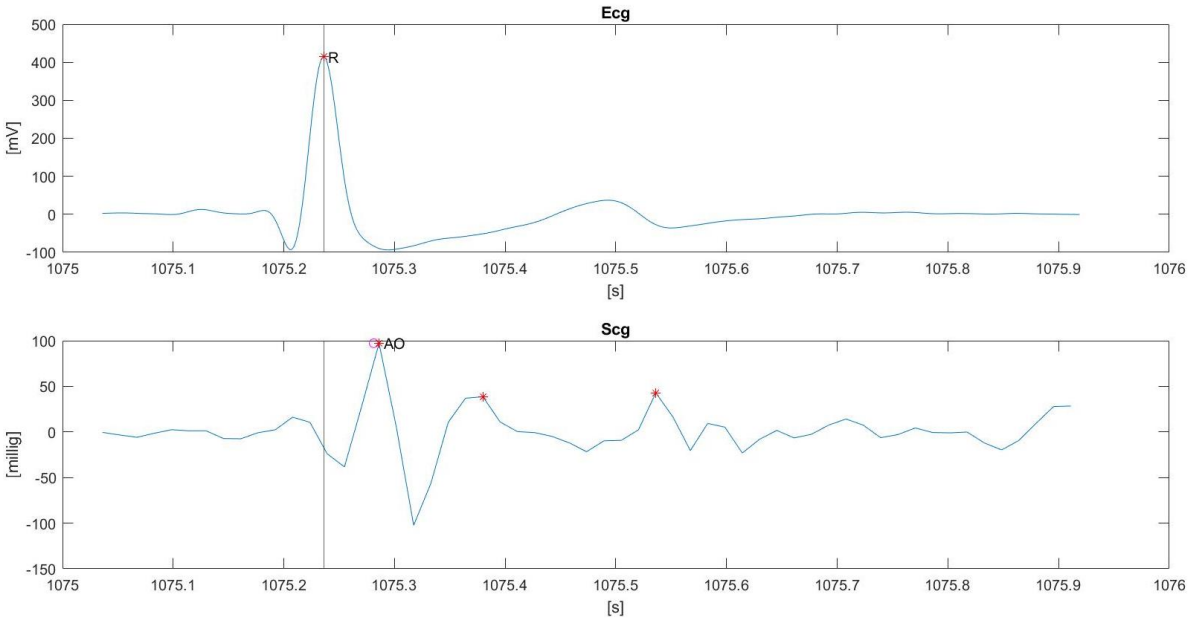

Figure 2.8: *Top*: *ECG signal together with R peak. Bottom: SCG signal along with the systolic complex identified in Section 2.2.3.b (pink circle) and the three maximum peaks occurring after R (red asterisks). AO was found as the first maximum point after R*

2.2.4.a.2 Mitral valve closure - MC

The Mitral valve closes (MC) at the beginning of ventricular systole when ventricular pressures rise above atrial pressures (*Section 1.3*). Then, soon after MC, the action potential depolarizes the wall of ventricles up to their apexes and R peak occurs. Next, when the pressure inside the left ventricle rises above the pressure in aorta, the aortic valve opens (AO) and the left ventricle ejects blood into the body through the aorta (RE).

For each segment, the MC point was identified as the maximum before AO (*Figure 2.9*). The position of MC with respect to R was a crucial condition to decide whether to consider or not such fiducial point: if MC was identified outside a maximum allowed distance from the R peak, then the SCG window was not further analyzed.

The maximum limit position for MC was found applying the Trapezium method [91]. The trapezium's area method is based on the calculation of successive areas of a rectangular trapezium with three fixed vertexes (x_m,y_m), (x_r,y_r), (x_r,y_m) and one mobile vertex (x_i,y_i). The mobile vertex is shifted from (x_m,y_m) to (x_r,y_r) while the total area is computed. The formula of the area is:

$$A = 0.5(y_m - y_i)(2x_r - x_i - x_m) \tag{2.4}$$

where:

- (x_m,y_m) are the abscissa and ordinate of a point with the highest absolute derivative inside a window ranging from R peak to 100 ms from R peak.
- (x_r,y_r) are the abscissa and ordinate of a reference point located approximately on the S-T isoelectric segment. The algorithm searches in a window between x_m and 100 ms from R peak, preferably with a value of the first derivative near to zero. The window amplitude was selected empirically.
- (x_i,y_i) are the abscissa and the ordinate of a mobile point among the two points mentioned before.

The maximum limit position for MC is defined as the point where the area A of the trapezium is maximum. It has been empirically found that this distance never exceeds 0.04 ms from the R peak.

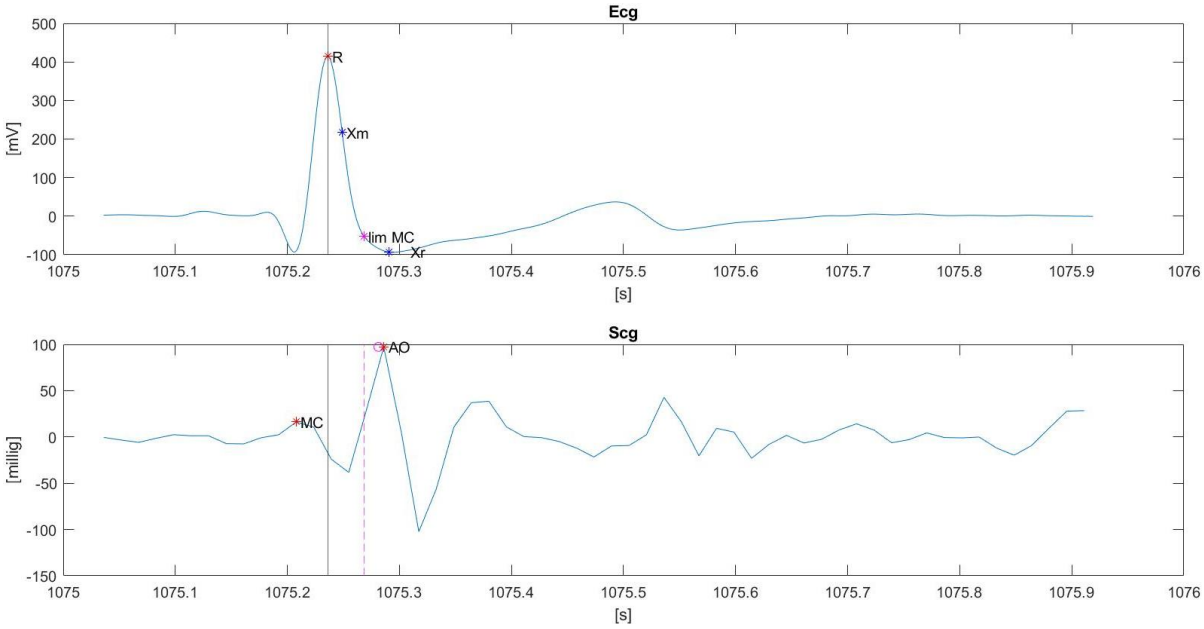

Figure 2.9: *Top: ECG signal together with R peak, Xm, Xr (blue asterisks) and the computed limit position for MC (pink asterisk). Bottom: SCG signal along with the systolic complex identified in Section 2.2.3.b (pink circle) and AO. The maximum allowed position for MC is reflected by the pink vertical line. MC was found as the maximum point before AO and before the maximum allowed MC position*

2.2.4.a.3 Isovolumic contraction – IVC

For each segment, the IVC point was identified as the minimum peak between the closure of mitral valve (MC) and the opening of aortic valve (AO) (*Figure 2.10*). Again, the position of IVC with respect to R was an important condition to decide the reliability of the extracted point and whether further analyze the specific SCG window. The isovolumetric contraction happens after the descent depolarization along the walls of the ventricles up to the apex, thus after R peak. If IVC was identified before R, this position was discharged and the first minimum point after R was labelled as IVC.

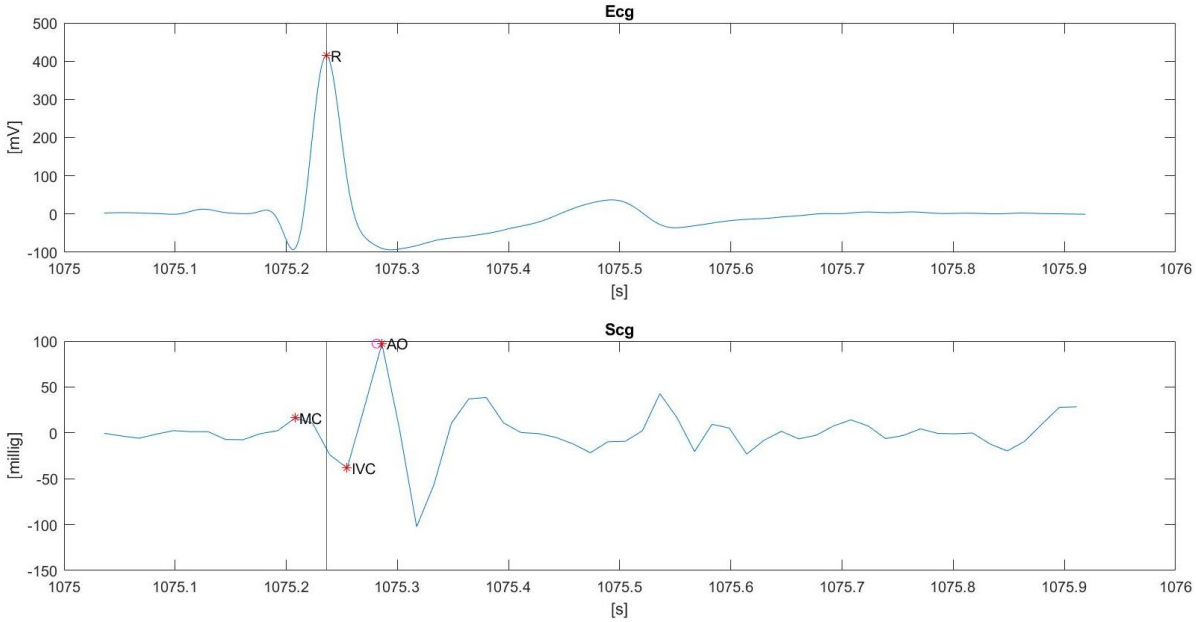

Figure 2.10: *Top: ECG signal together with R peak. Bottom: SCG signal along with the systolic complex identified in Section 2.2.3.b (pink circle), AO and MC. IVC was found as the minimum point between MC and AO*

2.2.4.a.4 Rapid Ejection – RE

As seen is *Section 1.3*, soon after the aortic valve opening the blood is ejected into the vascular tree (rapid ejection).

The RE fiducial point was identified as the peak following the aortic valve opening (*Figure 2.11*).

In addition, the negative peak between AO and RE was also extracted and used for further analysis (*Figure 2.11*).

If there were more than one negative values between AO and RE, the minimum peak between them was labelled as fiducial point.

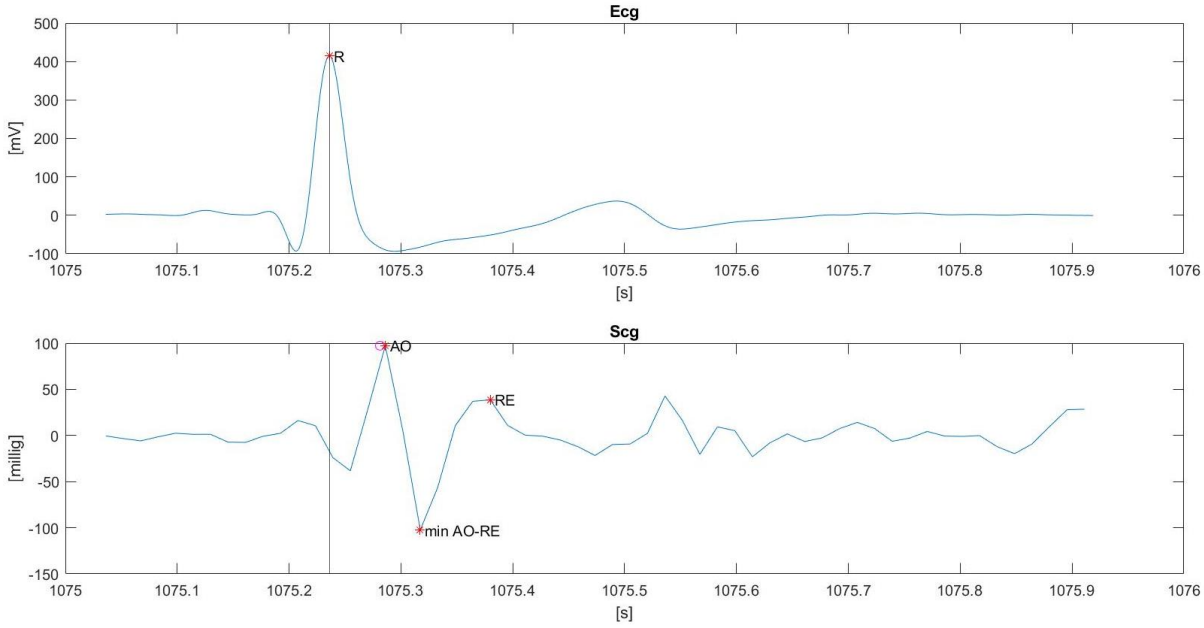

Figure 2.11: Top: ECG signal together with R peak. Bottom: SCG signal along with the systolic complex identified in Section 2.2.3.b (pink circle), AO, RE and the minimum point between AO and RE. RE was found as the peak after AO. The point with the minimum value between AO and RE as min AO-RE

2.2.4.a.6 Aortic valve closure – AC

Towards the end of the T wave on the ECG, the aortic valve closes and the left ventricle enters in the isovolumic relaxation phase, which marks the beginning of ventricular diastole. To detect AC, several steps were applied:

- Identification of T peak
  For each segment, the T peak was identified as the maximum peak after R (*Figure 2.12*).
  If more than one peak was identified after the QRS complex (the algorithm may have identified U peak or a motion artifact), the two maxima peaks after R were identified and the first one in time order was labelled as T peak.
  However, to avoid an erroneous identification, it was necessary for the peak to occur in the systolic phase. Given an R_iR_{i+1} interval, the systolic phase has been defined as 1/3 R_iR_{i+1} [103].
  Due to noise artifacts superimposed to the ECG signal, the systolic phase was enlarged to 40% of R_iR_{i+1}. If the T peak was identified outside, then the ECG and SCG windows were not further analyzed.

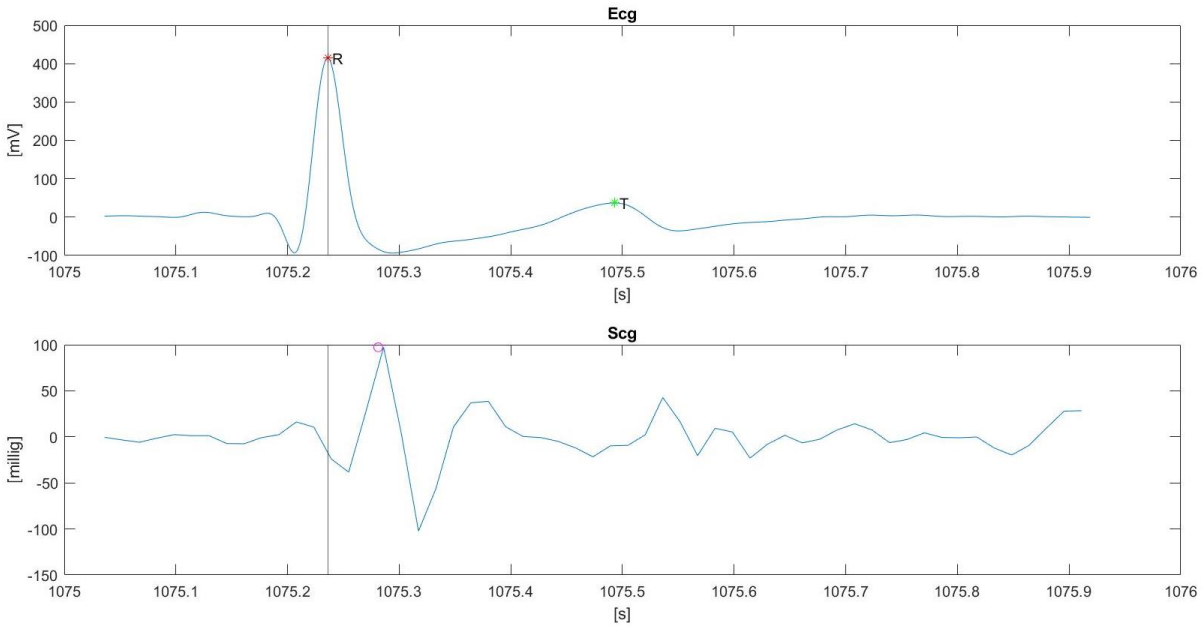

Figure 2.12: *Top: the ECG signal together with R peak and T peak. Bottom: SCG signal along with the systolic complex identified in Section 2.2.3.b (pink circle)*

Another important control condition to be met was related to the interval QT_c (Bazett's correction). If QT_c – computed using the T and Q peaks was longer than physiological QT_c values – then the ECG and SCG signals for that beat were not further analyzed. Corrected QT interval threshold values were defined

as 450 ms for adult males and 470 ms for adult females, according to the Committee for Proprietary Medical Products.

	Adult Males	**Adult Females**
Normal	< 430 ms	*< 450 ms*
Borderline	431 – 450 ms	*451 – 470 ms*
Prolonged	> 450 ms	*> 470 ms*

Table 2.2: Corrected QT intervals values according to the Committee for Proprietary Medical Products [104]

- Identification of T-wave end point
  The T-wave end location was identified based on the computation of trapezium's areas, an algorithm for T-end location that is least sensitive to the presence of broad-band noise or Gaussian white noise [91], also introduced before.
  Only monophasic T-waves (positive or negative) were considered.
  The trapezium's area method is based on the calculation of successive areas of a rectangular trapezium with three fixed vertexes (x_m,y_m), (x_r,y_r), (x_r,y_m) and one mobile vertex (x_i,y_i). The mobile vertex is shifted from (x_m,y_m) to (x_r,y_r) while the total area is computed (*Figure 2.13*). The formula of the area is:

$$A = 0.5(y_m - y_i)(2x_r - x_i - x_m) \quad (2.6)$$

  where:
  - (x_m,y_m) are the abscissa and the ordinate of a point with the highest absolute derivative inside the T-wave and after the T peak.
    The algorithm searches in a 40 ms window, starting from the T-wave peak. The window amplitude was selected empirically.
  - (x_r,y_r) are the abscissa and the ordinate of a reference point located approximately on the T-P isoelectric segment.
    The algorithm searches in a window between 40 ms and 80 ms from the peak of the T-wave, preferably with a value of the first derivative near to zero. If no point satisfies the condition, the central point is chosen.
    The window amplitude was selected empirically.
  - (x_i,y_i) are the abscissa and the ordinate of a mobile point among the two points mentioned before.

The T-end point is defined as the point where the area A of the trapezium is maximum (*Figure 2.13*).

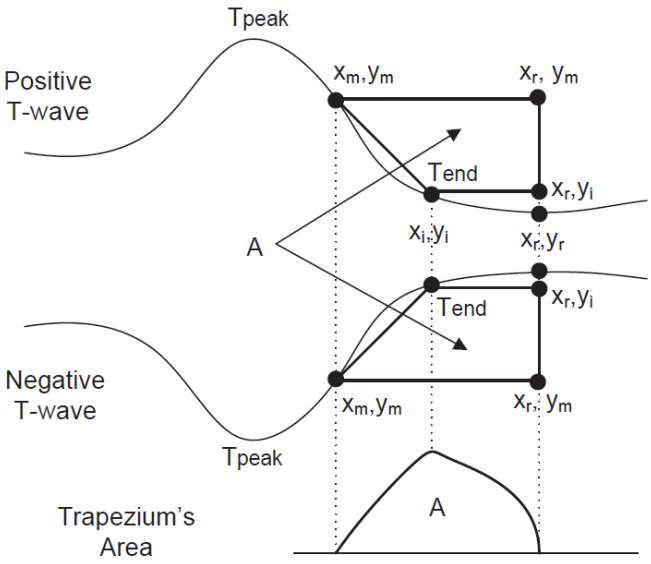

Figure 2.13: Determination of the T-wave end for a monophasic wave by the computation of the area of several trapezes formed by three fixed points and one mobile point (x_i,y_i) [91]

- Identification of AC
  Given the T-wave end point position, AC was identified as the first peak in time after it (*Figure 2.15*).
  Due to the low sampling frequency of SCG signal, we decided to consider valid the position of AC until the point was identified at most 4 ms after T-end peak.

  The position of AC with respect to Q was a crucial condition to decide whether to consider or not the detected fiducial points for that beat.
  For each ECG segment, Q-peak and the negative peak before Q-peak were identified. The negative peak before Q peak was identified as the minimum point inside a window ranging from 80 ms before R peak to the R peak. Then, Q peak was searched in a window ranging from 80 ms before R peak to the previously identified peak (negative peak before Q peak). The 80 ms window was chosen to be sure to exclude the P wave from this analysis.
  By computing the first derivative inside that window, the Q peak was selected as the point closest to the negative peak before Q peak, that met two conditions: the derivative in the previous points was close to zero and the derivative in the subsequent points was less than zero (due to the descending slope of the Q wave) (*Figure 2.14*).

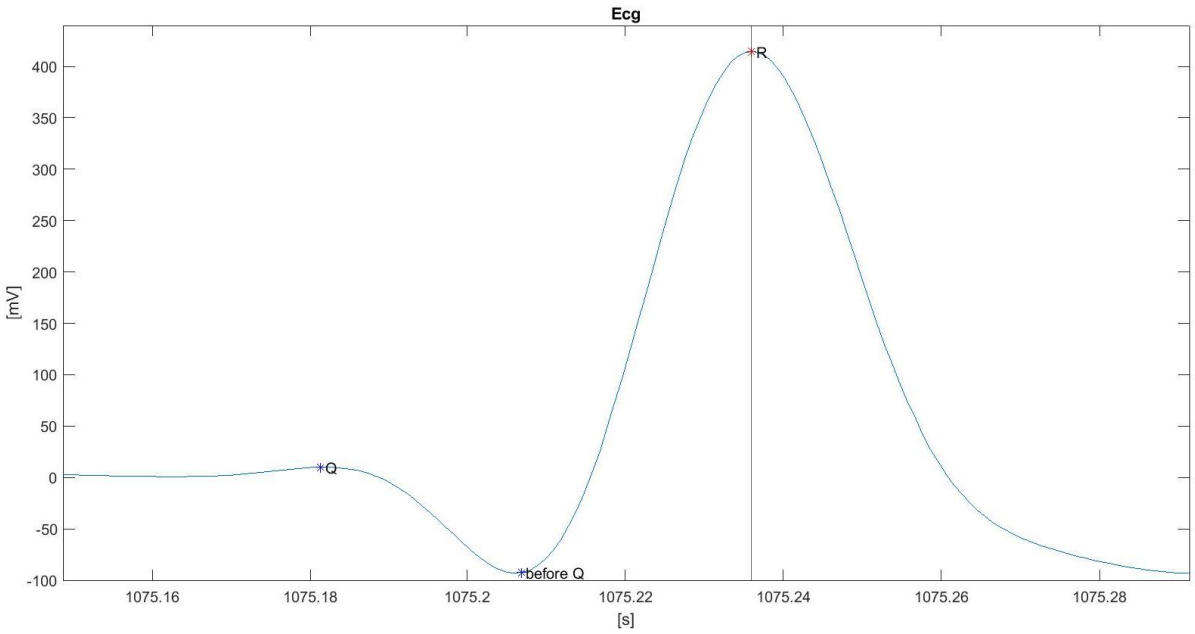

Figure 2.14: ECG signal together with the point before Q peak and Q peak

Then, the QS2 distance was computed as the time interval from the start of the electrical stimulation (i.e. Q wave) to the closure of the aortic valve (i.e AC) through *Formula 1.5* for male and female subjects. HR was calculated from the relationship 60/average RR intervals, where the average R_iR_{i+1} intervals was calculated from the mean value on 30 consecutive beat.
If AC was identified after the QS2 value previously computed, then the SCG was not further analyzed.

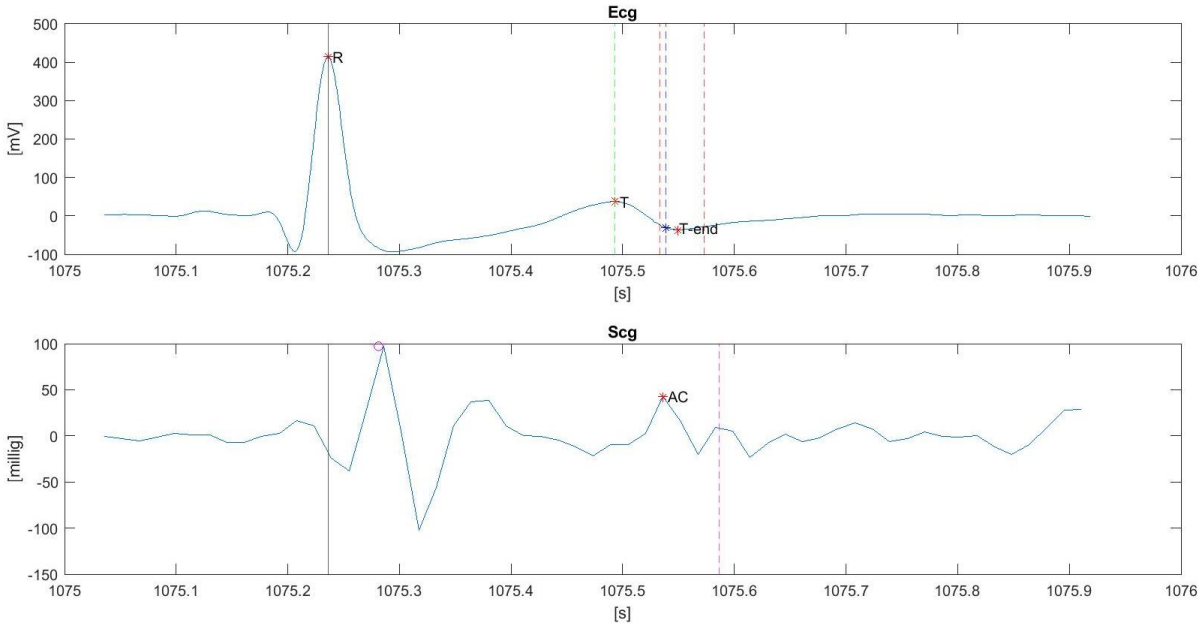

Figure 2.15: *Top: the ECG together with R peak and Tpeak. (Xm,Ym) is identified by the pink asterisk inside the window ranging between T-peak (green vertical line) and T-peak + 40 ms (first pink vertical line); (Xr,Yr) is identified by the pink asterisk inside the window ranging between T-peak + 40 ms (first pink vertical line) and T-peak + 80 ms (second pink vertical line). T-end peak is displayed with a blue asterisk. Bottom: SCG signal along with the systolic complex identified in Section 2.2.3.b (pink circle) and AC. The pink line corresponds to the maximum allowed QS2 distance*

2.2.4.a.7 Minimum before AC

Given the position of the fiducial point corresponding to the closure of the aortic valve, the minimum before AC was extracted as the negative peak prior to AC (*Figure 2.16*).

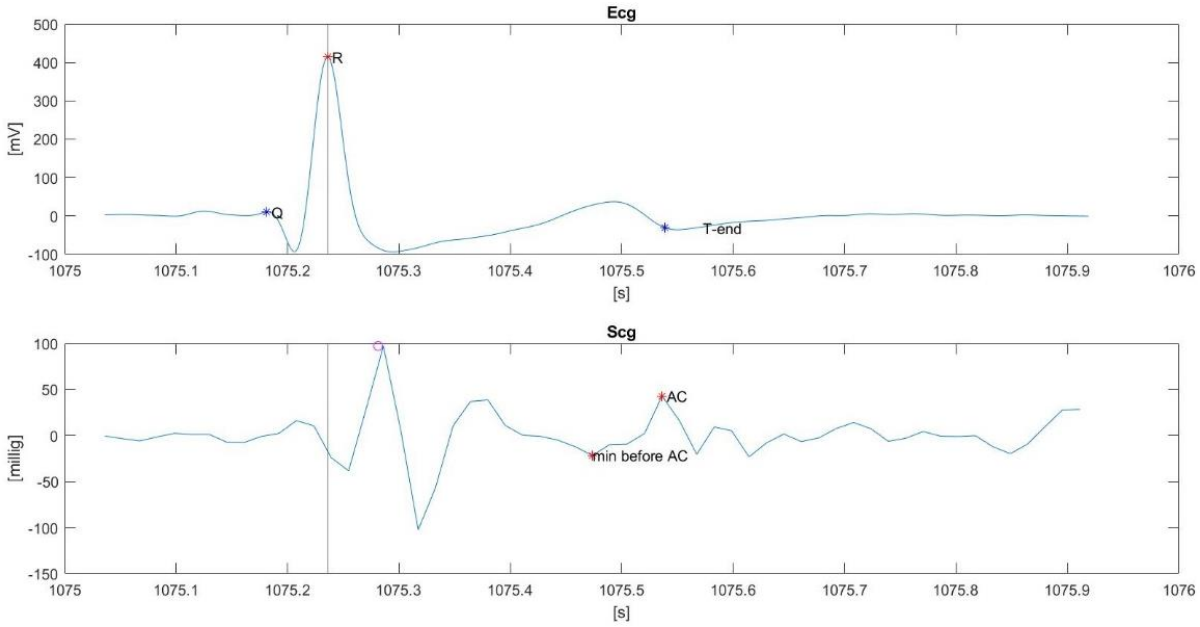

Figure 2.16: Top: ECG signal together with R peak and T-end peak. Bottom: SCG signal along with the systolic complex identified in Section 2.2.3.b (pink circle) and AC. The minimum peak before AC is labelled as min before AC

2.2.4.b Tags – Beat to Beat Labelling

To evaluate the feasibility of the proposed SCG analysis, a tag value was associated to each window (i.e., beat as defined by two consecutive R peaks on the ECG) based on the detected fiducial points. In total 10 different tag values were defined, of which:

- 6 are associated to windows in which there were "errors" and therefore no fiducial points from the SCG could be extracted;
- 2 are associated to windows in which only the SCG fiducial points relevant to early systole were extracted;
- 1 is associated to "perfect" windows, in which all fiducial points from the SCG could be extracted, except RE;
- 1 is associated to "perfect" windows, in which all fiducial points from the SCG could be extracted.

Table 2.3 shows the 10 tags with an explanation of the situation encountered and whether the window has been analyzed or not:

Tag	Description	Window further analysed
0	Perfect ECG and SCG window. All fiducial points are identified	*Yes*
1	At least one of two consecutive R_iR_{i+1} intervals are outlier	*No*
2	No correspondence between R peak and systolic complex in the specific window (0 systolic complex found)	*No*
3	Not possible to identify at least three peaks in the beat window (i.e., typical SCG beat waveform not identifiable)	*No*
4	Typical ECG beat waveform not identifiable	*No*
5	Wrong identification of T peak: T is found in the diastolic phase or QT_c is longer than the physiological value or T is not visually found	*Only Early Systole*
6	Cardiac cycle too short	*No*
7	RE coincides with AC, RE not reliable	*Yes (no RE)*
8	MC was identified after R peak: data from both early and late systole are not reliable	*No*
9	AC was identified after the maximum distance allowed from Q (QS2 max): data from late systolic phase are not reliable	*Only Early Systole*

Table 2.3: Tag values identified during the analysis. Each row represents a specific value: the first column displays the name of the tag, the second column describes it, and the third column explains the consequence related to that specific tag value (window analyzed, window not analyzed, only early systolic phase of the window analyzed)

Below an example of the "good" beat - associated to tags 0, 5, 7 and 9 - described above (*Figure 2.17*)

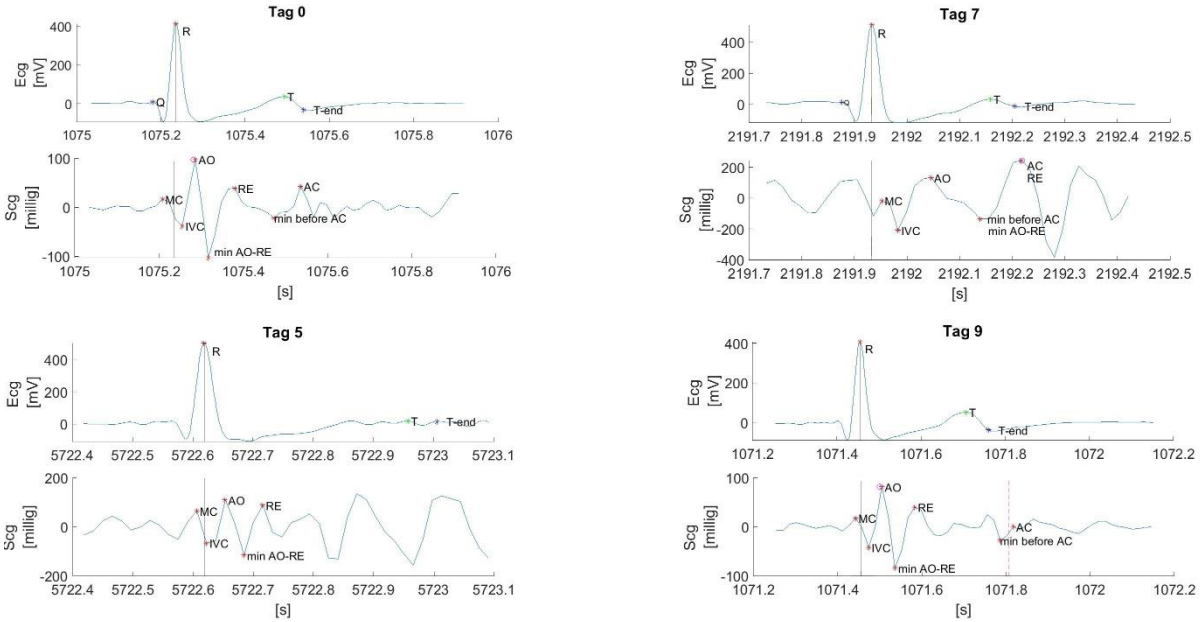

Figure 2.17: Examples of "good" heartbeats. Top left: ECG and SCG signals labelled as tag 0 (all fiducial points identified); Top right: ECG and SCG signals labelled as tag 7 (all fiducial points identified but RE non reliable); Bottom left: ECG and SCG signals labelled as tag 5 (early systolic fiducial points identified); Bottom right: SCG and ECG signals labelled as tag 9 (early systolic fiducial points identified). SCs identified through the SCG template matching algorithm are displayed as black squares

An example of "bad" heartbeats – labelled as tags 2, 3, 4,6 and 9 – are displayed in *Figure 2.18*. Beats associated to tag 1 are not shown because it was not possible to define and extract ECG and SCG windows associated to this event.

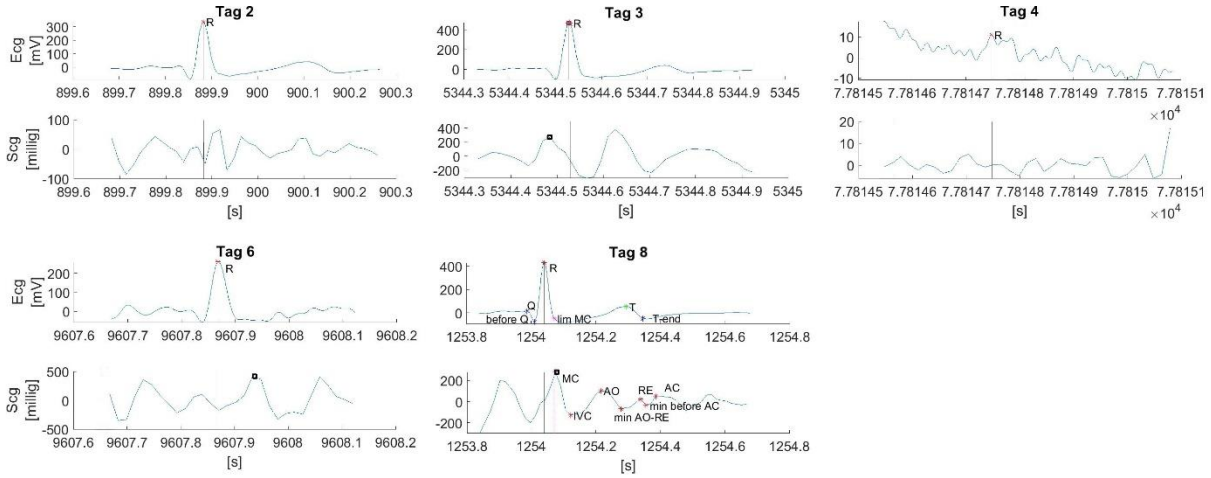

Figure 2.18: Examples of "bad" heartbeats. Top left: ECG and SCG signals labelled as tag 2 (no correspondence between R peak and SC); Top centre: ECG and SCG signals labelled as tag 3 (typical SCG waveform not identifiable); Top right: ECG and SCG signals labelled as tag 4 (typical ECG waveform not identifiable); Bottom left: ECG and SCG signals labelled as tag 6 (cardiac cycle too short); Bottom right: SCG and ECG signals labelled as tag 8 (MC was identified after the R peak). SCs identified through the SCG template matching algorithm are displayed as black squares

The beat-to-beat labeling and the number of heartbeats corresponding to each tag are functional to the subsequent feasibility analysis, whose objective is to understand what percentage of the 24h signals can be used to extract SCG parameters to compute normality ranges and circadian analysis, and what percentage instead needs to be discarded. In addition, the following analysis was carried out separately for daytime and nighttime to understand if there is a particular period within the 24 hours of recording, in which a greater percentage of the signal can be better analyzed.

Considering the tag values relevant to the positive extraction of SCG fiducial points relevant to the early systolic phase (tags 0,5,7 and 9), it was also important to quantify the maximum number of consecutive heartbeats detected as such, to determine whether a HRV analysis (ultra short-term or short-term) could also be performed.

2.2.5 Computation of SCG parameters

For each time window, the detected fiducial points were used to calculate the following parameters:

Parameters *[millig]*	**Description**	**How is computed**	**Cardiac phase**
ΔA(IVC-AO)	Difference in amplitude between IVC and AO	$Amp_{AO} - Amp_{IVC}$	*Early Systole*
ΔA(IVC-MC)	Difference in amplitude between IVC and MC	$Amp_{MC} - Amp_{IVC}$	*Early Systole*
ΔA(AO-RE)	Difference in amplitude between AO and RE	$Amp_{AO} - Amp_{IVC}$	*Early Systole*
ΔA(RE-minAORE)	Difference in amplitude between RE and the minAO-RE	$Amp_{minAORE} - Amp_{RE}$	*Early Systole*
ΔA(AO-AC)	Difference in amplitude between AO and AC	$Amp_{AO} - Amp_{IVC}$	*Late Systole*
ΔA(AO-minAORE)	Difference in amplitude between AO and minAO-RE	$Amp_{minAORE} - Amp_{AO}$	*Early Systole*
ΔA(AC-minAC)	Difference in amplitude between AC and min bef AC	$Amp_{minAC} - Amp_{AC}$	*Late Systole*

Table 2.4: Amplitude parameters computed using previously obtained fiducial points. Each row represents one amplitude parameter: the first column displays the name of the parameter, the second column describes it and the third column shows the formula applied to compute the data. The fourth column displays to which cardiac phase the parameter corresponds (early or late systole).

Parameters *[millig/ms]*	**Description**	**How is computed**	**Cardiac phase**
SLOPE(IVC-AO)	Slope between IVC and AO	$\frac{Amp_{AO} - Amp_{IVC}}{T_{AO} - T_{IVC}}$	*Early Systole*
SLOPE(minAC-AC)	Slope between minAC and AC	$\frac{Amp_{AC} - Amp_{minAC}}{T_{AC} - T_{minAC}}$	*Late Diastole*
SLOPE(minAORE-RE)	Slope between minAORE and RE	$\frac{Amp_{RE} - Amp_{minAORE}}{T_{RE} - T_{minAORE}}$	*Early Systole*

Table 2.5: Slope parameters computed using previously obtained fiducial points. Each row represents one slope parameter: the first column displays the name of the parameter, the second column describes it and the third column shows the formula applied to compute the data. The fourth column displays to which cardiac phase the parameter corresponds (early or late systole).

Parameters *[ms]*	**Description**	**How is computed**	**Cardiac phase**
ΔT(IVC-AO)	Time delay between IVC and AO	$T_{AO} - T_{IVC}$	*Early Systole*
ΔT(IVC-MC)	Time delay between IVC and MC	$T_{IVC} - T_{MC}$	*Early Systole*
ΔT(AO-RE)	Time delay between AO and RE	$T_{AO} - T_{RE}$	*Early Systole*
ΔT(AO-AC)	Time delay between AO and AC	$T_{AC} - T_{AO}$	*Late Systole*
ΔT(AO-minAORE)	Time delay between AO and minAO-RE	$T_{minAORE} - T_{AO}$	*Early Systole*
ΔT(AC-minAC)	Time delay between AC and min bef AC	$T_{minAC} - T_{AC}$	*Late Systole*
LVET	Time delay between AO and AC	$T_{AC} - T_{AO}$	*Late Systole*
QS2	Time delay between Q and AC	$T_{AC} - T_{Q}$	*Late Systole*
QT	Time delay between Q and T-end	$T_{T\text{-}end} - T_{Q}$	*Late Systole*
QT_c	Time delay between Q and T-end (corr)	$(T_{T\text{-}end} - T_{Q})/sqrt(RR)$	*Late Systole*
PEP	Time delay between Q and AO	$T_{AO} - T_{Q}$	*Early Systole*
ΔT(R-AO)	Time delay between R and AO	$T_{AO} - T_{R}$	*Early Systole*
ΔT(R-AC)	Time delay between R and AC	$T_{AC} - T_{R}$	*Late Systole*
ΔT(R-MC)	Time delay between R and MC	$T_{MC} - T_{R}$	*Early Systole*
R_iR_{i+1}	Time delay between R_i and R_{i+1}	$R_{i+1} - R_i$	*Early Systole*
AO_iAO_{i+1}	Time delay between AO_i and AO_{i+1}	$AO_{i+1} - AO_i$	*Early Systole*

Table 2.6: Temporal parameters computed using previously obtained fiducial points. Each row represents one slope parameter: the first column displays the name of the parameter, the second column describes it and the third column shows the formula applied to compute the data. The fourth column displays to which cardiac phase the parameter corresponds (early or late systole)

2.2.6 Circadian Rhythms Analysis

Cardiac circadian rhythms analysis aims to evaluate whether there is a circadian behavior in the considered parameter of cardiac mechanical activity.

Visual analysis is the first step of circadian analysis (*Subsection 2.2.6.a*). Visual analysis is crucial to understand if indeed it makes sense to carry out a circadian analysis and in what parameters a circadian pattern is expected. Only some parameters were selected for further steps.

Then, Cosinor analysis was applied on previously selected parameters (*Subsection 2.2.6.b*).

2.2.6.a Visual Analysis

The visual analysis uses previously calculated parameters to create approximate representation of the distribution of data through histograms. These visual representations display the comparisons of parameters between daytime and nighttime, to understand if the analyzed parameter is likely to have a circadian rhythm. Moreover, for each parameter, day-night differences were verified through Wilcoxon Signed Rank test ($p < 0.05$).

Accordingly, for each parameter a cumulative representations using data coming from all healthy volunteers participating in the study was computed together with median value, 25th-75th percentiles and 2.5th and 97.5th percentiles. This allows to determine a range of normality for each parameter.

When needed, parameters were normalized to allow the comparison between different subjects. Some amplitude parameters (Δ(IVC-AO), Δ(IVC-MC)) were normalized by the absolute value of the amplitude of IVC computed for the current cardiac cycle, following the *Formula 2.7*:

$$Amp\ parameter\ normalized = \frac{Amp\ parameter}{|Amplitude\ IVC|} \quad (2.7)$$

The remaining amplitude parameters (Δ(AO-RE),Δ(AO-minAORE), Δ(RE-minAORE), Δ(AO-AC) and Δ(AC-minAC)), were normalized by the absolute value of the amplitude of AO computed for the current cardiac cycle, following the *Formula 2.8*:

$$Amp\ parameter\ normalized = \frac{Amp\ parameter}{|Amplitude\ AO|} \quad (2.8)$$

Temporal parameters were normalized by the R_iR_{i+1} interval computed for the current cardiac cycle, as described in *Formula 2.9*:

$$Temporal\ parameter\ normalized = \frac{Temporal\ parameter}{RR\ interval} \quad (2.9)$$

2.2.6.b Cosinor Analysis

The traditional method to analyze circadian rhythm is the Cosinor analysis, which quantifies the circadian 24 hours cycle by means of examining the degree of fit (using the least squares method) between the experimental time series data and a model consisting of a superposition of cosine functions [105,106].

Cosinor analysis allows calculating the following circadian parameters (*Figure 2.19*) [107].

- Mesor: midline of the oscillation corresponding to the circadian activity;
- Amplitude: distance between the peak of the Cosinor curve and the mesor, measuring half variation within a night-day cycle ;
- Acrophase: time corresponding to the peak (positive) of the curve;
- p-value: assessed by the Zero-Amplitude Test with the null-hypothesis that the amplitude of the series is zero and thus that there is no rhythm in it (p>0.05)

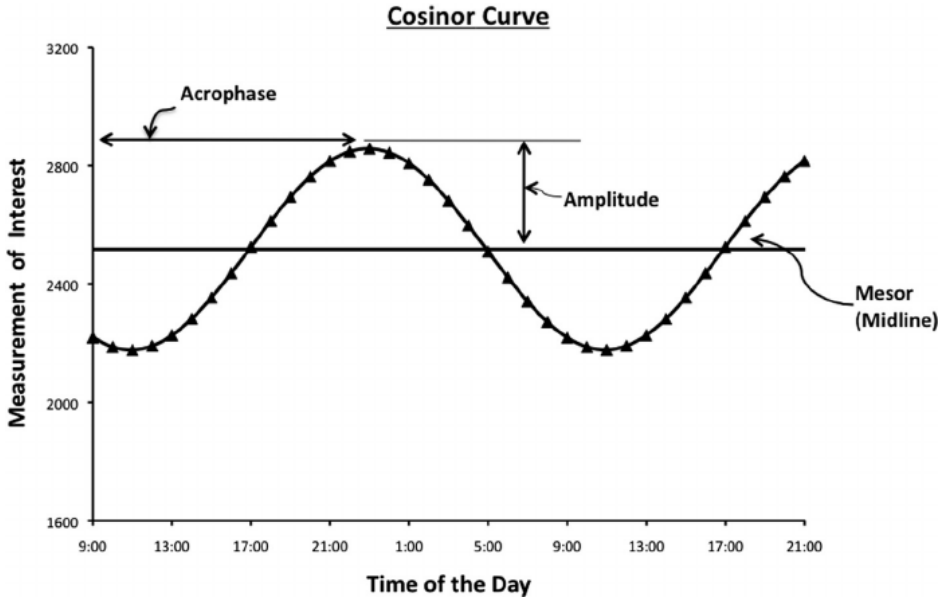

Figure 2.19: Example of cosinor curve and terms used to describe the circadian rhythm: mesor, amplitude and acrophase [107]

Cosinor analysis was computed both as a separate and cumulative analyses. As regards to the separate Cosinor analysis, before applying it, points were translated to ensure that all recordings started at 8 AM. This procedure aims to compare results of the Cosinor analysis -and in particular the acrophase - between all the participating volunteers. Cosinor analysis was not computed using beat-to-beat values but considering a moving average window lasting 5 minutes – without overlapping. Outliers were removed if the current parameter's value was bigger than 30% of the

average between the previous and next parameter's value. For each volunteer participating to the study, mesor, amplitude, acrophase (measured as hours and minutes) and the ratio between amplitude and mesor [108] of each clinical parameter previously identified, were computed. This analysis allowed to better understand the day-night cycle of the parameters describing the mechanical activity of the heart.

For each subject and each parameter, the results of the statistical analysis were evaluated to access circadianity ($p < 0.05$).

Regarding cumulative Cosinor analysis, points were translated to ensure that all recordings started when the subject goes to bed (i.e. approximately beginning of the annotated sleeping period). For each parameter, data coming from all healthy participating volunteer were merged to create one template. Then, the median template for each parameter was computed and outliers were removed. Then, mesor, amplitude, acrophase (measured as radians and hours - minutes) and the ratio between amplitude and mesor previously identified, were computed.
The results of the statistical analysis ($p < 0.05$) were evaluated for each parameter.

The coupling between the cardiac electro-mechanical activity was evaluated through a statistical test (Wilcoxon Signed Rank, $p<0.05$) of the acrophases of R_iR_{i+1} and AO_iAO_{i+1}.

3. Results

The following chapter is subdivided into 5 different sections: *Section 3.1* describes results about the feasibility analysis while *Section 3.2* reports results about the visual analysis, specifically the comparison of parameters extracted during day and night, to evaluate if there could be a circadian pattern during the 24 hours.

Section 3.3 and *Section 3.4* describe the results of Cosinor and its statistical analysis.

3.1 Feasibility Analysis

For each subject, the number of R peaks identified from the ECG and the number of systolic complexes identified from the SCG were compared during 24 hours, and separately day and night. The analysis was based on the data obtained after the signal post processing phases (RR outliers are included in the number of R peaks identified and are set to NaN).

Table A.1 shows the comparison between systolic complexes and R peaks depicted during 24 hours in each healthy volunteer participating to the study. Despite the fact that the percentage of SCs peaks identified compared to identified R peaks varied greatly from subject to subject, the median value was equal to 71.75% (62.09% as 25th percentile and 80.91% as 75th percentile). In thirteen subjects the percentage of SCs identified was greater than 70%.

Regarding the comparison of SCs and R peaks identified during daytime and night-time (*Table A.2*), the percentage of SCs (with respect to R peaks) identified during night-time was always higher than the percentage identified during day-time. Indeed, the median percentage value reached during night-time was 95.72% (92.04%; 98.3%), while the median percentage value computed during day-time was 64.18% (53.03% ; 74.16%).

To evaluate possible influence of body mass on the feasibility of the analysis due to signal quality, given for each participating volunteer the weight [Kg] and the height [m], the body mass index [Kg/m²] (BMI) was computed. Then, the correlation between BMI and the percentage of identified beats (data reported in *Table A.1*) was investigated by a linear regression model to describe the relationship between the response (percentage of identified beats) and predictor (BMI) variables (*Figure 3.1*).

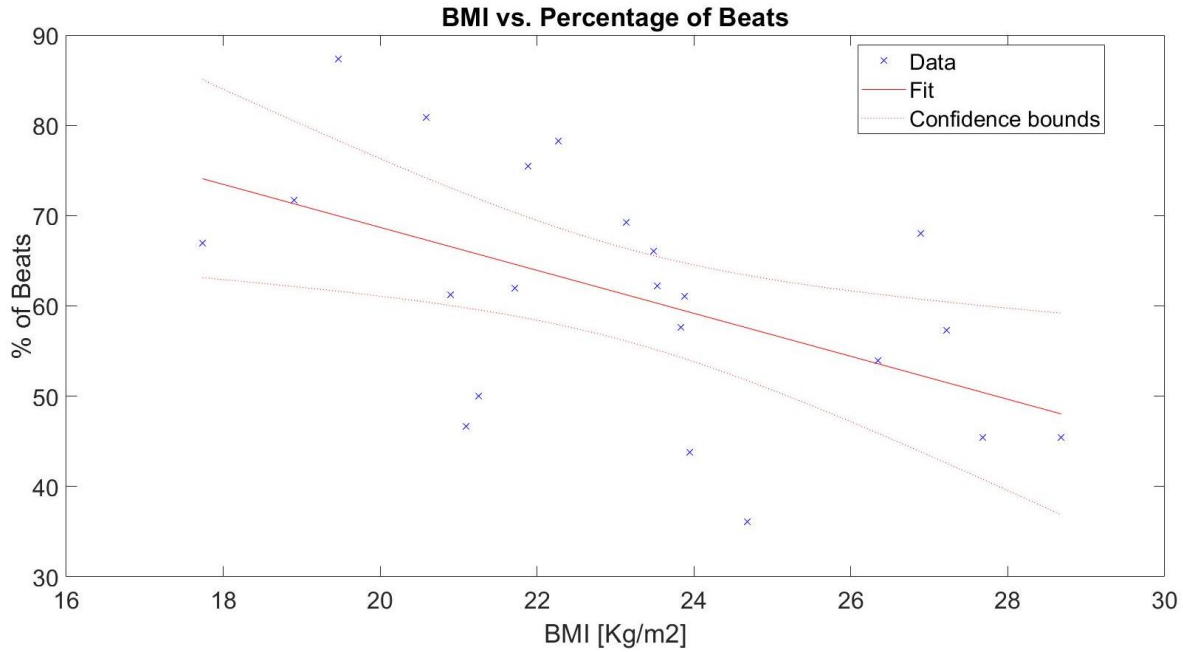

Figure 3.1: *Linear regression model representing the relationship between the predictor (BMI) and the response (percentage of beats) variables. The x-axis represents the body mass index [Kg/m²], while the y-axis represents the percentage of identified beats. Each blue dot represents a patient, while the red line displays the estimated model (straight line) and the dotted line displays the 95% confidence bounds*

Obtained results showed a significant ($R^2 = 0.278$ with $p < 0.05$) existing inverse correlation, resulting in a lower percentage of beats properly identified with higher BMI.

Another crucial part of the feasibility analysis was to establish for which subjects the T wave was visible in most beats (R_iR_{i+1} intervals).
A visual analysis was carried out on healthy participants and T-waves were visible and it was possible to identify T peaks in 15 volunteers only, while they were not visible and identifiable in 7 subjects.
In subjects in which the T wave was not identified (*Figure 3.2*), fiducial points and parameters in the late systolic phase were not sought in the subsequent analysis.

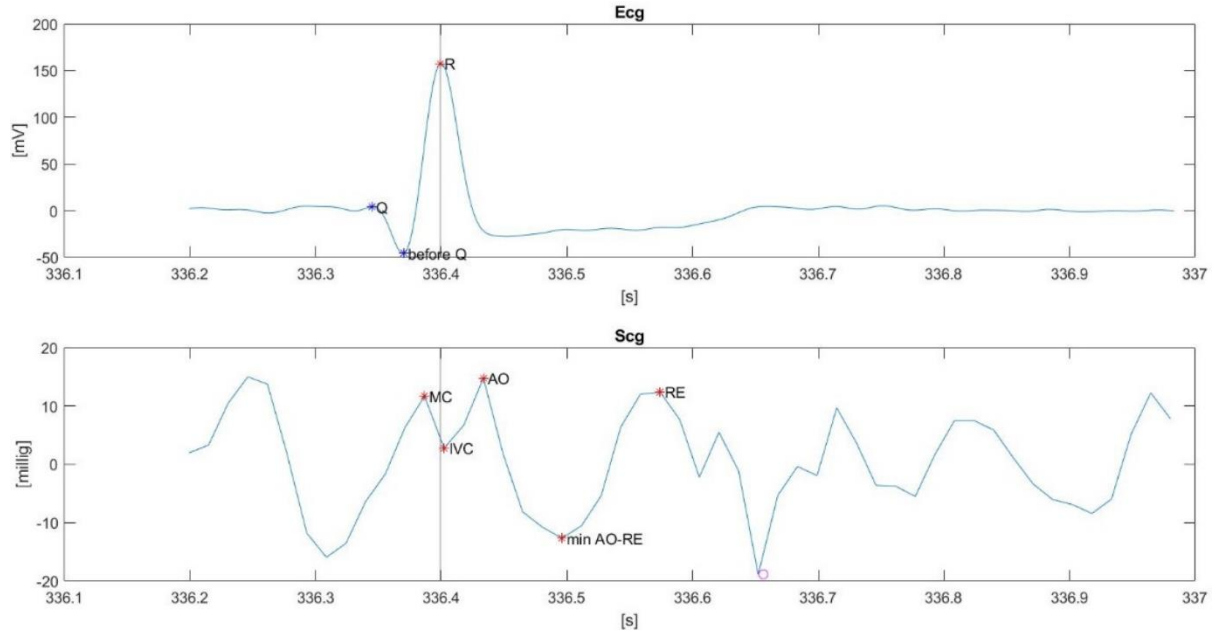

Figure 3.2: Example of a participating volunteer in which is not possible to identify the T peak wave

The second step of feasibility analysis was beat-to-beat labelling. For each subject, each beat was associated with one of the previously identified 10 tags. This operation allowed to establish what percentage of the acquired signals could be used for subsequent circadian analysis (tag 0,5,7 and 9) and what percentage would need to be discarded (other tags).
The analysis was carried out separately for day and night, and among subjects in which it was possible to identify the T wave or not.
We used three different colors to differentiate between "perfect-almost perfect" tags for which all parameters could be extracted (tags 0 and 7, in green), "good" tags, from which only parameters of the systolic complex could be identified (tags 5 and 9, in

yellow), and "bad" tags, associated to heartbeats to be fully discarded (remaining tags, in orange).

In subjects in which was possible to identify T wave peaks, all 10 tags were included. *Table A.3* and *Table A.4* display respectively day and night beat-to-beat labeling results.

Tags concerning the late-systolic phase (tags 7 and 9) were equal to N/A (i.e. not available) in subjects in which the T wave could not be identified. *Table A.6* and *Table A.5* display respectively day and night beat-to-beat labeling results for subjects in which it was not possible to identify T wave peaks.

Table 3.1 shows the distribution of beats (median, 25th and 75th percentile) associated to each tag, divided by day and night, considering all the 15 participating volunteers in which it was possible to identify the T wave peak.

Tag	**Distribution – Day**	**Distribution - Night**
Tag 0	*14.86 (4.07 ; 21.37) %*	*19.79 (6.90 ; 47.68) %*
Tag 1	*2.93 (1.41 ; 5.48) %*	*0 (0 ; 0) %*
Tag 2	*34.84 (28.08 ; 41.10) %*	*7.71 (5.75 ; 10.63) %*
Tag 3	*0.52 (0.03 ; 0.60) %*	*0 (0 ; 0.02) %*
Tag 4	*0.02 (0 ; 0.13) %*	*0 (0 ; 0) %*
Tag 5	*11.54 (7.05 ; 21.47) %*	*1.27 (0.81 ; 6.96) %*
Tag 6	*0 (0 ; 0.01) %*	*0 (0 ; 0) %*
Tag 7	*0.27 (0.13 ; 0.57) %*	*0.01 (0.01 ; 0.04) %*
Tag 8	*9.49 (6.12 ; 12.06) %*	*8.96 (1.24 ; 17.70) %*
Tag 9	*19.77 (12.28 ; 30.93) %*	*50.12 (29.98 ; 65.69) %*
Selected Tags	*51.82 (43.26 ; 56.98) %*	*82.51 (69.08 ; 92.14) %*

Table 3.1: Distribution results (median, 25th and 75th percentile) for each tag divided between day and night of subjects in which is possible to identify T peaks. For the further analysis we consider heartbeats corresponding to tag 0 (perfect heartbeat – early and late systole), tag 5 (only early systole), tag 7 (early and late systole, except for RE) and tag 9 (only early systole)

In general, less perfect beats (tags 0 and 9) were observed during day-time than during night-time.
Regarding tags 5 and 7, during day-time, they show a larger number of heartbeats.
Heartbeats associated with tag 1 (at least one of two consecutive R_iR_{i+1} intervals are outliers) were present only during day-time.

Beats labelled with tag 2 are the majority during the day, as a result of the non identification of the SCs by the SCG template matching algorithm in the considered time window.

Also tag 8 (MC was identified after R peak: data from early and late systolic phases were not reliable) was associated with several beats (around 10%) both during day and night.

Table 3.2 shows the distribution results (median, 25th and 75th percentile) associated to each tag, divided by day and night, considering all the 7 participating volunteers in which it was not possible to identify the T wave peaks.

Tag	**Distribution – Day**	**Distribution - Night**
Tag 0	*1.26 (0.89 ; 3.85) %*	*7.92 (1.89 ; 28.62) %*
Tag 1	*22.99 (5.16 ; 36.47) %*	*0 (0 ; 0) %*
Tag 2	*40.26 (17.72 ; 48.12) %*	*10.74 (6,05 ;17.43) %*
Tag 3	*2.10 (0.34 ; 3.16) %*	*0 (0 ; 0.17) %*
Tag 4	*0.27 (0.03 ; 1.38) %*	*0.01 (0 ; 0.05) %*
Tag 5	*30.51 (22.39 ; 34.73) %*	*54.9 (46.57 ; 73.49) %*
Tag 6	*0,01 (0 ; 0.1) %*	*0 (0 ; 0.04) %*
Tag 7	*N/A*	*N/A*
Tag 8	*5.31 (1.9 ; 11.18) %*	*13.70 (5.78 ; 27.70) %*
Tag 9	*N/A*	*N/A*
Selected Tags	*33.23 (26.24 ; 41.92) %*	*79.48 (56.79 ; 81.41) %*

Table 3.2: Distribution results (median, 25th and 75th percentile) for each tag divided between day and night of subjects in which is not possible to identify T peaks. For the further analysis we consider heartbeats corresponding to tag 0 (perfect heartbeat – early and late systole), tag 5 (only early systole), tag 7 (early and late systole, except for RE) and tag 9 (only early systole). Information about tags 7 and 9 are not available

The previously made considerations also apply in this case.

The tags labelled as 0, 5, 7 and 9 present in subsequent beats were considered for each participating volunteer to evaluate the maximum and median duration potentially analyzable in terms of beat-to-beat variability. Results are displayed in *Table A.7*.

The number of analyzable successive heartbeats was very dependent on the subject, but showed in general a very low median value (<= 2) during the day and similar in the night (only 4/22 had >20 beats during the night). However, considering the maximum strip of good beats, in 18/22 subjects during the day and in 19/22 during the night, at least 60 consecutive beats could be identified.

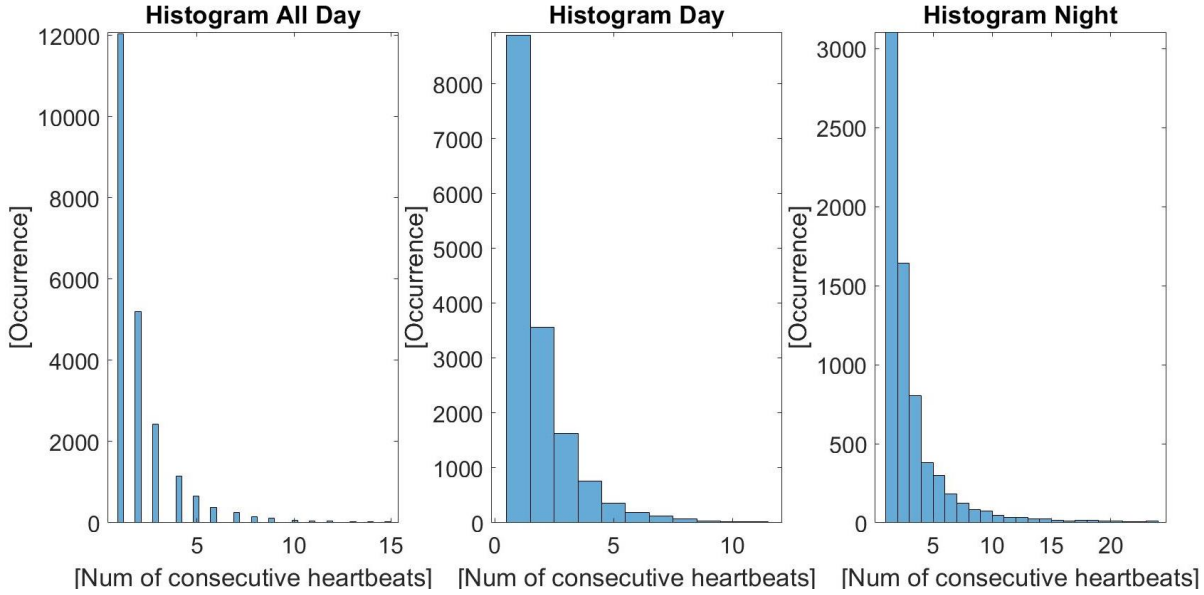

Figure 3.3: Consecutive heartbeats labelled as tag 0, 5, 7 and 9 identified into 24 hours (left panel), day-time (central panel) and night-time (right panel). The x-axis represents the number of consecutive heartbeats, while the y-axis represents the occurrence (num of times)

3.2 Visual Analysis – Day vs Night

Only beats associated with tags 0,5,7 and 9 were considered, and for each the fiducial points and the amplitude, temporal and slope parameters were extracted. For each parameter, a visual analysis was conducted by plotting the respective histogram for day and night.

Based on such visual analysis, the following parameters (13 out of 26 parameters) were selected, excluding those for which the sampling rate of the SCG prevented the extraction of meaningful distributions:

- AO_iAO_{i+1} intervals;
- ΔA(IVC-AO);
- ΔA(IVC-MC);
- ΔA(AO-RE);
- ΔA(AO-minAORE);
- ΔA(RE-minAORE);
- ΔA(AO-AC);
- ΔA(AC-minAC);
- LVET;
- PEP;
- QT intervals;
- R_iR_{i+1} intervals;
- SLOPE(IVC-AO);

For each parameter, the cumulative histograms among all subjects were computed with the respective median, 2,5th, 25th, 75th and 97.5th percentiles, in order to identify a normality range, separately for day and night.

Since the time duration of the period in which the subject was awake (i.e. day) was larger than the duration of the sleeping time (i.e. night), the day-time's histograms have y-values (Occurrence) much greater than those of the night.

Amplitude and temporal parameters (except for R_iR_{i+1}, AO_iAO_{i+1}, QT and QTc) were also represented as normalized (as explained in *Section 2.2.6.a*).

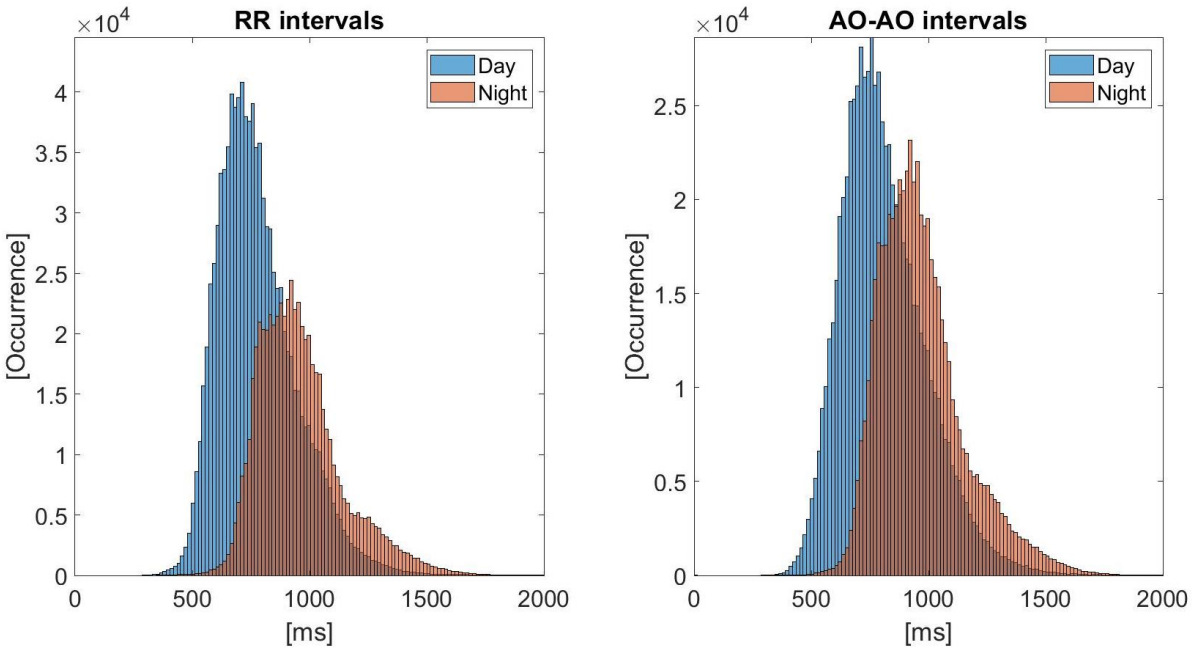

Figure 3.4: Left panel: cumulative distribution of R_iR_{i+1} intervals ; Right panel: cumulative distribution of AO_iAO_{i+1} intervals. The x-axis represents the temporal distance [ms] while the y-axis represents the occurrence (number of times) the that specific value takes place

Parameter	**Day**	**Night**	**24 hours**
R_iR_{i+1} Not Norm	*751.95*	*931.64 **	*822.27*
$(25^{th} – 75^{th})$	*(657.23; 872.07)*	*(829.10; 1048.80)*	*(707.03 ; 960.94)*
$(2.5^{th} – 97.5^{th})$	*(523.40 ; 1163.10)*	*(693.40 ; 1410.20)*	*(542 ; 1309.60)*
AO_iAO_{i+1} Not Norm	*785.16*	*941.41**	*860.35*
$(25^{th} – 75^{th})$	*(682.62 ; 916.02)*	*(839.80 ; 1062.50)*	*(742.19 ; 994.14)*
$(2.5^{th} – 97.5^{th})$	*(524.40 ; 1219.70)*	*(698.20 ; 1430.70)*	*(551.80 ; 1345.70)*

Table 3.3: Cumulative results of R_iR_{i+1} and AO_iAO_{i+1} intervals.. Not normalized results (median : first row, 25^{th}-75^{th} percentiles: second row; $2.5^{th} – 97.5^{th}$ percentile: third row) are reported for day-time, night-time and 24 hours. The existence of a significant difference between day and night distribution is highlighted by an asterisk

The distributions show different values between day and night (significant difference between day and night in both parameters) hence with values slightly different from those obtained by the gold standard R_iR_{i+1}.

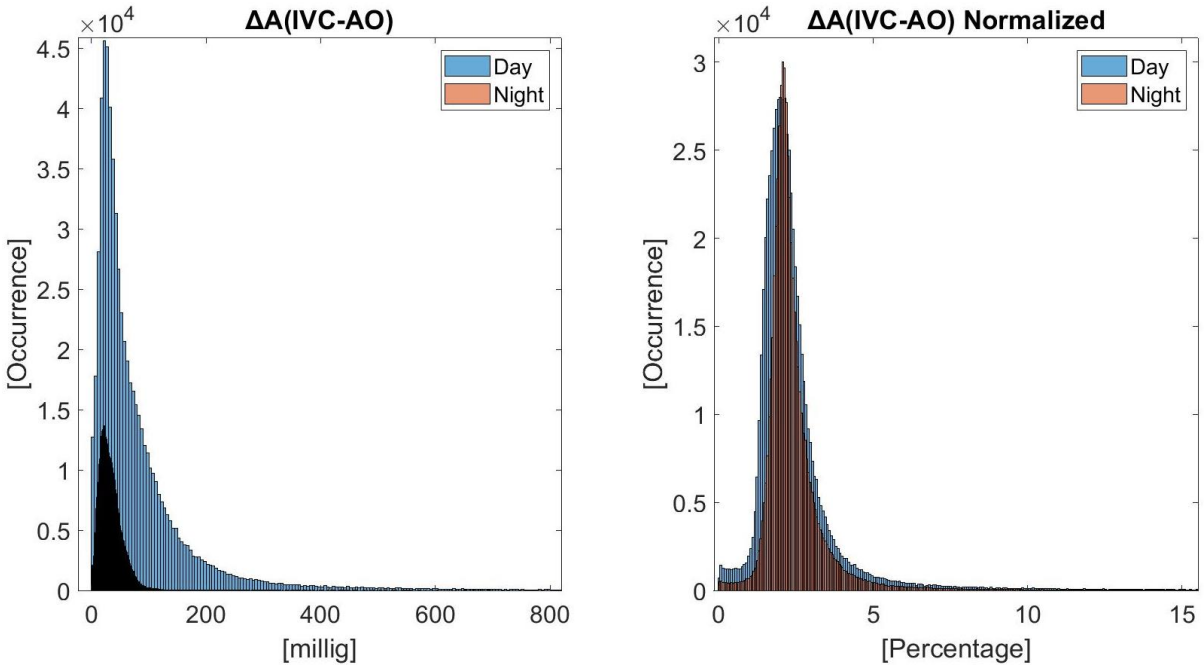

Figure 3.5: Cumulative distribution of ΔA(IVC-AO). The left panel displays the non normalized distribution, while the right panel shows the normalized distribution (normalized over the absolute value of IVC amplitude). The x-axis represents the amplitude [millig] while the y-axis represents the occurrence (number of times) the that specific value takes place

ΔA(IVC-AO)	**Day**	**Night**	**24 hours**
Not normalized	*65.31*	*30.51 **	*36.95*
(25th – 75th)	*(30.67 ; 127.01)*	*(19.00 ; 45.11)*	*(22.15 ; 63.37)*
(2.5th – 97.5th)	*(6.13 ; 378.10)*	*(5.67 ; 79.68)*	*(5.88 ; 269.41)*
Normalized by IVC amplitude	*2.14*	*2.2 **	*2.17*
(25th – 75th)	*(1.74 ; 2.69)*	*(1.93 ; 2.63)*	*(1.84 ; 2.66)*
(2.5th – 97.5th)	*(0.87 ; 8.90)*	*(1.03 ; 7.29)*	*(1.25 ; 5.79)*
Amp IVC [millig]	*-26.21*	*-13.49*	*-18.12*
(25th – 75th)	*(-51.81 ; -13.21)*	*(-20.07 ; -8.23)*	*(-33.96 ; -10.19)*
Amp AO [millig]	*35.34*	*15.88*	*23.32*
(25th – 75th)	*(16.29 ; 71.95)*	*(10.13 ; 23.9)*	*(12.91 ; 50)*

Table 3.4: Cumulative results of ΔA(IVC-AO). The first row displays not normalized results (median, 25th-75th percentiles and 2.5th-97.5th percentiles) reported for day-time, night-time and 24 hours; while the second row displays normalized results (median, 25th-75th percentiles and 2.5th-97.5th percentiles) reported for day-time, night-time and 24 hours. The existence of a significant difference between day and night distribution is highlighted by an asterisk

As regards the ΔA(IVC-AO), a difference between day and night was visible while not normalized, while visually disappeared when normalization was applied. Despite this behavior, normalized and not-normalized ΔA(IVC-AO) showed a significant difference between day and night. Considering the absolute values of the respective fiducial points, they both reduced in amplitude during the night compared to day.

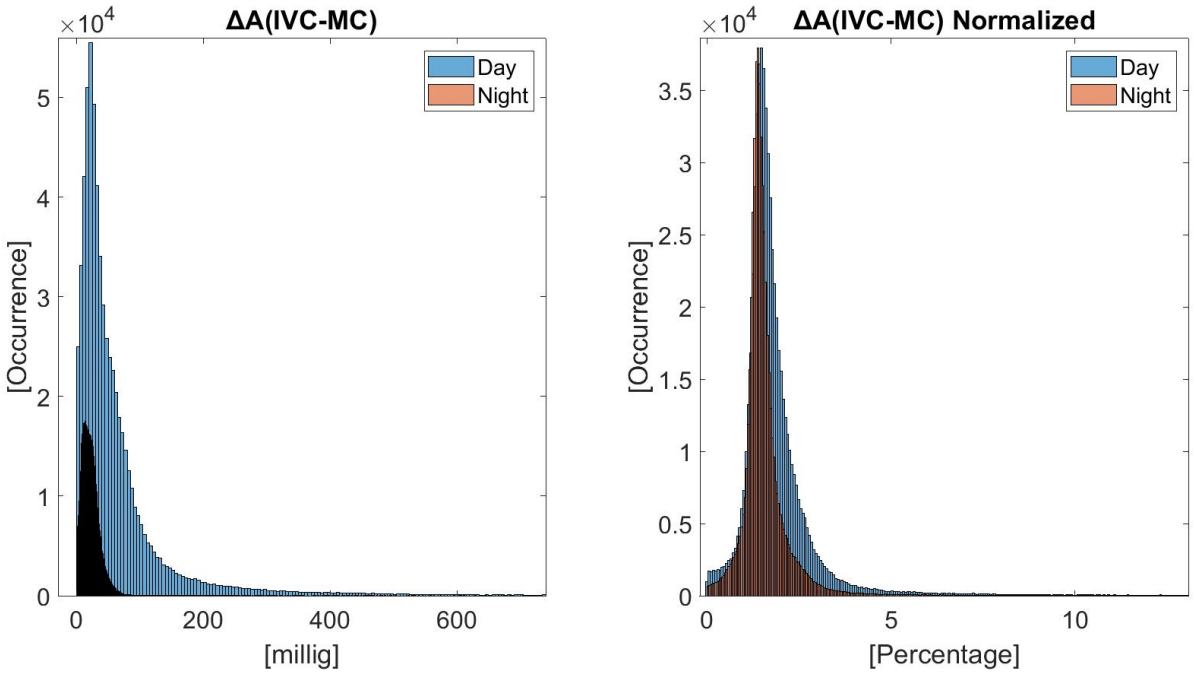

Figure 3.6: Cumulative distribution of ΔA(IVC-MC). The left panel displays the non normalized distribution, while the right panel shows the normalized distribution (normalized over the absolute value of IVC amplitude). The x-axis represents the amplitude [millig] while the y-axis represents the occurrence (number of times) the that specific value takes place

ΔA(IVC-MC)	**Day**	**Night**	**24 hours**
Not normalized	*46.19*	*20.38 **	*26.51*
(25th – 75th)	*(23.75 ; 85.13)*	*(11.82 ; 29.91)*	*(15.30 ; 47.35)*
(2.5th – 97.5th)	*(3.42 ; 356.38)*	*(2.41 ; 55.81)*	*(2.84 ; 242.74)*
Normalized by IVC amplitude	*1.63*	*1.44 **	*1.53*
(25th – 75th)	*(1.37 ; 2.08)*	*(1.27 ; 1.70)*	*(1.31 ; 1.90)*
(2.5th – 97.5th)	*(0.52 ; 6.30)*	*(0.57 ; 3.51)*	*(0.55 ; 4.90)*
Amp IVC [millig]	*-26.21*	*-13.49*	*-18.12*
(25th – 75th)	*(-51.81 ; -13.21)*	*(-20.07 ; -8.23)*	*(-33.96 ; -10.19)*
Amp MC [millig]	*15.66*	*6.36*	*9.39*
(25th – 75th)	*(7.44 ; 33.42)*	*(3.5 ; 9.59)*	*(4.92 ; 20.47)*

Table 3.5: Cumulative results of ΔA(IVC-MC). The first row displays not normalized results (median, 25th-75th percentiles and 2.5th-97.5th percentiles) reported for day-time, night-time and 24 hours; while the second row displays normalized results (median, 25th-75th percentiles and 2.5th-97.5th percentiles) reported for day-time, night-time and 24 hours. The existence of a significant difference between day and night distribution is highlighted by an asterisk

As regards the ΔA(IVC-MC), a significant difference between day and night was visible while not normalized and normalized (significant difference of the distributions between day and night). Considering the absolute values of the respective fiducial points, they both reduced in amplitude during the night compared to day.

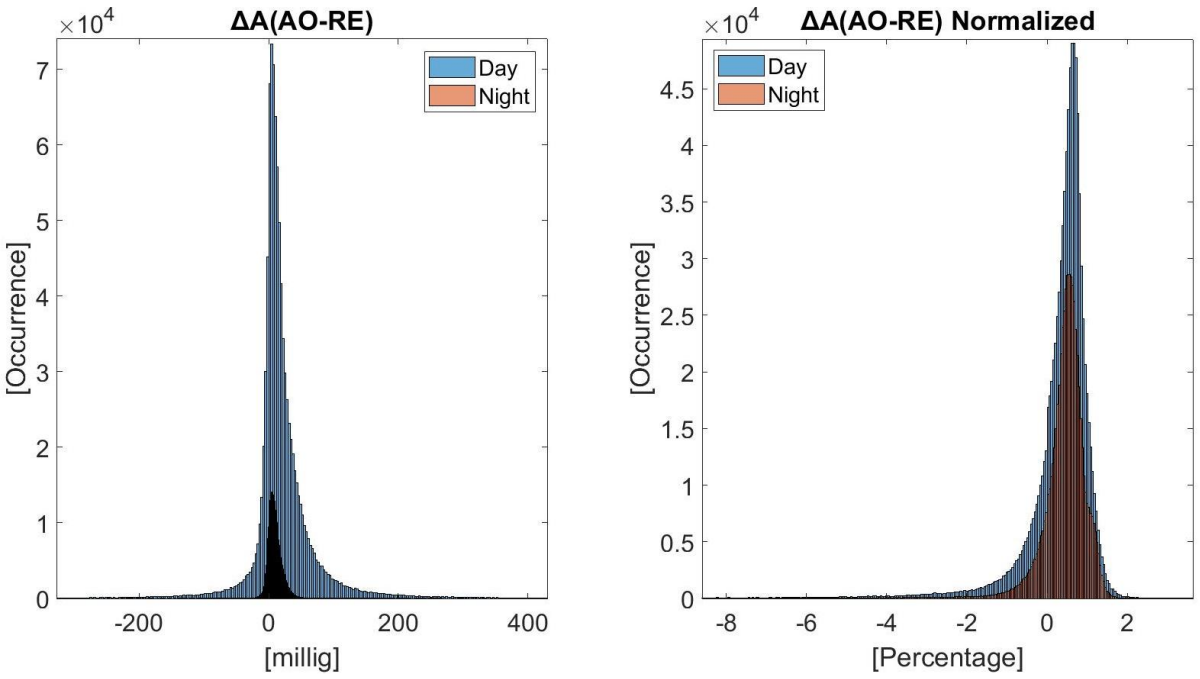

Figure 3.7: Cumulative distribution of ΔA(AO-RE). The left panel displays the no normalized distribution, while the right panel shows the normalized distribution (normalized over the absolute value of AO amplitude). The x-axis represents the amplitude [millig] while the y-axis represents the occurrence (number of times) the that specific value takes place

ΔA(AO-RE)	**Day**	**Night**	**24 hours**
Not normalized	*12.90*	*8.14 **	*10.26*
(25th – 75th)	*(2.24 ; 32.84)*	*(2.65 ; 15.15)*	*(2.46 ; 23.15)*
(2.5th – 97.5th)	*(-70.2 ; 153.6)*	*(-7.04 ; 35.7)*	*(-41.2 ; 117.06)*
Normalized by AO amplitude	*0.52*	*0.51*	*0.51*
(25th – 75th)	*(0.13 ; 0.75)*	*(0.23 ; 0.74)*	*(0.18 ; 0.75)*
(2.5th – 97.5th)	*(-2.9 ; 1.28)*	*(-1.19 ; 1.25)*	*(-2.32 ; 1.27)*
Amp AO [millig]	*35.34*	*15.88*	*23.32*
(25th – 75th)	*(16.29 ; 71.95)*	*(10.13 ; 23.9)*	*(12.91 ; 50)*
Amp RE [millig]	*15.46*	*7.76*	*10.97*
(25th – 75th)	*(6.2 ; 33.73)*	*(3.84 ; 12.32)*	*(4.99 ; 22.74)*

Table 3.6: Cumulative results of ΔA(AO-RE). The first row displays not normalized results (median, 25th-75th percentiles and 2.5th-97.5th percentiles) reported for day-time, night-time and 24 hours; while the second row displays normalized results (median, 25th-75th percentiles and 2.5th-97.5th percentiles) reported for day-time, night-time and 24 hours. The existence of a significant difference between day and night distribution is highlighted by an asterisk

As regards the ΔA(AO-RE), a significant difference between day and night was visible while not normalized, while disappeared when normalization was applied. Considering the absolute values of the respective fiducial points, they both reduced in amplitude during the night compared to day.

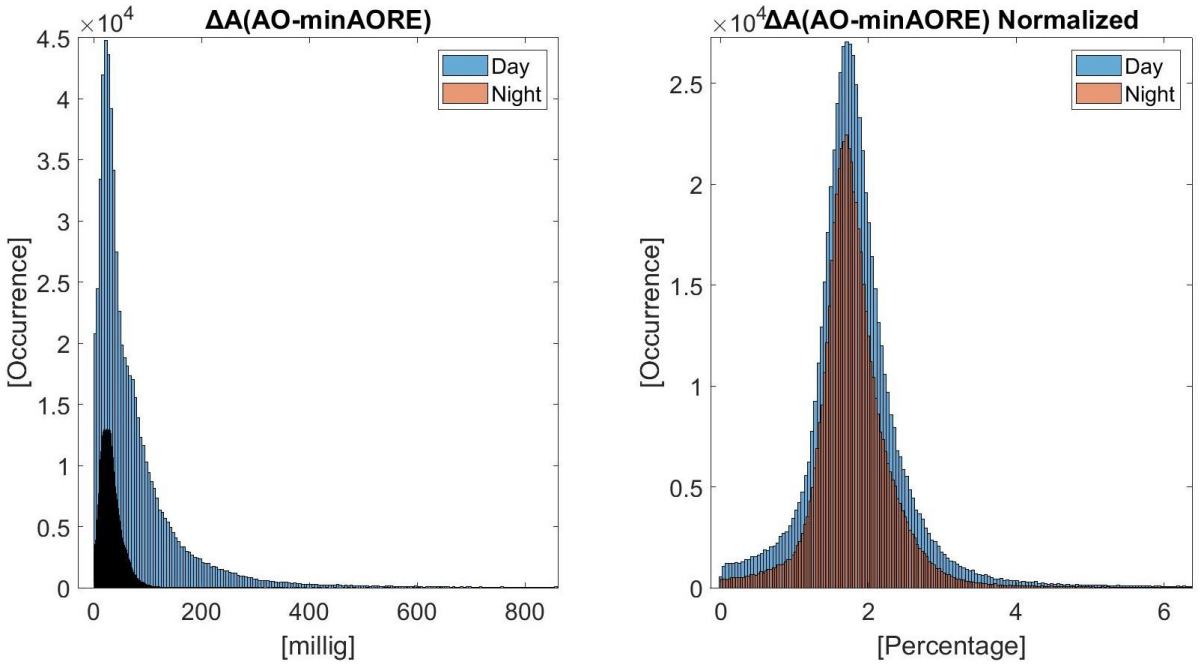

Table 3.7: Cumulative results of ΔA(AO-minAORE). The first row displays not normalized results (median, 25th-75th percentiles and 2.5th-97.5th percentiles) reported for day-time, night-time and 24 hours; while the second row displays normalized results (median, 25th-75th percentiles and 2.5th-97.5th percentiles) reported for day-time, night-time and 24 hours. The existence of a significant difference between day and night distribution is highlighted by an asterisk

As regards the ΔA(AO-minAORE), a significant difference between day and night was visible while not normalized, while disappeared when normalization was applied. Considering the absolute values of the respective fiducial points, they both reduced in amplitude during the night compared to day.

ΔA(AO-minAORE)	**Day**	**Night**	**24 hours**
Not normalized	*46.27*	*28.86 **	*34.58*
(25th – 75th)	*(24.16 ; 93.52)*	*(18.05 ; 41.91)*	*(20.57 ; 62.06)*
(2.5th – 97.5th)	*(1.33 ; 296.68)*	*(0.95 ; 58,48)*	*(1.13 ; 205.39)*
Normalized by AO amplitude	*1.78*	*1,75*	*1.76*
(25th – 75th)	*(1.51 ; 2.10)*	*(1.53 ; 2.02)*	*(1.52 ; 2.06)*
(2.5th – 97.5th)	*(0.08 ; 6.59)*	*(0.07 ; 4.05)*	*(0.07 ; 5.31)*
Amp RE [millig]	*35.34*	*15.88*	*23.32*
(25th – 75th)	*(16.29 ; 71.95)*	*(10.13 ; 23.9)*	*(12.91 ; 50)*
Amp min AORE [millig]	*-24.37*	*-12.28*	*-16.24*
(25th – 75th)	*(-55.29 ; -10.91)*	*(-18.53 ; -7.27)*	*(-33.02 ; -8.69)*

Figure 3.8: Cumulative distribution of ΔA(AO-minAORE). The left panel displays the no normalized distribution, while the right panel shows the normalized distribution (normalized over the absolute value of AO amplitude). The x-axis represents the amplitude [millig] while the y-axis represents the occurrence (number of times) the that specific value takes place

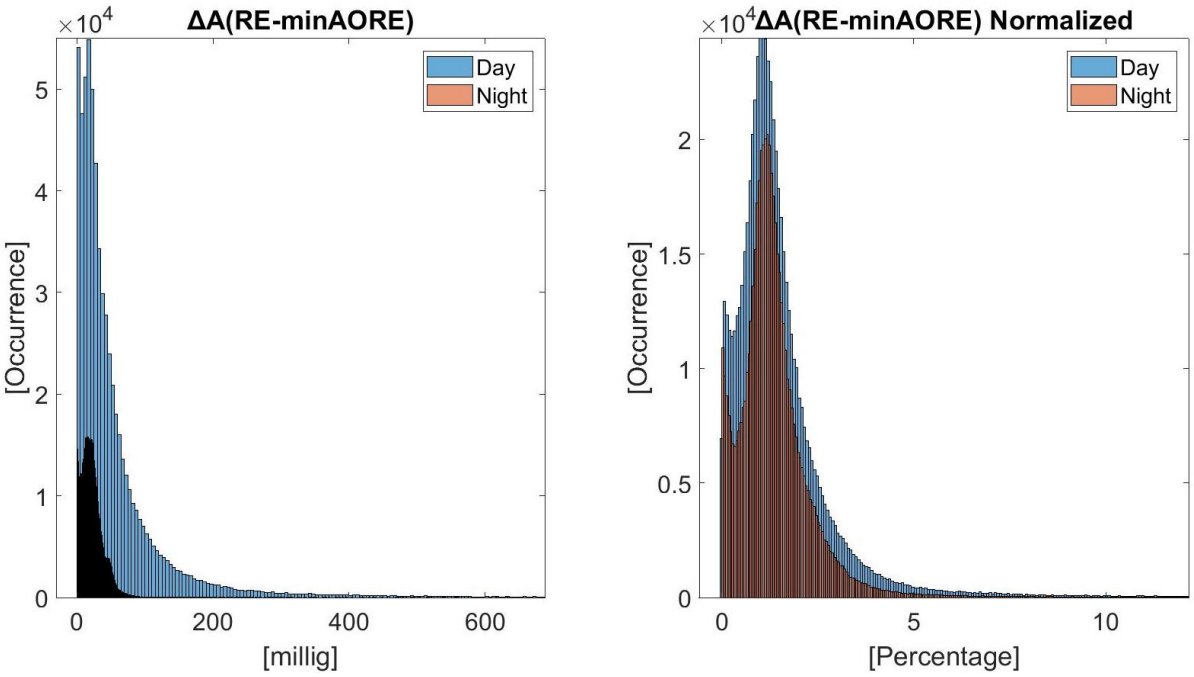

Figure 3.9: Cumulative distribution of ΔA(RE-minAORE).. The left panel displays the no normalized distribution, while the right panel shows the normalized distribution (normalized over the absolute value of AO amplitude). The x-axis represents the amplitude [millig] while the y-axis represents the occurrence (number of times) the that specific value takes place

As regards the ΔA(RE-minAORE), a significant difference between day and night was visible while not normalized, while disappeared when normalization was applied. Considering the absolute values of the respective fiducial points, they both reduced in amplitude during the night compared to day.

ΔA(RE-minAORE)	**Day**	**Night**	**24 hours**
Not normalized	*32.12*	*19.80 **	*24.13*
(25th – 75th)	*(15.46 ; 65.91)*	*(10.83 ; 30.02)*	*(12.75 ; 44.20)*
(2.5th – 97.5th)	*(3.89 ; 340.13)*	*(4.11 ; 79,72)*	*(3.99 ; 253.2)*
Normalized by AO amplitude	*1.24*	*1.23*	*1.23*
(25th – 75th)	*(0.78 ; 1.89)*	*(0.83 ; 1.72)*	*(0.81 ; 1.80)*
(2.5th – 97.5th)	*(0.52 ; 3.84)*	*(0.74 ; 3.04)*	*(0.60 ; 3.44)*
Amp AO [millig]	*15.46*	*7.76*	*10.97*
(25th – 75th)	*(6.2 ; 33.73)*	*(3.84 ; 12.32)*	*(4.99 ; 22.74)*
Amp min AORE [millig]	*-24.37*	*-12.28*	*-16.24*
(25th – 75th)	*(-55.29 ; -10.91)*	*(-18.53 ; -7.27)*	*(-33.02 ; -8.69)*

Table 3.8: Cumulative results of ΔA(RE-minAORE).. The first row displays not normalized results (median, 25th-75th percentiles and 2.5th-97.5th percentiles) reported for day-time, night-time and 24 hours; while the second row displays normalized results (median, 25th-75th percentiles and 2.5th-97.5th percentiles) reported for day-time, night-time and 24 hours. The existence of a significant difference between day and night distribution is highlighted by an asterisk

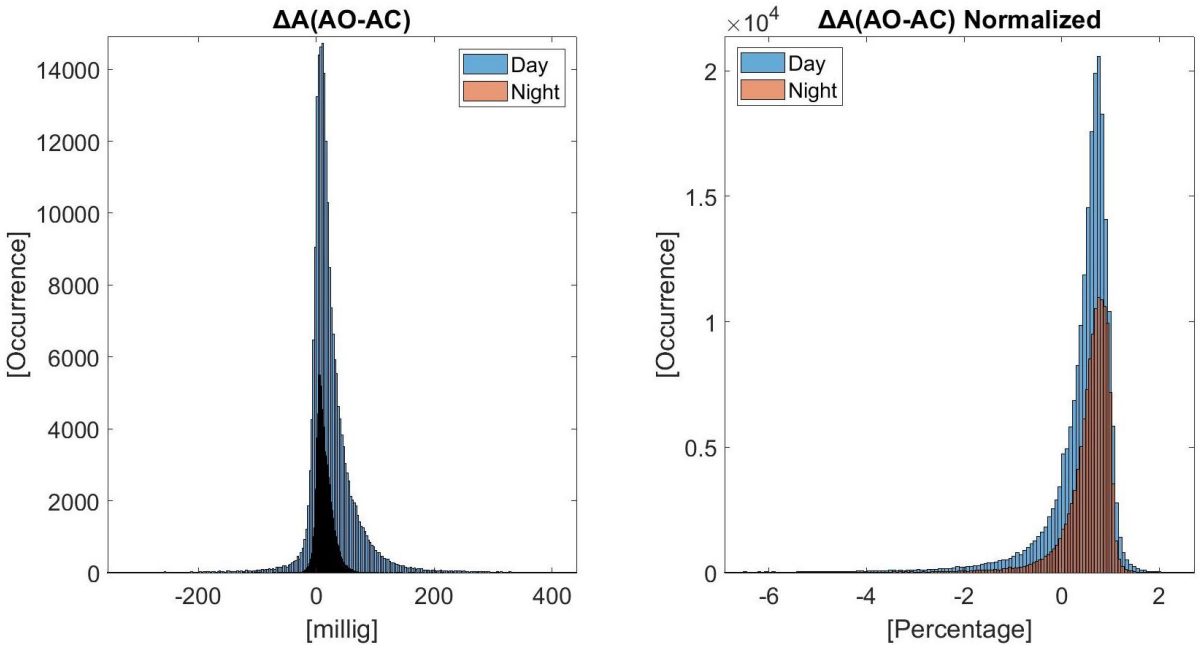

Figure 3.10: *Cumulative distribution of ΔA(AO-AC). The left panel displays the no normalized distribution, while the right panel shows the normalized distribution (normalized over the absolute value of AO amplitude). The x-axis represents the amplitude [millig]] while the y-axis represents the occurrence (number of times) the that specific value takes place*

As regards the ΔA(AO-AC), a significant difference between day and night was visible while not normalized, while disappeared when normalization was applied. Considering the absolute values of the respective fiducial points, they both reduced in amplitude during the night compared to day.

ΔA(AO-AC)	**Day**	**Night**	**24 hours**
Not normalized	*15.52*	*11.14 **	*13.42*
(25^{th} – 75^{th})	*(4.31 ; 35.80)*	*(4.72 ; 20.92)*	*(4.52 ; 28.05)*
(2.5^{th} – 97.5^{th})	*(-34.96 ; 130.1)*	*(-7.08 ; 45.54)*	*(19.07 ; 105.5)*
Normalized by AO amplitude	*0.61*	*0.67*	*0.63*
(25^{th} – 75^{th})	*(0.26 ; 0.80)*	*(0.41 ; 0.80)*	*(0.32 ; 0.83)*
(2.5^{th} – 97.5^{th})	*(-2.48 ; 1.12)*	*(-1.18 ; 1.07)*	*(-1.99 ; 1.10)*
Amp AO [millig]	*35.34*	*15.88*	*23.32*
(25^{th} – 75^{th})	*(16.29 ; 71.95)*	*(10.13 ; 23.9)*	*(12.91 ; 50)*
Amp AC [millig]	*8.51*	*5.18*	*6.43*
(25^{th} – 75^{th})	*(4.7 ; 16.66)*	*(2.86 ; 8.26)*	*(3.43 ; 10.67)*

Table 3.9: Cumulative results of ΔA(AO-AC). The first row displays not normalized results (median, 25^{th}-75^{th} percentiles and 2.5^{th}-97.5^{th} percentiles) reported for day-time, night-time and 24 hours; while the second row displays normalized results (median, 25^{th}-75^{th} percentiles and 2.5^{th}-97.5^{th} percentiles) reported for day-time, night-time and 24 hours The existence of a significant difference between day and night distribution is highlighted by an asterisk

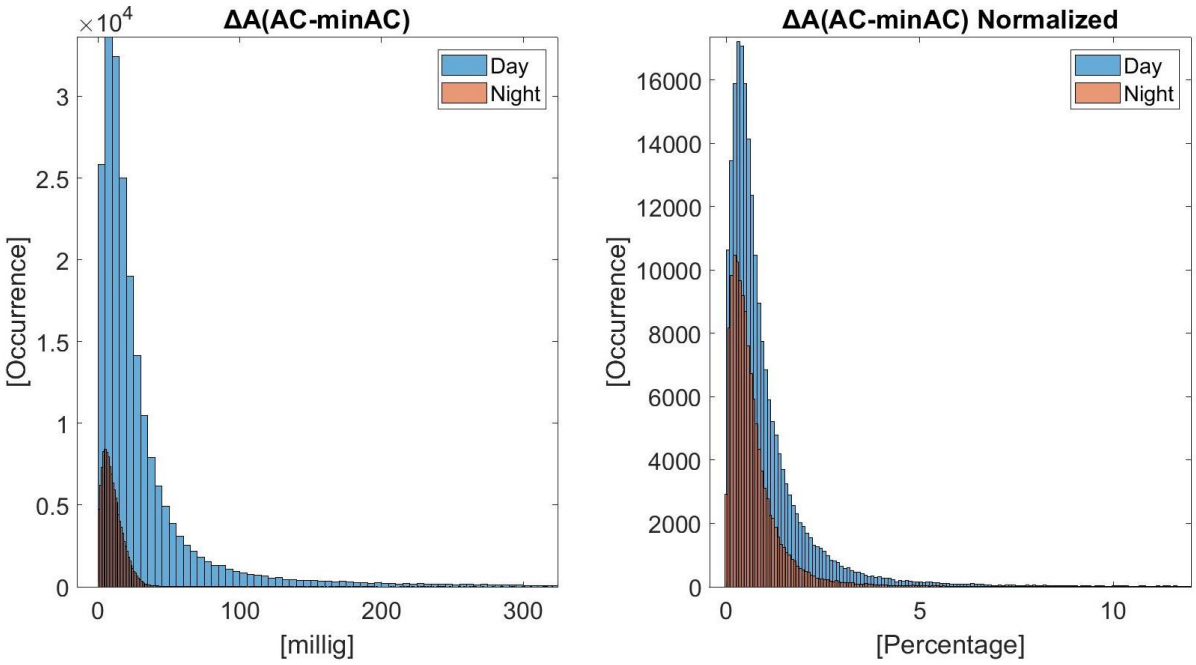

Figure 3.11: Cumulative distribution ΔA(AC-minAC).. The left panel displays the no normalized distribution, while the right panel shows the normalized distribution (normalized over the absolute value of AO amplitude). The x-axis represents the amplitude [millig] while the y-axis represents the occurrence (number of times) the that specific value takes place

As regards the ΔA(AC-minAC), a significant difference between day and night was visible while not normalized, while visually disappeared when normalization was applied even if it was characterized by a significant difference between day and night. Considering the absolute values of the respective fiducial points, they both reduced in amplitude during the night compared to day

ΔA(AC-minAC)	**Day**	**Night**	**24 hours**
Not normalized	*17.89*	*8.84 **	*13.16*
(25th – 75th)	*(9.15 ; 35.27)*	*(4.75 ; 14.42)*	*(6.74 ; 24.64)*
(2.5th – 97.5th)	*(1.27 ; 239.09)*	*(0.75 ; 28.92)*	*(0.98 ; 168.99)*
Normalized by AO amplitude	*0.64*	*0.50 **	*0.58*
(25th – 75th)	*(0.34 ; 1.23)*	*(0.26 ; 0.88)*	*(0.30 ; 1.08)*
(2.5th – 97.5th)	*(0.05 ; 5.45)*	*(0.04 ; 3.04)*	*(0.04 ; 4.55)*
Amp AC [millig]	*8.51*	*5.18*	*6.43*
(25th – 75th)	*(4.7 ; 16.66)*	*(2.86 ; 8.26)*	*(3.43 ; 10.67)*
Amp min AC [millig]	*-5.68*	*-3.07*	*-3.88*
(25th – 75th)	*(-12.99 ; -2.77)*	*(-4.94 ; -1.57)*	*(-7.06 ; -1.94)*

Table 3.10: Cumulative results of ΔA(AC-minAC). The first row displays not normalized results (median, 25th-75th percentiles and 2.5th-97.5th percentiles) reported for day-time, night-time and 24 hours; while the second row displays normalized results (median, 25th-75th percentiles and 2.5th-97.5th percentiles) reported for day-time, night-time and 24 hours. The existence of a significant difference between day and night distribution is highlighted by an asterisk

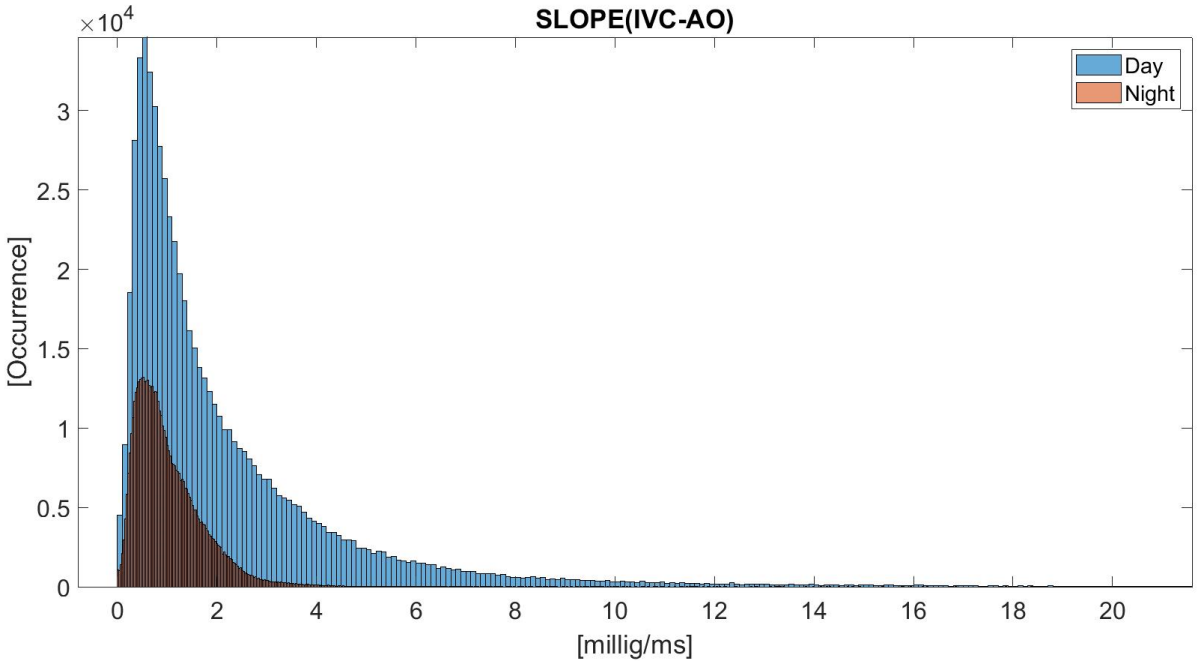

Figure 3.12: Cumulative distribution of SLOPE(IVC-AO). The x-axis represents the value of the slope [millig/ms] while the y-axis represents the occurrence (number of times) the that specific value takes place

SLOPE(IVC-AO)	**Day**	**Night**	**24 hours**
Not Normalized	*1.84*	*0.87 **	*1.06*
(25^{th} – 75^{th})	*(0.81 ; 3.81)*	*(0.52 ; 1.43)*	*(0.61 ; 1.93)*
(2.5^{th} – 97.5^{th})	*(0.22 ; 9.62)*	*(0.18 ; 2.75)*	*(0.2 ; 7.27)*

Table 3.11: Cumulative results of SLOPE(IVC-AO). Not normalized results (median: first row; 25^{th}- 75^{th} percentiles: second row; 2.5^{th} – 97.5^{th} percentiles: third row) are reported for day-time, night-time and 24 hours. The existence of a significant difference between day and night distribution is highlighted by an asterisk

The distribution of the SLOPE(VC-AO) shows different values between day and night (significant difference between day and night in both parameters).

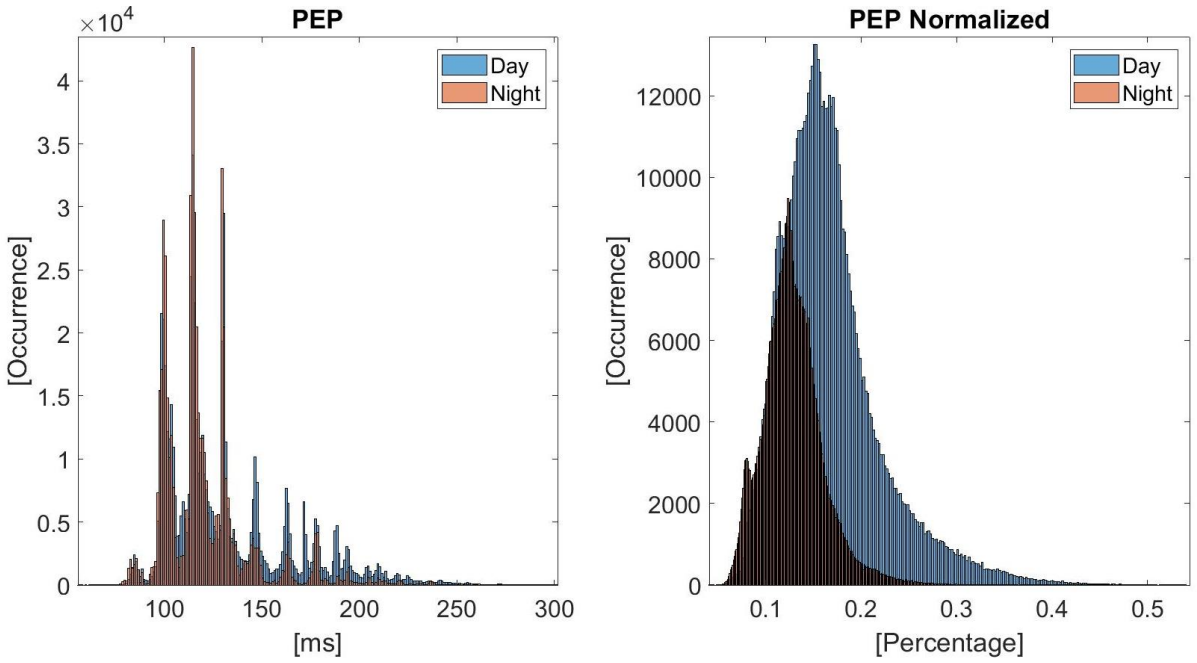

Figure 3.13: Cumulative distribution of the PEP. The left panel displays the no normalized distribution, while the right panel shows the normalized distribution (normalized over R_iR_{i+1}). The x-axis represents the temporal distance [mw] while the y-axis represents the occurrence (number of times) the that specific value takes place

PEP	**Day**	**Night**	**24 hours**
Not normalized	*117.30*	*115.35 **	*117.31*
(25th – 75th)	*(103.63 ; 141.72)*	*(103.63 ; 130)*	*(104.61 ; 133.91)*
(2.5th – 97.5th)	*(96.80 ; 213.01)*	*(93.87 ; 187.62)*	*(94.84 ; 206.17)*
Normalized by			
R_iR_{i+1}	*0.16*	*0.13 **	*0.14*
(25th – 75th)	*(0.13 ; 0.19)*	*(0.11 ; 0.15)*	*(0.12 ; 0.17)*
(2.5th – 97.5th)	*(0.09 ; 0.31)*	*(0.08 ; 0.28)*	*(0.08 ; 0.20)*

Table 3.12: Cumulative results of PEP. The first row displays not normalized results (median, 25th and 75th percentiles) reported for day-time, night-time and 24 hours; while the second row displays normalized results (median, 25th and 75th percentiles) reported for day-time, night-time and 24 hours. The existence of a significant difference between day and night distribution is highlighted by an asterisk

Not-normalized PEP distribution didn't have a visible difference between day and night, even if it resulted as significant. However, when normalization was applied a significant difference between day and night distributions appeared.

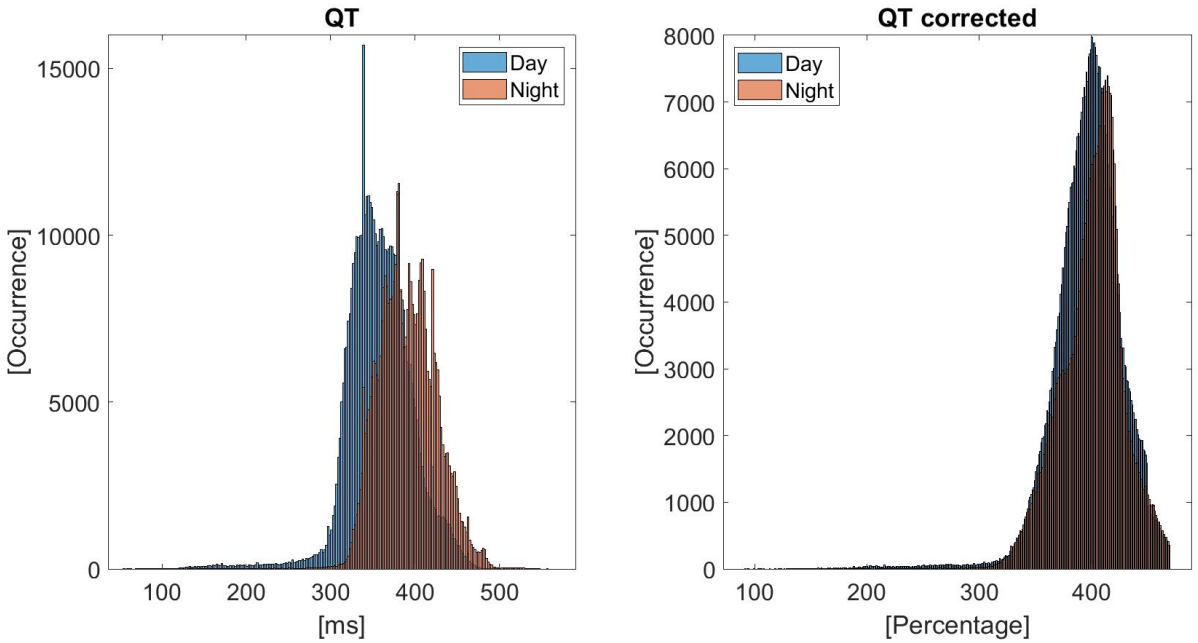

Figure 3.14: Cumulative distribution of QT. The x-axis represents the temporal distance [ms] while the y-axis represents the occurrence (number of times) the that specific value takes place

QT	Day	Night	24 hours
Not Normalized	*358.52*	*394.65 **	*372.19*
(25th – 75th)	*(338.98 ; 380.98)*	*(371.21 ; 417.11)*	*(346.80 ; 399.53)*
(2.5th – 97.5th)	*(286.25 ; 436.64)*	*(333.13 ; 460.08)*	*304.81 ; 450.31)*
Normalized			
(QTc)	*397.71*	*404.02*	*372.19*
(25th – 75th)	*(378.81 ; 414.94)*	*(384.13 ; 418.32)*	*(381.94 – 417.04)*
(2.5th – 97.5th)	*(336.66 ; 450.82)*	*(341.93 ; 454.16)*	*339.58 ; 452.53)*

Table 3.13: Cumulative results of QT. Not normalized results (median, 25th and 75th percentiles) are reported for day-time, night-time and 24 hours. The existence of a significant difference between day and night distribution is highlighted by an asterisk

Not-normalized QT distributions showed a visible difference between day and night which resulted as significant. However, when normalization (corrected QT) was applied the visible and significant difference between day and night distributions disappeared.

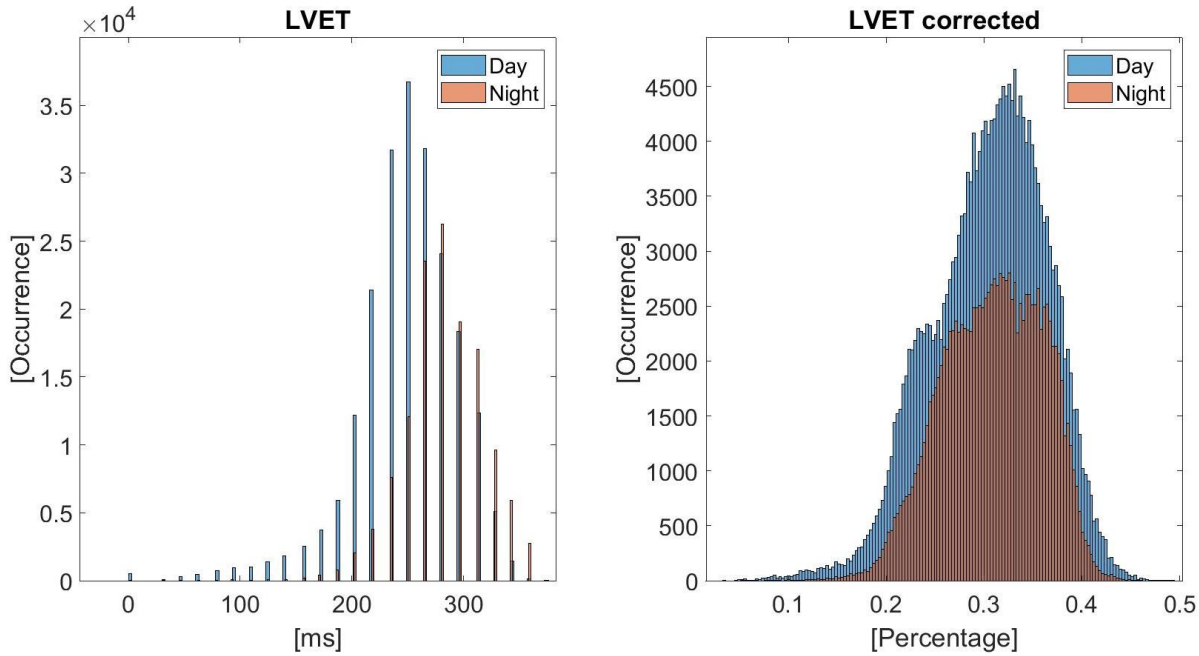

Figure 3.15: *Cumulative distribution of LVET. The left panel displays the no normalized distribution, while the right panel shows the normalized distribution (normalized over R_iR_{i+1}). The x-axis represents the temporal distance [mw] while the y-axis represents the occurrence (number of times) the that specific value takes place*

LVET	**Day**	**Night**	**24 hours**
Not normalized	*265.63*	*296.88 **	*265.63*
(25th – 75th)	*(234.38 ; 281.25)*	*(265.63 ; 312.50)*	*(234.75 ; 296.88)*
(2.5th – 97.5th)	*(125 ; 328.13)*	*(203.13 ; 343.75)*	*(156.25 ; 343.75)*
Normalized by			
R_iR_{i+1}	*0.31*	*0.31*	*0.31*
(25th – 75th)	*(0.27 ; 0.35)*	*(0.27 ; 0.35)*	*(0.27 ; 0.35)*
(2.5th – 97.5th)	*(0.18 ; 0.41)*	*(0.21 ; 0.39)*	*(0.19 ; 0.40)*

Table 3.14: Cumulative results of the LVET. The first row displays not normalized results (median, 25th and 75th percentiles) reported for day-time, night-time and 24 hours; while the second row displays normalized results (median, 25th and 75th percentiles) reported for day-time, night-time and 24 hours. The existence of a significant difference between day and night distribution is highlighted by an asterisk

Not normalized LVET distributions showed a visible difference between day and night which resulted as significant. However, when normalization was applied the visible and significant difference between day and night distributions disappeared

3.3 Cosinor Analysis

The subsequent step was to apply the Cosinor analysis to evaluate if there is a circadian rhythm. For this step, we considered the slope parameters, not normalized amplitude parameters (they displayed a greater difference between day and night) and not normalized temporal parameters.
Two different Cosinor analyses were performed: the first one considering separately each participating volunteers, and the second one considering all the subjects together.

3.3.1 Separate analysis

Before applying Cosinor analysis, points were translated to ensure that all recordings start at 8 AM. This procedure aims to compare results of the Cosinor analysis -and in particular the acrophase - between all the participating volunteers.

For each healthy volunteer, the median template for each parameter was computed, considering a moving window lasting 5 minutes – without overlapping.
Outliers were removed if the current parameter's value was bigger than 30% of the average between the previous and next parameters' values.
Then, mesor, amplitude, acrophase (measured as radians and hours - minutes) and the ratio between amplitude and mesor were computed for each parameter of the each subject.
Finally, the median (25th and 75th percentile) for the mesor, amplitude, the ratio between amplitude and mesor and the acrophase [Hours:Minutes] was computed among subjects, and results are reported in *Table 3.15*.

Parameter	**Mesor**	**Amplitude**	$\frac{Amplitude}{Mesor}$ **[a.u.]**	**Acrophase [Hours:Minutes]**
ΔA(IVC-AO) *[millig]*	*46.33* *(35.41 ; 75.45)*	*16.43* *(8.11 ; 31.67)*	*0.34* *(0.23 ; 0.49)*	*15:20* *(13:32 ; 18:35)*
ΔA(IVC-MC) *[millig]*	*40.49* *(32.05 ; 61.53)*	*17.35* *(8.71 ; 29.46)*	*0.39* *(0.30 ; 0.52)*	*14:52* *(13:46 ; 17:45)*
ΔA(AO-RE) *[millig]*	*10.13* *(6.89 ; 19.82)*	*4.33* *(2.63 ; 8.42)*	*0.35* *(0.28 ; 0.51)*	*15:49* *(12:58 ; 17:22)*
ΔA(AO-AC) *[millig]*	*12.96* *(8.54 ; 26.39)*	*4.21* *(3.49 ; 10.73)*	*0.41* *(0.25 ; 0.81)*	*14:50* *(08:00 ; 19:29)*

ΔA(AO-minAORE) *[millig]*	*43.28* *(33.47 ; 75.79)*	*16.13* *(8.16 ; 30.42)*	*0.37* *(0.22 ; 0.47)*	*15:06* *(13:51 ; 18:27)*
ΔA(RE-minAORE) *[millig]*	*31.99* *(25.84 ; 50.47)*	*13.31* *(6.98; 21.99)*	*0.41* *(0.24 ; 0.56)*	*14:17* *(12:32 ; 17:12)*
ΔA(AC-minAC) *[millig]*	*30.74* *(19.83 ; 55.80)*	*20.93* *(8.37 ; 29.80)*	*0.62* *(0.38 ; 0.76)*	*15:20* *(13:01 ; 17:54)*
LVET *[ms]*	*233* *(199 ; 248)*	*310* *(197 ; 383)*	*0.12* *(0.08 ; 0.18)*	*04:38* *(03:06 ; 07:17)*
QT *[ms]*	*353* *(337 ; 373)*	*250* *(144 ; 335)*	*0.07* *(0.04 ; 0.10)*	*05:28* *(02:54 ; 06:42)*
PEP *[ms]*	*130* *(113 ; 137)*	*5.3* *(1.9 ; 9.9)*	*0.04* *(0.02 ; 0.07)*	*14:33* *(11:56 ; 17:39)*
R_iR_{i+1} *[ms]*	*763.13* *(730.38 ; 881.90)*	*115.71* *(53.60 ; 181.36)*	*0.15* *(0.07 ; 0.20)*	*04:13* *(02:55 ; 06:10)*
AO_iAO_{i+1} *[ms]*	*792.17* *(753.21 ; 889.34)*	*114.40* *(56.07 ; 177.29)*	*0.14* *(0.07 ; 0.18)*	*04:34* *(03:17 – 06:30)*
SLOPE(IVC-AO) *[millig/ms]*	*1138.88* *(898 ;1840.70)*	*427.94* *(178.87;803.58)*	*0.34* *(0.16 ; 0.45)*	*15:20* *(13:16 ; 17:40)*

Table 3.15: Cumulative results of Cosinor analysis: median, 25th and 75th percentiles. For each parameter (row), the first column displays the values of the mesor, the second column displays the values of the amplitude, the third column shows the ratio between amplitude and mesor and the fourth column shows the values of the acrophase expressed in hours-minutes [Hours: Minutes]

Two similar patterns can be identified among the analysed data. Temporal parameters R_iR_{i+1}, AO_iAO_{i+1}, QT and LVET intervals presented the acrophase early in the morning, in particular for R_iR_{i+1}, AO_iAO_{i+1}, LVET is around 4 AM. The other parameters presented the acrophase between 3 PM and 4 PM.

3.3.2 Cumulative analysis

In this case, points were translated to ensure that all recording started when the subject goes to bed. The beginning of the sleep period varies from subject to subject, with a median time at 0:45 AM (22 PM ; 2 AM).

For each parameter, data coming from all participating volunteer were merged to create one template. Then, the median template for each parameter was computed, considering a moving window lasting 5 minutes – without overlapping.
Again, outliers for each parameter were removed if the current parameter's value was bigger than 30% of the average between the previous and next parameters' values.
Then, mesor, amplitude, acrophase (measured as radians and hours - minutes) and the ratio between amplitude and mesor of each clinical parameter previously identified, were computed.

Table 3.16 displays the mesor, amplitude, the ratio between amplitude and mesor and the acrophase [Hours:Minutes] for each parameter.

Parameter	**Mesor**	**Amplitude**	$\frac{Amplitude}{Mesor}$ **[a.u.]**	**Acrophase [Hours:Minutes]**
ΔA(IVC-AO) *[millig]*	*40.37*	*12.40*	*0.31*	*14:09*
ΔA(IVC-MC) *[millig]*	*30.89*	*10.81*	*0.35*	*13:59*
ΔA(AO-RE) *[millig]*	*10.59*	*3.82*	*0.36*	*13:11*
ΔA(AO-AC) *[millig]*	*12.59*	*3.66*	*0.29*	*12:53*
ΔA(AO-minAORE) *[millig]*	*38.57*	*1.09*	*0.28*	*14:16*
ΔA(RE-minAORE) *[millig]*	*27.13*	*6.84*	*0.25*	*14:49*
ΔA(AC-minAC) *[millig]*	*15.11*	*5.61*	*0.37*	*14:16*
LVET *[ms]*	*257.60*	*16.65*	*0.06*	*05:48*
QT *[ms]*	*367*	*15.27*	*0.04*	*05:32*
PEP *[ms]*	*120.37*	*3.58*	*0.03*	*13:24*
R_iR_{i+1} *[ms]*	*812.70*	*88.61*	*0.11*	*04:49*

AO_iAO_{i+1} *[ms]*	*838.261*	*79.18*	*0.09*	*05:11*
SLOPE(IVC-AO) *[millig/ms]*	*1110.79*	*3060.47*	*0.28*	*14:14*

Table 3.16: Cumulative results of Cosinor analysis: median, 25th and 75th percentiles. For each parameter (row), the first column displays the values of the mesor, the second column displays the values of the amplitude, the third column shows the ratio between amplitude and mesor and the fourth column shows the values of the acrophase expressed in hours-minutes [Hours: Minutes]

Nine out of thirteen parameters presented the acrophase around 14 hours after the moment in which the subject went to bed (more or less at 3 PM, considering the median time value). On the contrary, the acrophase was around 5 hours after the beginning of the sleep period for temporal parameters as R_iR_{i+1}, AO_iAO_{i+1}, QT intervals and LVET (around 6 AM, considering the median time value).

3.4 Statistical Analysis

The statistical analysis concerns the evaluation of the presence of circadian rhythm in the extracted mechanical parameters.

3.4.1 Circadian Rhythm

Table 3.17 displays the results of the statistical analysis and in particular the evaluation of the presence of circadian rhythm in slope, amplitude and temporal selected mechanical parameters. We considered a parameter significant when its p-value was lower than 0.05.

As a result of the first Cosinor analysis, given the fact that we computed the analysis for each separate participating volunteer, the significance of each parameter is assessed for each subject. The systolic parameters, being also calculated for the 7 subjects in which is not possible to identify the T wave, can be significant for up to 22 subjects (all participating volunteers). Instead, diastolic parameters can be significant for up to 15 subjects (all participating volunteers except the 7 subjects in which is not possible to identify the T wave).

As the second Cosinor analysis evaluates a single template for each parameter - built up by the union of parameters for all participating volunteers. Thus, as a result of the analysis, just one p-value was computed. The parameter is significant at the 95% of confidence if the p-value is lower than 0.05 (“Yes”), otherwise it is not significant (“No”).

Parameter	Significance *Separate Subjects*		Significance *All together Subjects*
	[Number Subjects]	**[%]**	**[Yes/No]**
ΔA(IVC-AO)	*19/22*	*86.36 %*	*Yes*
ΔA(IVC-MC)	*19/22*	*86.36 %*	*Yes*
ΔA(AO-RE)	*22/22*	*100 %*	*Yes*
ΔA(AO-AC)	*12/15*	*80 %*	*Yes*
ΔA(AO-minAORE)	*21/22*	*95.46 %*	*Yes*
ΔA(RE-minAORE)	*21/22*	*95.46 %*	*Yes*
ΔA(AC-minAC)	*14/15*	*93.33 %*	*Yes*
LVET	*15/15*	*100 %*	*Yes*
QT	*15/15*	*100 %*	*Yes*
PEP	*18/22*	*81.82 %*	*Yes*
R_iR_{i+1}	*22/22*	*100 %*	*Yes*
AO_iAO_{i+1}	*22/22*	*100 %*	*Yes*
SLOPE(IVC-AO)	*18/22*	*81.82 %*	*Yes*

Table 3.17: Significance analysis results of circadian rhythm. For each parameter (row), the first column displays the significance [Number of subject - Percentage] resulting from the first Cosinor analysis (separate analysis), while the second column displays the significance resulting from the second Cosinor analysis (cumulative analysis) [Yes/No]

Regarding the first Cosinor analysis (separate analysis), every parameter reached a significance level in >= 80% of the subjects; while 100% significance levels were obtained for each studied parameter in the second Cosinor analysis (cumulative analysis).

4. Discussion

In this study, 24-hours long acquisitions of both electrical (ECG) and mechanical heart activity (SCG) were analysed through an innovative algorithm that combines signal's information, cardiac properties, and physiological knowledge. As a result, heartbeats were identified and labelled with different tags to discern the analysable heartbeats from the not-analysable ones. From the former, fiducial points were extracted and morphological (amplitude, slope) and temporal parameters were calculated. Also, Cosinor analysis was applied to evaluate the circadian rhythm of cardiac mechanical activity in the computed parameters in normal-day life. Finally, normality ranges were defined to be utilized as possible reference for comparison in future studies.

The following chapter is subdivided into 2 different sections: *Section 4.1* focuses on discussing the feasibility of the proposed approach, while *Section 4.2* considers the obtained results, their interpretation, including limitations, compared to literature.

4.1 Feasibility Analysis

Through feasibility analysis the possibility to analyze the 24h SCG recordings to extract cardiac mechanical activity parameters was evaluated. Results of the comparison between the total number of identified R peaks in the ECG signal and the total number of SCs identified in the SCG signal, reaching a median percentage value of SCs with respect to R peaks of 72 % (maximum value: 94 %), shows that such approach is feasible, despite the low sampling frequency of the SCG signal (64 Hz). This is important as many wearable devices now include recordings of signals acquired with inertial sensors in order to evaluate body posture, but without exploiting their possible use in measuring the SCG [109]. This study proves that, for the device utilized and the relevant sampling rate, also this additional information could be derived in a long-term acquisition.

Given the long-duration recordings, the percentage of identified SCs with respect to R peaks could be addressed as accuracy of the detection.

To this aim, different studies proved the ability to detect heartbeat using three-axial SCG with much greater values, up to 96% [110]. However, the protocol being used in such studies involved measurements relevant to short-duration recordings (from 30 seconds to 5 minutes), made under idealized laboratory conditions (i.e. rest position and breathing control), which tend to minimize all sources of artifacts in the signal. On the contrary, in this study 24h measurements were performed in a normal daily-life setting, acquiring a much broader and representative range of signals, and requiring the implementation of a novel strategy to first understand the "good beats" and then extract only from them the relevant fiducial points. Both R peaks and SCs were identified using an almost automatic pipeline and algorithm, therefore prone to some errors. To this point it is worth to underline again that the aim was not to develop an error-free algorithm, but a strategy by which beats recognized as good on the SCG signal could be further evaluated by computing time and amplitude parameters, to allow understanding their relationship with cardiac electrical activity and derive normality ranges during the day and the night periods.

The percentage of identified peaks was found higher during night-time rather than day-time; as possible explanation, it can be assumed that during night-time the subject rests still in a horizontal position and consequently the SCG signal is less subject to movement's artifacts. An additional reason that will require further investigation could also be due to the methodology applied to initially identify the SCs: the SCG template matching algorithm required a template of 10 sec chosen by the operator for the first computational step of correlation. As a consequence, to prevent using a 10 sec template with artifacts, this was generally chosen during the night period. However, as the duration and morphology of the SCG signal vary during the 24 hours [66], correlating the day-signals with a template extracted during night could have led to erroneously misidentifying SCG peaks, despite precautions introduced. Possibly due to a low threshold imposed to the cross-correlation [111].

As results varied much among subjects (day-time: min 49.63 % max: 90.93; night-time: min we could nevertheless assume that the main source of failure was due to movement artifacts affecting the SCG signal, in some subjects more evident than others, instead than a systematic bias introduced by the 10-sec manual selection. Interestingly, an inverse linear correlation with the BMI of the subject was also found [112], which could be related to the larger dumping of the vibrations generated by the heart when the body structure is such to increase the distance between the external sensor and the source of vibrations, or when fat tissue is present in larger thickness. To compensate for this effect, an equivalent alternative placement option for the sensor could be at the sternum (breastbone), located closest to heart, which offers a rigid

mechanical bone structure that should efficiently transmit the mechanical vibrations, independently from BMI or gender-related body differences.

The innovative algorithm for heartbeats classification and extraction of fiducial points relied on the synchronously acquired 1-lead ECG signal, used as gold-standard. To this point, it was thus important to verify that all parts of the ECG signal were analyzable and, in particular the T-wave peak. Through a visual analysis of a large number of random heartbeats, there was a chance to identify the T wave peaks in 15 out of 22 participating volunteers.

As a matter of fact, the standard 12-lead ECG is the most frequently used as diagnostic test in cardiology practice [113], while EcgMove 4 device acquires a single channel ECG signal (single lead: V4-V5) and this could be reason why it was more difficult to identify the T wave on such signal. In those subjects where the T wave peak could not be identified, beat-to-beat labeling and fiducial points extraction was conducted only on the first part of the systolic phase, in order not to exclude such subjects from the analysis, but avoiding including possible unreliable measures in late systolic parameters.

Beat-to-beat labeling aimed at classifying heartbeats, assigning a label to each of them, to identify analyzable ones and to categorize the reasons why this was not possible. Labels were defined empirically, based on the various morphologies and scenarios observed in multiple patients during the analyses, and constitute a novelty of the proposed approach. Also, this step will constitute the basis of future work for the development of machine learning algorithms for automated classification of beats on the SCG signal, as the provided labels can be used in a supervised learning approach.

Even if the % of analyzable heartbeats among those identified on the SCG was still high, a significant number was excluded. A possible explanation could be due to the fact that the innovative labelling algorithm associated a label to each SCG heartbeat based on its morphology, assuming as correct reference morphology the one in which AO, RE and AC represented the most prominent peaks [114].Previous work observed that the SCG signal presents different morphologies, with three of them as the most common (*Figure 4.1*), despite not giving proper justification for this phenomenon [115]. As a result, SCG beats with a morphology different from the assumed reference could have been classified with a label implying their elimination from further analysis. Additionally, it has been proven that fiducial points are not always corresponding to clear peaks (for MC, RE, AO and AC) or valleys (for IVC) but sometimes are defined only by an inflection point on the SCG, thus making more difficult to identify them (*Figure 4.2*) [116]. Although the origin of this phenomenon is still unexplored, it might

depend on a transient, slight physiological, de-synchronization between left and right heart mechanics, coupled with the effects of breathing activity and its impact on preload and afterload.

Interestingly, in all subjects the % of beats labelled as analyzable during night-time was higher than the one during day-time.

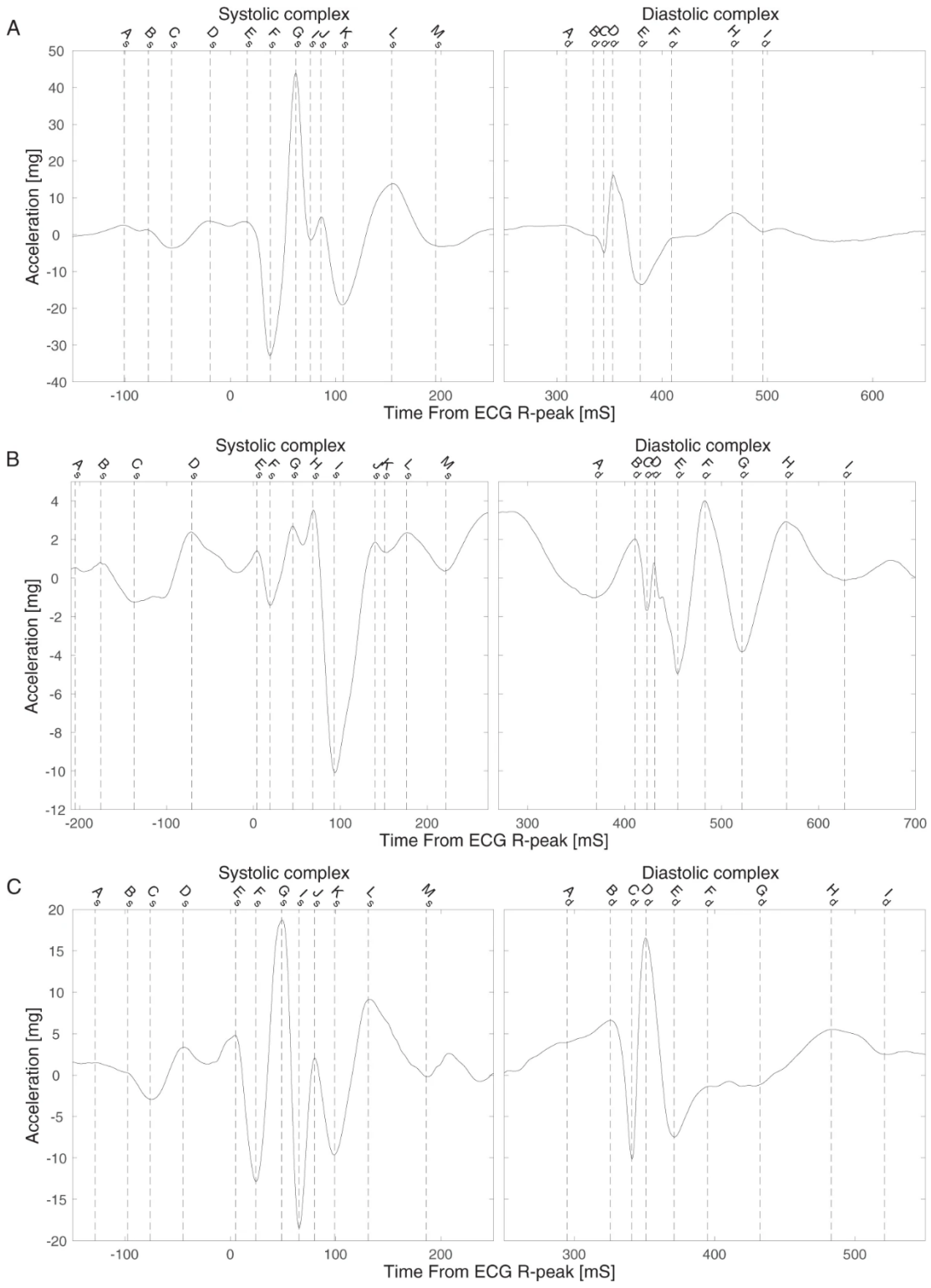

Figure 4.1: The three most common morphologies for the SCG signal [115]

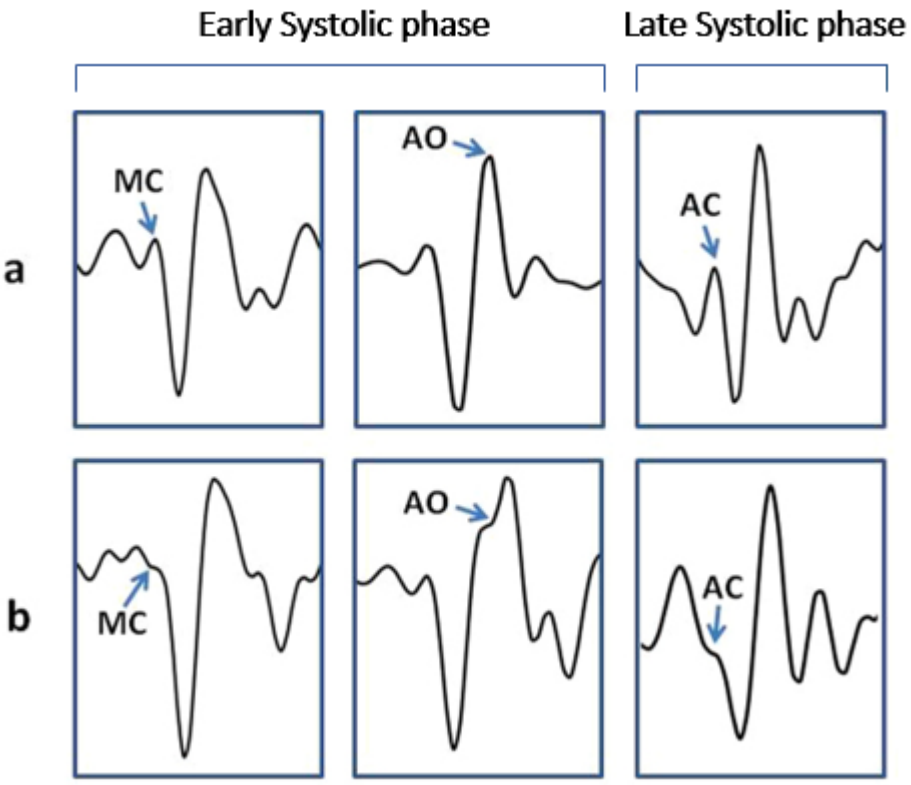

Figure 4.2: Panel a: Examples of beats in which MC, AO and AC fiducial points are characterized by the expected clear-cut peaks; Panel b: other beats in which the fiducial points are marked only by an inflection point. Adapted from [116]

The tags relevant to analyzable consecutive heartbeats were also computed for each participant, to evaluate by their maximum and median number the possibility to extract from the acquired 24h signal some intervals in which to evaluate heart rate variability (HRV) analysis of the extracted parameters, related to dynamic non-linear autonomic nervous system (ANS) processes. HRV reflects regulation of autonomic balance, blood pressure, gas exchange, gut, heart and vascular tone and an optimal level of HRV is associated with health, self-regulatory capacity and adaptability or resistance. Unfortunately, we didn't have a sufficient number of consecutive analyzable heartbeats to conduct a systematic HRV analysis during the 24 hours and we can assume it is due to the relationship between respiratory phases and SCG. It has in fact been proven that there is a relationship between respiratory rate and stroke volume [117] and, additionally, the SCG has been proposed in previous studies as a methodology to estimate stroke volume and myocardial contractility [118]. However, it was still possible to identify and extract - especially during the sleeping period – a sufficient number of analyzable consecutive heartbeats (i.e. 20 seconds) to conduct an ultra-short HRV (USHRV). USHRV parameters could be very useful to access and

monitor patients with CV diseases and physiological status, as diabetes mellitus [119], diabetic neuropathy [120], myocardial dysfunction [121], and stress conditions [87].

To extract fiducial points from analysable heartbeats over the 24h signals, an innovative algorithm that combines signal's information (i.e. peaks and valleys), cardiac properties, and physiological information (i.e. QS2, QTc intervals, etc) was developed. New morphological and temporal biomarkers were then computed as amplitude and time differences and slopes between previously identified fiducial points.

Unfortunately, due to the lack of imaging techniques, and the different sampling rate between the ECG and the SCG, it was not possible to validate that the position of fiducial points perfectly corresponds with a precise physiological event. However, it has been demonstrated that physiological events don't exactly coincide with local maxima of the SCG signal [122] but they occur before or after (they take place on the slope of the signal) (*Figure 4.3*)[115].

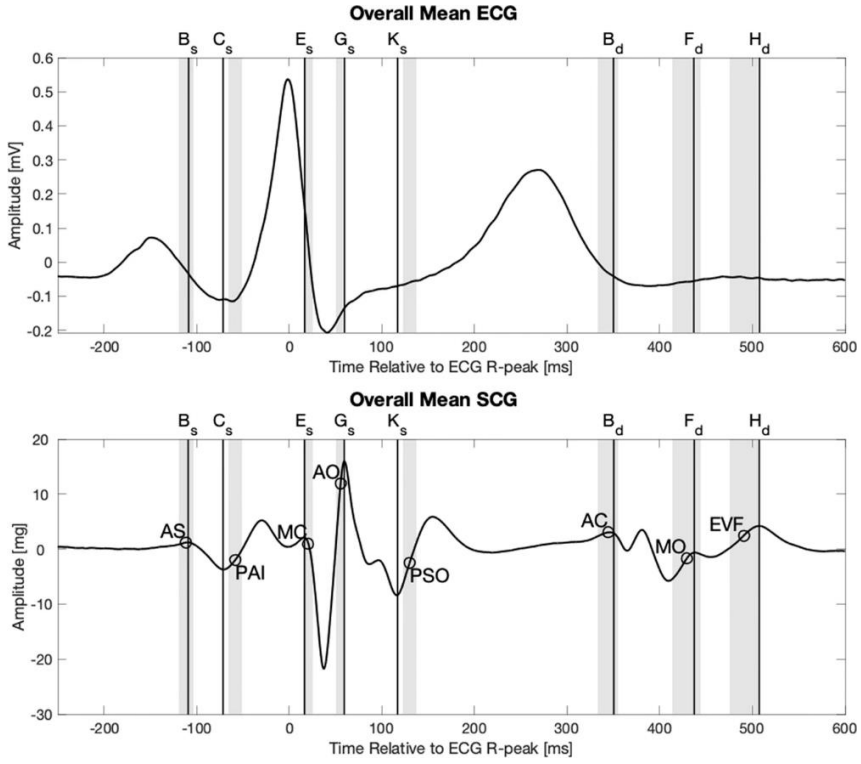

Figure 4.3: Top panel: ECG signal; Bottom panel: SCG signal, the circles indicate the mean location of physiological events found through ultrasound imaging. The grey areas indicate the 95% confidence intervals of the means for the physiological events found in the ultrasound images [115]

New biomarkers were identified and could be used to study electro-mechanical cardiac activity and make intra- and inter-subject comparisons. In previous studies, cardiac kinetic energy was proposed to characterize the cardiovascular status [123,124,125], representing the useful work of the heart in ejecting blood [126]. Using specific algorithms, kinetic energy and its temporal integral were computed from BCG and SCG waveforms as scalar parameters, both in a linear and in a rotational dimension. For example, the rotational kinetic energy obtained from tri-axial gyroscopes could accurately identify the first and second peak of the SCG [124]. However, given the intrinsic dependency from kinetic energy, it hasn't been possible to use energy derived parameters as biomarkers. In fact, kinetic energy is related to the position and posture of the subject, to the position of the device (even if we place the sensor in the same area, it is not possible to place it in the exact previously position) and thus is not possible to acquire repeated acquisitions under the same conditions, and thus to make comparison between the obtained data.

4.2 Circadian rhythm

All temporal parameters were characterized by a significant difference between day and night and the presence of a circadian rhythm was validated through the Cosinor analysis (cumulative analysis). All acrophases occurred between 05:00 and 07:00, a circadian behavior in accordance with the R_iR_{i+1} [66]. Indeed, it has already been proven that some temporal parameters as ΔT(Q-MC), ΔT(R-MC), ΔT(R-AO), ΔT(MC-AO), ΔT(R-IVC), are correlated with myocardial contractility and stroke volume [127,54].

Interesting considerations about the coupling between the electrical and mechanical activities could be derived from the comparison between AO_iAO_{i+1} and R_iR_{i+1} intervals. Given the results of the Cosinor analysis and of the day-night comparison, we can deduce that the mechanical temporal variability of AO_iAO_{i+1} (as demonstrated by the ratio between the amplitude and the mesor) reflects the electrical temporal variability of R_iR_{i+1}, while the maximum value of the AO_iAO_{i+1} (acrophase) occurred after the one of R_iR_{i+1}, we can thus speculate that the cardiac electrical activity reaches its higher value before the cardiac mechanical activity.

PEP is used as an estimate of the sympathetic nervous system influence on the heart and is defined as the sympathetically mediated time interval between the start of the electrical systole and the ejection of blood into the aorta [128]. In particular, PEP becomes shorter as sympathetic activity increases, which is higher at day-time [129], and thus longer PEP values were observed at night between 4:00 and 7:00 [130]. However, the acrophase obtained in this study though the Cosinor analysis occurs in the afternoon, and it is not in accordance with previous results. We could speculate that this difference is possibly related to the method used to derive the parameter of interest. In [130] PEP was derived from recordings of ECG (V5) and arterial pressure (by means of an ear densitogram utilizing a photoelectric transducer attached to an ear ring) and computed through an analog pre-processing methodology [131] while in this research only information coming from the EcgMove4 sensors were acquired and extracted through the pipeline previously described. An alternative reason could be related to the low sampling frequency of SCG (64 Hz) and to the applied normalization (normalized by R_iR_{i+1}). Indeed, not significant differences between day and night were visible in the not-normalized PEP, while appeared after the normalization procedure. It is indeed possible that the not-normalized PEP was characterized by a low circadian rhythm (not visible due to the low SCG sampling frequency) and, normalizing by R_iR_{i+1} intervals in which the circadian rhythm is very evident, resulting acrophases of the normalized PEP could have been altered.

Additionally, the ratio between the amplitude and the mesor was higher in R_iR_{i+1} intervals (0.11) with respect to PEP (0.03), thus showing a greater temporal variability in R_iR_{i+1}.

LVET is inversely related to HR and has been used for several decades to assess left ventricular function, contractility, and myocardial efficiency [132] being also directly correlated with the left ventricular ejection function and stroke volume. A significant difference between day and night was depicted in the non-normalized LVET, probably due its correlation to R_iR_{i+1} intervals, while no day-night oscillation was displayed in the normalized LVET. Non-normalized LVET reached the highest values in the early morning, with acrophase at 7:00. Additionally, the ratio between the amplitude and the mesor was higher in R_iR_{i+1} intervals (0.11) with respect to LVET (0.03), demonstrating a greater temporal variability in the first parameter.

QT interval shortening is induced by the sympathetic nervous system and is associated with increased ventricular contractility [133]. *Bonneimer et. al* [134] proved that QT and R_iR_{i+1} intervals revealed a characteristic day-night-pattern: diurnal profiles of QT interval variability exhibited a significant increase in the morning hours (6-9 AM) and a consecutive decline to baseline levels. Furthermore, the diurnal course of the QT interval variability strongly suggested that it is related to cardiac sympathetic activity [134]. The acrophase of QT occurred after the acrophase of the R_iR_{i+1} intervals and from the comparison between the ratio between amplitude and mesor, we derived that R_iR_{i+1} had a greater temporal variability with respect to QT.

Morphological parameters were characterized by a significant difference between day and night and the presence of a circadian rhythm was validated through the Cosinor analysis (cumulative analysis). All acrophases, following the circadian pattern of stroke volume and myocardial contractility as described in literature [135] occurred between the 15:00 and 16:00. Indeed, it has already been proven that BSG and SCG amplitudes and in particular amplitudes of AO, MC and IVC, SLOPE(IVC-AO) and SLOPE(MC-IVC) are correlated to the stroke volume and myocardial contractility.
All non-normalized pathological parameters displayed a significant difference between day and night, while disappeared in normalized parameters Δ(AO-RE), Δ(RE-minAORE) and Δ(AO-minAORE) (normalized by the amplitude of AO).

Since the SCG was calibrated in terms of acceleration and thus, force, amplitude of fiducial points and derived morphological parameters could be interpreted as the force of the heart's contraction and of the blood ejected into the vascular tree. Instead, the SLOPE(IVC-AO) is related to the velocity of the contraction of the heart.

In particular, a linear regression model to study the correlation between stroke volume and morphological SCG parameters has been developed and it has been proven that the amplitude of MC and AO are two crucial terms to estimate the stroke volume starting from the SCG signal [136].

Normality ranges for amplitude, mesor, amplitude/mesor and acrophase were computed from all the participating volunteers for intra-inter subject's comparisons of cardiac mechanical parameters.

5. Conclusions

This research was the first attempt to evaluate the circadianity of cardiac electro-mechanical activity parameters though Holter (24h) acquisitions during the participant's normal daily life and activity.

An innovative approach that combines signal's morphology, cardiac properties and physiological information was developed to identify analyzable heartbeats over 24h signals and to extract cardiac mechanical parameters. Normality ranges were then defined from 22 healthy participating volunteers.

New parameters identified in this study could be used as important biomarkers for comparisons when monitoring pathological patients and as a prevention tool in healthy subjects in longitudinal studies.

These results also provide evidence of the possibility to study the electro-mechanical activity of the heart and health status outside of the clinical setting through new wearable, user-friendly and non-invasive devices. This approach combined with machine learning techniques will open the opportunity to evaluate more reliably the CV system through SCG acquisitions of different duration. The labelling introduced for all the acquired beats indeed will constitute the basis to proceed to train machine learning models in order to automatically identify the correct beats and extract relevant parameters. Such models could then be used also for the analysis of short-term SCG signals acquired using embedded smartphone to constitute a new tool for self-tracking of cardiac activity.

Furthermore, this study lays the foundation providing normal reference values for future research on the coupling of electro-mechanical cardiac activity in different scenarios currently under evaluation, such as during underwater immersions and during prolonged isolation.

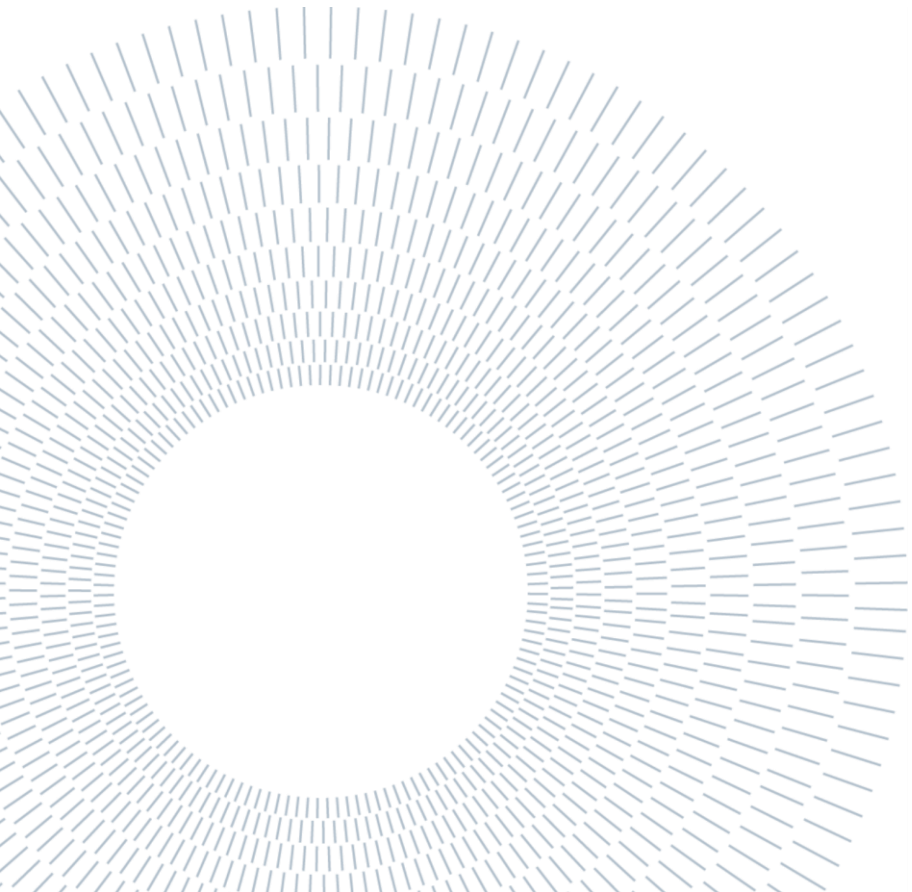

Bibliography

[1] Thiriet, M (2015). Cardiac Pump: An Introduction. In: Lanzer, p.(eds) PanVascularMedicine. Spieger, Berlin, Heidelberg. Doi: 10.1007/978-3-642-37078-6_25

[2] Peate, Ian. (2018). Anatomy and physiology, 8. The circulatory system. British Journal of Healthcare Assistants. 12. 62-67. Doi: 10.12968/bjha.2018.12.2.62

[3] URL https://pediaa.com/difference-between-pulmonary-and-systemic-circulation/

[4] Rhian M. Touyz, Christian Delles (2019). Textbook of Vascular Medicine (pp: 13-22). Springer, Berlin, Heidelberg

[5] URL:https://www.shalom-education.com/courses/gcse-biology/lessons/transport systems/topic/the-human-circulatory-system/

[6] Whitaker, R. H. (2014). Anatomy of the heart. In *Medicine (United Kingdom)* (Vol. 42, Issue 8, pp. 406–408). Elsevier Ltd. Doi: 10.1016/j.mpmed.2014.05.007

[7] Malmivuo, Jaakko & Plonsey, Robert. (1995). Bioelectromagnetism. 6. The Heart.

[8] URL:https://socratic.org/questions/which-is-the-cardiac-muscle-layer-of-the-heart

[9] URL:https://www.shutterstock.com

[10] URL:https://nurseslabs.com/cardiovascular-system-anatomy-physiology/

[11] URL:https://www.drugs.com/health-guide/heart-valve-problems.html

[12] Penn, Gleeson Murphy, Cardiovascular System, Encyclopedia of Toxicology (Second Edition), Elsevier, **2005** (pp. 467-485), Doi: 10.1016/B0-12-369400-0/00193-9.

[13] Grant, A. O. (2009). Cardiac ion channels. In *Circulation: Arrhythmia and Electrophysiology* (Vol. 2, Issue 2, pp. 185–194), Doi: 10.1161/CIRCEP.108.789081

[14] URL:http://www.pathophys.org/physiology-of-cardiac-conduction-and-contractility/

[15] Sánchez-Quintana, D., Ho, S. Y., & Sánchez-Quintana, D. (2003). R EVIEW A RTICLE Anatomy of Cardiac Nodes and Atrioventricular Specialized Conduction System. In *Rev Esp Cardiol* (Vol. 56, Issue 11)

[16] URL:https://www.heart.org/en/healthy-living/fitness/fitness-basics/target-heart-rates

[17] Mangoni ME, Nargeot J. Genesis and regulation of the heart automaticity. Physiol Rev. 2008 Jul;88(3):919-82. Doi: 10.1152/physrev.00018.2007.

[18] URL:https://www.slideserve.com/wolfe/electrical-conduction-in-myocardial-cells

[19] Pollock JD, Makaryus AN. Physiology, Cardiac Cycle. [Updated 2021 Oct 9]. In: StatPearls [Internet]. Treasure Island (FL): StatPearls Publishing; 2022 Jan

[20] URL:https://www.utmb.edu/pedi_ed/CoreV2/Cardiology/cardiologyV2/cardiologyV22.html

[21] Homan TD, Bordes S, Cichowski E. Physiology, Pulse Pressure. [Updated 2021 Jul 15]. In: StatPearls [Internet]. Treasure Island (FL): StatPearls Publishing; 2022 Jan

[22] URL:https://123sonography.com/ebook/assess-pulmonary-hypertension

[23] Hoeper MM, Bogaard HJ, Condliffe R, et al. Definitions and diagnosis of pulmonary hypertension. J Am Coll Cardiol 2013; **62**: D42–D50

[24] URL https://commons.wikimedia.org/wiki/File:Wiggers_Diagram_2.svg

[25] De, N., Ferreira, P., Gehin, C., Massot, B., & Massot, B. A. (2020). A Review of Methods for Non-Invasive Heart Rate Measurement on Wrist. *Review of Methods for Non-Invasive Heart Rate Measurement on Wrist. Innovation and Research in BioMedical Engineering*, 10. Doi: 10.1016/j.irbm.2020.04.001ï

[26] Lukkarinen, S. Phonocardiography: Development of a Clinical System and Its Application to Screening for Paediatric Heart Murmurs. Ph.D. Thesis, Aalto University, Espoo, Finland, 2012.

[27] Einthoven,W. The string galvanometer and the human electrocardiogram. Knaw Proc. **1903**, 6, 107–115.

[28] Bour, J.; Kellett, J. Impedance cardiography—A rapid and cost-effective screening tool for cardiac disease. Eur. J. Intern. Med. **2008**, 19, 399–405.

[29] Edler, I.; Lindström, K. The history of echocardiography. Ultrasound Med. Biol. **2004**, 30, 1565–1644.

[30] Starr, I.; Rawson, A.; Schroeder, H.; Joseph, N. Studies on the estimation of cardiac ouptut in man, and of abnormalities in cardiac function, from the heart's recoil and the blood's impacts; the ballistocardiogram. Am. J. Physiol.-Leg. Content **1939**, 127, 1– 28.

[31] Mounsey, P. Praecordial ballistocardiography. Br. Heart J. **1957**, 19, 259.

[32] Tadi, M.J.; Lehtonen, E.; Pankäälä, M.; Saraste, A.; Vasankari, T.; Terás, M.; Koivisto, T. Gyrocardiography: A new non-invasive approach in the study of mechanical motions of the heart. Concept, method and initial observations. In Proceedings of the 2016 38th Annual International Conference of the IEEE Engineering in Medicine and Biology Society (EMBC), Orlando, FL, USA, 16–20 August 2016; pp. 2034–2037.

[33] InformedHealth.org [Internet]. Cologne, Germany: Institute for Quality and Efficiency in Health Care (IQWiG); 2006-. What is an electrocardiogram (ECG)? 2019 Jan 31

[34] URL:https://jakenmedical.com/blog/12lead-resting-ekg-electrode-placement/
[35] URL:https://en.wikipedia.org/wiki/Electrocardiography#/media/File:EKG_leads.png
[36] URL:https://ecgwaves.com/topic/introduction-electrocardiography-ecg-book/
[37] Akhras F, Rickards AF. The relationship between QT interval and heart rate during physiological exercise and pacing. Jpn Heart J. 1981 May;22(3):345-51. Doi:10.1536/ihj.22.345.
[38] Viskin S. Long QT syndromes and torsade de pointes. Lancet. 1999 Nov 6;354(9190):1625-33. Doi: 10.1016/S0140-6736(99)02107-8.
[39] Johnson JN, Ackerman MJ. QTc: how long is too long?. *Br J Sports Med*. 2009;43(9):657-662. Doi:10.1136/bjsm.2008.054734
[40] Mason JW, et al. Electrocardiographic reference ranges derived from 79,743 ambulatory subjects. *J. Electrocardiol.* 2007;40:228–234. Doi: 10.1016/j.jelectrocard.2006.09.003
[41] URL:https://amscardiology.com/conditions-procedures/bradycardia-and-tachycardia/
[42] Antzelevitch C, Burashnikov A. Overview of Basic Mechanisms of Cardiac Arrhythmia. *Card Electrophysiol Clin*. 2011;3(1):23-45. Doi:10.1016/j.ccep.2010.10.012
[43] W.Gordon, Certain molar movements of the human body produced by the circulation of the blood, *J.Anat. Physiol*, vol. 11, pp. 533-536, 1877
[44] I.Srarr, A.J. Rawson, H. A. Schroeder et al., Studies on the estimation of cardiac output in man, and of abnormalities in cardiac function, from the heart's recoil and the blood's impacts; the ballistocardiogram. *Amer. J. Physiol*., vol. 127, pp. 1-28, 1939
[45] Bozhenko, B. S. Seismocardiography–a new method in the study of functional conditions of the heart. *Ter. Arkh.* **33**, 55 (1961).
[46] D. M. Salerno and J.Zanetti, Seismocardiography for monitoring changes in left ventricular function during ischemia, *Chest J.*, vol. 100, pp. 991-993, 1991
[47] L. Giovagrandi, O. T. Inan, R. M. Wiard *et al*., Ballistocardiography: A method worth revisiting, in *Proc. IEEE Annu. Int. Conf. Eng. Med. Biol. Soc.*, 2011, pp- 4279-4282
[48] Akhbardeh, A.; Tavakolian, K.; Gurev, V.; Lee, T.; New, W.; Kaminska, B.; Trayanova, N. Comparative analysis of three different modalities for characterization of the seismocardiogram. In Proceedings of the 2009 Annual International Conference of the IEEE Engineering in Medicine and Biology Society, Minneapolis, MN, USA, 3–6 September 2009; pp. 2899–2903.
[49] Lee, H., Lee, H., & Whang, M. (2018). An enhanced method to estimate heart rate from seismocardiography via ensemble averaging of body movements at six degrees of freedom. *Sensors (Switzerland)*, *18*(1). Doi:10.3390/s18010238

[50] Friedrich, David & Aubert, Xavier & Fuehr, Hartmut & Brauers, Andreas. (2010). Heart Rate Estimation on a Beat-to-Beat Basis via Ballistocardiography - A hybrid Approach.. Conference proceedings : ... Annual International Conference of the IEEE Engineering in Medicine and Biology Society. IEEE Engineering in Medicine and Biology Society. Conference. 2010. 4048-51. 10.1109/IEMBS.2010.5627626.

[51] Işilay Zeybek, Z. M., Racca, V., Pezzano, A., Tavanelli, M., & di Rienzo, M. (2022). Can Seismocardiogram Fiducial Points Be Used for the Routine Estimation of Cardiac Time Intervals in Cardiac Patients? *Frontiers in Physiology*, *13*. Doi:10.3389/fphys.2022.825918

[52] Crow, R. S., Hannan, P., Jacobs, D., Hadquist, L. & Salerno, D. M. Relationship between Seismocardiogram and Echocardiogram for Events in Cardiac Cycle. *Am. J. Noninvasive Cardiology* **8**, 39–46 (1994).

[53] Mohammed Owahidur Rahman, Raiker Witter, Ago Samoson; Development of a signal processing algorithm for automatic identification of the cardiac events in the seismocardiogram, Cardiology, pp. 41, Doi: 10.1159/000431110

[54] Di Rienzo, Marco & Vaini, Emanuele & Lombardi, Prospero. (2017). An algorithm for the beat-to-beat assessment of cardiac mechanics during sleep on Earth and in microgravity from the seismocardiogram. Scientific Reports. 7. Doi:10.1038/s41598-017-15829-0.

[55] Tavakolian K, Portacio G, Tamddondoust NR, Jahns G, Ngai B, Dumont GA, Blaber AP. Myocardial contractility: a seismocardiography approach. Annu Int Conf IEEE Eng Med Biol Soc. 2012;2012:3801-4. Doi: 10.1109/EMBC.2012.6346795.

[56] Weissler AM, Harris WS, Schoenfeld CD. Systolic time intervals in heart failure in man. *Circulation* 1968; 37:149-159

[57] H. Boudoulas, S.E.Rittgers, R.P. Lewis, C.V. Leier A.M. Weissler. "Changes in diastolic time with various pharmacologic agents: implication for myocardial perfusion.". Circulation. Jul;60(1):164-9, 1979

[58] Garrod, A. H.: On some points connected with circulation of the blood arrived at from a study of the sphygmograph. Proc Roy Soc London 23: 140, 1874-5.

[59] Weissler, A. M., Harris, W. S., & Schoenfeld, C. D. (1968). XXXVII NO. 2 AN OFFICIAL JOlURNAL ofet1i AMERICAN IEART ASSOCIATION. In *American Heart Association. Circulation: Vol. XXXVII*.

[60] Lauboeck H. Echocardiographic study of the isovolumetric contraction time. J Biomed Eng. 1980 Oct;2(4):281-4. Doi: 10.1016/0141-5425(80)90121-1

[61] Inductance cardiography (thoracocardiography): A novel, non invasive technique for monitoring left ventricular filling. *Journal of Critical Care*, Volume 14, Issue 4, Pages 177-185

[62] Shapiro LM, Thwaites BC. Measurement of isovolumic relaxation: comparison of echocardiographic mitral valve opening and Doppler mitral valve flow. Cardiovasc Res.1987; 21:489-491

[63] Portaluppi F., Hermida R.C. Circadian rhythms in cardiac arrhythmias and opportunities for their chronotherapy. *Adv Drug Deliv Rev.* 2007;**59**:940–951

[64] Cooke HM, Lynch A. Biorhythms and chronotherapy in cardiovascular disease. Am J Hosp Parm 1994;51:2569–2580.

[65] Gander PH, Connell LJ, Graeber RC. Masking of the circadian rhythms of heart rate and core temperature by the rest-activity cycle in man. J Biol Rhythms. 1986 Summer;1(2):119-35. Doi: 10.1177/074873048600100203

[66] Dilaveris PE, Farbom P, Batchvarov V, Ghuran A, Malik M. Circadian behavior of P-wave duration, P-wave area, and PR interval in healthy subjects. Ann Noninvas Electrocardiol 2001;6:92–97.

[67] Oda E, Aizawa Y, Arai Y, Shibata A. Diurnal variation of QT interval in patients with VVI pacemaker. Tohoku J Exp Med 1985;145:419–426.

[68] Molnar J, Zhang F, Weiss J, Ehlert FA, Rosenthal JE. Diurnal pattern of QTc interval: How long is prolonged? Possible relation to circadian triggers of cardiovascular events. J Am Coll Cardiol 1996;27:76–83

[69] Yamasaki Y, Kodama M, Matsuhisa M, Kishimoto M, Ozaki H, Tani A, Ueda N, Ishida Y, Kamada T. Diurnal heart rate variability in healthy subjects: Effects of aging and sex difference. Am J Physiol 1996;271:H303–310

[70] Natarajan, A., Pantelopoulos, A., Emir-Farinas, H., & Natarajan, P. (2020). Heart rate variability with photoplethysmography in 8 million individuals: a cross sectional study. *The Lancet Digital Health*, *2*(12), e650–e657. Doi:10.1016/S2589-7500(20)30246-6

[71] Shaffer F, Ginsberg JP. An Overview of Heart Rate Variability Metrics and Norms. Front Public Health. 2017 Sep 28;5:258. Doi:10.3389/fpubh.2017.00258

[72] Massin MM, Maeyns K, Withofs N, Ravet F, Gerard P. Circadian rhythm of heart rate and heart rate variability. Arch Dis Child 2000;83:179–182.

[73] Korpelainen JT, Sotaniemi KA, Huiluri HV, Myllyla VV. Circadian rhythm of heart rate variability is reversibly abolished in ischemic stroke. Stroke 1997;28:2150–2154.

[74] Lombardi F, Sandrone G, Mortara A, La Rovere MT, Colombo E, Guzzetti S, Malliani A. Circadian variation of spectral indices of heart rate variability after myocardial infarction. Am Heart J 1992;123: 1521–1529.

[75] Portaluppi F, Tiseo R, Smolensky MH, Hermida RC, Ayala DE, Fabbian F. Circadian rhythms of cardiovascular health. Sleep Med Rev. 2012; 16:151-166. Doi: 10.1016/j.smrv.2011.04.003

[76] Richards AM, Nicholls MG, Espiner EA, Ikram H, Cullens M, Hinton D. Diurnal patterns of blood pressure, heart rate and vasoactive hormones in normal man. Clin Exp Hypertens A. 1986; 8:153-166. Doi: 10.3109/10641968609074769

[77] J. Ramos-Castro et al., "Heart rate variability analysis using a seismocardiogram signal," in 2012 Annual International Conference of the IEEE Engineering in Medicine and Biology Society, 2012, pp. 5642–5645.

[78] C. Gavriel, K. H. Parker, and A. A. Faisal, "Smartphone as an ultra-low cost medical tricorder for real-time cardiological measurements via ballistocardiography," in 2015 IEEE 12th International Conference on Wearable and Implantable Body Sensor Networks (BSN), 2015, pp. 1–6.

[79] Hazar Ashouri et al. 2017. Universal Pre-Ejection Period Estimation using Seismocardiography: Quantifying the Effects of Sensor Placement and Regression Algorithm. *IEEE Sensors Journal* (2017)

[80] Mojtaba Jafari Tadi et al. 2015. A new algorithm for segmentation of cardiac quiescent phases and cardiac time intervals using seismocardiography. In *6th Int. Conference on Graphic and Image Processing (ICGIP 2014),* Vol. 9443

[81] Amirtaha Taebi et al. 2018. An Adaptive Feature Extraction Algorithm for Classification of Seismocardiographic Signals. *arXiv preprint arXiv:1803.10343(2018)*

[82] Zanetti J, Salerno D. Seismocardiography: A new technique for recording cardiac vibrations. concept, method, and initial observations. *J. Cardiovasc. Technol.* 1990;**9**:111–118

[83] Durichen, R., Verma, K. D., Yee, S. Y., Rocznik, T., Schmidt, P., Bodecker, J., & Peters, C. (2018). Prediction of electrocardiography features points using seismocardiography data: A machine learning approach. *Proceedings - International Symposium on Wearable Computers, ISWC*, 96–99. Doi: 10.1145/3267242.3267283

[84] Javaid, A.Q.; Fesmire, N.F.;Weitnauer, M.A.; Inan, O.T. Towards robust estimation of systolic time intervals using head-to-foot and dorso-ventral components of sternal acceleration signals. In Proceedings of the 2015 IEEE 12th international conference on wearable and implantable body sensor networks (BSN), Cambridge, MA, USA, 9–12 June 2015; pp. 1–5.

[85] Ramos-Castro, Juan & Moreno, Jordi & Miranda-Vidal, H & Garcia-Gonzalez, M & Fernández-Chimeno, Mireya & Rodas, Gil & Ortís, Lluís. (2012). Heart rate variability analysis using a seismocardiogram signal. Conference proceedings : ... Annual International Conference of the IEEE Engineering in Medicine and Biology Society. IEEE Engineering in Medicine and Biology Society. Conference. 2012. 5642-5. 10.1109/EMBC.2012.6347274.

[86] Munoz, M.L.; Van Roon, A.; Riese, H.; Thio, C.; Oostenbroek, E.; Westrik, I.; Snieder, H. Validity of (Ultra-)Short recordings for heart rate variability measurements. *PLoS ONE* **2015**, *10*, 1–15

[87] Taelman, J.; Vandeput, S.; Spaepen, A.; Van Huffel, S. Influence of Mental Stress on Heart Rate and Heart Rate Variability. In *Proceedings of the 4th European Conference of the International Federation for Medical and Biological Engineering (IFMBE)*; Vander Sloten, J., Verdonck, P., Nyssen, M., Haueisen, J., Eds.; Springer: Berlin/Heidelberg, Germany, 2009; Volume 22, pp. 395–400

[88] Solbiati, S., Paglialonga, A., Costantini, L., Šimunič, B., Pišot, R., Narici, M. v, & Caiani, E. G. (2021). *Assessing Cardiac Electro-Mechanical Deconditioning During Bed Rest Using Smartphone's Inertial Sensors; Assessing Cardiac Electro-Mechanical Deconditioning During Bed Rest Using Smartphone's Inertial Sensors*.Doi: 10.22489/CinC.2021.191

[89] URL:https://docs.movisens.com/Sensors/EcgMove4/#scope-of-application

[90] Friesen GM, Jannette TC, Jadallah M A, Yates SL, Quint SR, Nagle HT. A comparison of the noise sensitivity of nine QRS detection algorithms. IEEE Trans Biomed Eng. 1990;**37**:85–98. Doi: 10.1109/10.43620

[91] Carlos R Vázquez-Seisdedos1† , João Evangelista Neto2,3,4*† , Enrique J Marañón Reyes1 , Aldebaro Klautau2 and Roberto C Limão de Oliveira. New approach for T-wave end detection on electrocardiogram: Performance in noisy conditions

[92] Rai, D., Thakkar, H. K., Rajput, S. S., Santamaria, J., Bhatt, C., & Roca, F. (2021). A comprehensive review on seismocardiogram: Current advancements on acquisition, annotation, and applications. *Mathematics*, *9*(18). Doi:10.3390/math9182243

[93] Landreani, F., Faini, A., Martin-Yebra, A., Morri, M., Parati, G., & Caiani, E. G. (2019). Assessment of ultra-short heart variability indices derived by smartphone accelerometers for stress detection. *Sensors (Switzerland)*, *19*(17). Doi:10.3390/s19173729

[94] A. Q. Javaid, H. Ashouri, A. Dorier, M. Etemadi, J. A. Heller, S. Roy, and O. T. Inan, "Quantifying and reducing motion artifacts in wearable seismocardiogram measurements during walking to assess left ventricular health," IEEE Transactions on Biomedical Engineering, vol. 64, no. 6, pp. 1277–1286, 2017

[95] H. Lee, H. Lee, and M. Whang, "An enhanced method to estimate heart rate from seismocardiography via ensemble averaging of body movements at six degrees of freedom," Sensors, vol. 18, no. 1, p. 238, Jan 2018

[96] Tompkins, W. J. (1985). A Real-Time QRS Detection Algorithm. In *IEEE TRANSACTIONS ON BIOMEDICAL ENGINEERING* (Vol. 32, Issue 3).

[97] URL:https://www.mdapp.co/ecg-heart-rate-calculator-483/

[98] Siega Battel Lorenzo, *A deep learning approach for online fiducial points detection in seismo-cardiographic recordings* [master thesis]. Milano: Politecnico di Milano, 2021-2022

[99] Wichterle D, Simek J, La Rovere MT, *et al* Prevalent low-frequency oscillation of heart rate: Novel predictor of mortality after myocardial infarction. *Circulation* 2004;110:1183–1190

[100] Wiklund U, Hörnsten R, Karlsson M, Suhr OB, Jensen SM. Abnormal heart rate variability and subtle atrial arrhythmia in patients with familial amyloidotic polyneuropathy. *Ann Noninvasive Electrocardiol*. 2008;13(3):249-256. doi:10.1111/j.1542-474X.2008.00228.x

[101] Landreani, F.; Morri, M.; Martin-Yebra, A.; Casellato, C.; Pavan, E.; Frigo, C.; Caiani, E.G. Ultra-short-term heart rate variability analysis on accelerometric signals from mobile phone. In Proceedings of the E-Health and Bioengineering Conference (EHB), Sinaia, Romania, 22–24 June 2017; pp. 241–244

[102] A. Martín-Yebra *et al*., "Studying heart rate variability from ballistocardiography acquired by force platform: Comparison with conventional ECG," *2015 Computing in Cardiology Conference (CinC)*, 2015, pp. 929-932, Doi: 10.1109/CIC.2015.7411064.

[103] URL:https://www.physiologyweb.com/calculators/mean_arterial_pressure_calculator.

[104] The European Agency for the Evaluation of Medicinal Products (1997). *Committee for Proprietary Medicinal Products. Points to consider: The assessment of the potential for QT interval prolongation by non-cardiovascular medicinal products* (Report No. 3)

[105] Nelson W, Tong YL, Lee JK, Halberg F. Methods for cosinor-rhythmometry. Chronobiologia. 1979 Oct-Dec;6(4):305-23. PMID: 548245.

[106] Cornelissen, G. (2014). Cosinor-based rhythmometry. In *Theoretical Biology and Medical Modelling* (Vol. 11, Issue 1). BioMed Central Ltd. Doi:10.1186/1742-4682-11-16

[107] Refinetti R, Cornelissen G, Halberg F. Procedures for numerical analysis of circadian rhythms. Biological Rhythm Research. 2007; 38(4):275325. DOI: Doi:10.1080/09291010600903692

[108] Gallerani M, Portaluppi F, Maida G, Chieregato A, Calzolari F, Trapella G, Manfredini R. Circadian and circannual rhythmicity in the occurrence of subarachnoid hemorrhage. Stroke. 1996 Oct;27(10):1793-7

[109] Deep learning and domain adaptation acceleration-based techniques for human activity recognition in a hospital setting Tesi di Laurea Magistrale in Biomedical Engineering - Ingegneria Biomedica Author: Lorenzo Principi. A.A. 20/21

[110] Landreani, Federica & Gorlier, Damien & Hossein, Amin & Rabineau, Jeremy & Borne, Philippe & Caiani, Enrico & Migeotte, Pierre-François. (2018). Heartbeat

Detection Using Three-Axial Seismocardiogram Acquired by Mobile Phone. Doi:10.22489/CinC.2018.215

[111] F. Landreani *et al*., "Beat-to-beat heart rate detection by smartphone's accelerometers: Validation with ECG," *2016 38th Annual International Conference of the IEEE Engineering in Medicine and Biology Society (EMBC)*, 2016, pp. 525-528, Doi: 10.1109/EMBC.2016.7590755

[112] C. Gavriel, K. H. Parker and A. A. Faisal, "Smartphone as an ultra-low cost medical tricorder for real-time cardiological measurements via ballistocardiography," *2015 IEEE 12th International Conference on Wearable and Implantable Body Sensor Networks (BSN)*, 2015, pp. 1-6, Doi: 10.1109/BSN.2015.7299425

[113] Denes P. The importance of derived 12-lead electrocardiography in the interpretation of arrhythmias detected by Holter recording. Am Heart J. 1992 Oct;124(4):905-11. Doi: 10.1016/0002-8703(92)90971-w.

[114] Yao J, Tridandapani S, Wick CA, Bhatti PT. Seismocardiography-Based Cardiac Computed Tomography Gating Using Patient-Specific Template Identification and Detection. IEEE J Transl Eng Health Med. 2017 Jul 7;5:1900314. Doi: 10.1109/JTEHM.2017.2708100

[115] Sørensen, K., Schmidt, S.E., Jensen, A.S. *et al*. Definition of Fiducial Points in the Normal Seismocardiogram. *Sci Rep* **8**, 15455 (2018).Doi:10.1038/s41598-018-33675-6

[116] Di Rienzo M, Vaini E, Lombardi P. An algorithm for the beat-to-beat assessment of cardiac mechanics during sleep on Earth and in microgravity from the seismocardiogram. Sci Rep. 2017 Nov 15;7(1):15634. Doi: 10.1038/s41598-017-15829-0. PMID: 29142324

[117] Daniel De Backer, Fabio Silvio Taccone, Roland Holsten, Fayssal Ibrahimi, Jean-Louis Vincent; Influence of Respiratory Rate on Stroke Volume Variation in Mechanically Ventilated Patients. *Anesthesiology* 2009; 110:1092–1097 Doi:10.1097/ALN.0b013e31819db2a1

[118] Tavakolian, Kouhyar & Portacio, Gonzalo & Tamddondoust, Rosette & Jahns, Graeme & Ngai, Brandon & Dumont, Guy & Blaber, Andrew. (2012). Myocardial contractility: A seismocardiography approach. Conference proceedings : ... Annual International Conference of the IEEE Engineering in Medicine and Biology Society. IEEE Engineering in Medicine and Biology Society. Conference. 2012. 3801-4. Doi:10.1109/EMBC.2012.6346795.

[119] Nussinovitch, U., Cohen, O., Kaminer, K., Ilani, J., & Nussinovitch, N. (2012). Evaluating reliability of ultra-short ECG indices of heart rate variability in diabetes mellitus patients. *Journal of Diabetes and Its Complications*, *26*(5), 450–453. Doi:10.1016/j.jdiacomp.2012.05.001

[120] Pagani, M.; Malfatto, G.; Pierini, S.; Casati, R.; Masu, A.M.; Poli, M.; Malliani, A. Spectral analysis of heart rate variability in the assessment of autonomic diabetic neuropathy. *J. Auton. Nervous Syst.* **1988**, *23*, 143–153

[121] Nolan, J.; Flapan, A.D.; Capewell, S.; MacDonald, T.M.; Neilson, J.M.; Ewing, D.J. Decreased cardiac parasympathetic activity in chronic heart failure and its relation to left ventricular function. *Br Heart J.* **1992**, *67*, 482–485

[122] Crow, R. S., Hannan, P., Jacobs, D., Hedquist, L. & Salerno, D. M. Relationship between seismocardiogram and echocardiogram for events in the cardiac cycle. *Am. J. noninvasive Cardiol.* **8**, 39–46 (1994)

[123] Hossein A, Mirica DC, Rabineau J, Rio JI, Morra S, Gorlier D, Nonclercq A, van de Borne P, Migeotte PF. Accurate detection of dobutamine-induced haemodynamic changes by kino-cardiography: a randomised double-blind placebo-controlled validation study. Scientific reports. 2019 Jul 19;9(1):1-1

[124] Morra S, Pitisci L, Su F, Hossein A, Rabineau J, Racape J, Gorlier D, Herpain A, Migeotte PF, Creteur J, van de Borne P. Quantification of Cardiac Kinetic Energy and Its Changes During Transmural Myocardial Infarction Assessed by Multi-Dimensional Seismocardiography. Front Cardiovasc Med. 2021 Mar 8;8:603319. Doi: 10.3389/fcvm.2021.603319

[125] Solbiati, Sarah & Buffoli, A. & Megale, Valentino & Damato, Gianfranco & Lenzi, B. & Langfelder, G. & Caiani, Enrico. (2021). Detecting Heart Rate From Virtual Reality Headset-Embedded Inertial Sensors: a Kinetic Energy Approach. 1-4. Doi:10.1109/EHB52898.2021.9657564

[126] Wong J, Chabiniok R, Tibby SM, Pushparajah K, Sammut E, Celermajer D, Giese D, Hussain T, Greil GF, Schaeffter T, Razavi R. Exploring kinetic energy as a new marker of cardiac function in the single ventricle circulation. J Appl Physiol (1985). 2018 Sep 1;125(3):889-900. Doi: 10.1152/japplphysiol.00580.2017

[127] McKay WP, Gregson PH, McKay BW, Militzer J. Sternal acceleration ballistocardiography and arterial pressure wave analysis to determine stroke volume. Clin Invest Med. 1999 Feb;22(1):4-14

[128] Brenner and Beauchaine, 2011; Brenner et al., 2005; Fox et al., 2006

[129] Pressman MR, Fry JM. Relationship of autonomic nervous system activity to daytime sleepiness and prior sleep. Sleep. 1989 Jun;12(3):239-45.Doi: 10.1093/sleep/12.3.239

[130] Vr~ncianu, R., Filcescu, V., Ionescu, V., Groza, P., Persson, J., Kadefors, R., & Peterssn, I. (1982). The Influence of Day and Night Work on the Circadian Variations of Cardiovascular Performance*. In *European Journal of Applied Physiology and Occupational Physiology* (Vol. 48)

[131] Nygårds ME, Tranesjö J, Atterhög JH, Blomqvist P, Ekelund LG, Wigertz. On-line computer processing of pressure data from cardiac catheterizations. Comput Programs Biomed. 1976 Mar;5(4-2):272-82. Doi: 10.1016/0010-468x(76)90055-6.

[132] Knight DH, Sleeper MM. Pathophysiology of heart failure. In: Abbot JA, ed. *Small Animal Cardiology Secrets*. Philadelphia: Hanley & Belfus; 2000. Pp. 7-22

[133] Huang, M.H., Wolf, S.G. & Armour, J.A. Shortening of the QT interval of the EKG is associated primarily with increased ventricular contractility rather than heart rate. Integrative Physiological and Behavioral Science 30, 5-11 (1955). Doi: 10.1007/BF02691386

[134] Bonnemeier H, Wiegand UK, Braasch W, Brandes A, Richardt G, Potratz J. Circadian profile of QT interval and QT interval variability in 172 healthy volunteers. Pacing Clin Electrophysiol. 2003 Jan;26(1P2):377-82. Doi: 10.1046/j.1460-9592.2003.00053.x

[135] Koch, A.; McCormack, P.; Schwanecke, A.; Schnoor, P.; Buslaps, C.; Tetzlaff, K.; Rieckert, H. Noninvasive myocardial contractility monitoring with seismocardiography during simulated dives. Undersea Hyperb. Med. **2003**, 30, 19–28

[136] Gregson PH. Sternal acceleration ballistocardiography and arterial pressure wave analysis to determine stroke volume. Clin Invest Med. 1999 Feb;22(1):4-14

A. Appendix A

A.1 Feasibility Analysis

Subject	**Number of R peaks identified – ECG**	**Number of SCs identified - SCG**	
01	*85140*	*79745*	*93.55 %*
02	*126287*	*72585*	*57.48 %*
03	*104581*	*64969*	*62.12 %*
04	*118143*	*73050*	*61.83 %*
05	*86971*	*60120*	*69.13 %*
06	*82127*	*77080*	*93.86 %*
07	*84880*	*71691*	*84.46 %*
08	*92199*	*75390*	*81.77 %*
09	*113866*	*82447*	*72.41 %*
10	*115433*	*85169*	*73.78 %*
11	*180348*	*93950*	*52.09 %*
12	*117275*	*84373*	*71.95 %*
13	*108598*	*76853*	*70.77 %*
14	*115569*	*75976*	*65.74 %*
15	*113348*	*70247*	*61.98 %*
16	*115369*	*82531*	*71.54 %*
17	*108775*	*87690*	*80.62 %*
18	*107818*	*65890*	*61.11 %*
19	*99806*	*82184*	*82.34 %*

20	*126037*	*92700*	*73.55 %*
21	*105460*	*78484*	*74.42 %*
22	*111838*	*75814*	*67.79 %*

Table A.1: Comparison between the number of peaks extracted from the ECG and the number of systolic complexes extracted from the SCG. Close to the number of SCs, the percentage of SCs (from SCG) with respect to R peaks (from ECG) is displayed. All data derived after post processing phases. Analysis conducted over 24 hours

Subject	R peaks -Day	SCs - Day		R peaks – Night	SCs - Night	
01	*61754*	*57065*	*90.93%*	*23386*	*22680*	*96.98%*
02	*89135*	*36709*	*41.18%*	*37152*	*35876*	*96.57%*
03	*75818*	*36620*	*48.30%*	*28763*	*28349*	*98.56%*
04	*89368*	*45071*	*50.43%*	*28775*	*27979*	*97.23%*
05	*66260*	*39770*	*60.02%*	*20711*	*20350*	*98.26%*
06	*61218*	*55953*	*91.40%*	*20909*	*21127*	*101.04%*
07	*64670*	*52840*	*81.71%*	*20210*	*18851*	*93.28%*
08	*60805*	*46943*	*77.20%*	*31394*	*28447*	*90.61%*
09	*85478*	*55600*	*65.05%*	*28388*	*26847*	*94.57%*
10	*92001*	*61913*	*67.30%*	*23432*	*23256*	*99.25%*
11	*163266*	*84891*	*52.00%*	*17082*	*9059*	*53.03%*
12	*80960*	*49051*	*60.59%*	*36315*	*35322*	*97.27%*
13	*78615*	*47699*	*60.67%*	*29983*	*29154*	*97.24%*
14	*81491*	*43848*	*53.81%*	*34078*	*32128*	*94.28%*
15	*81544*	*40473*	*49.63%*	*31804*	*29774*	*93.62%*
16	*83484*	*53786*	*64.43%*	*31885*	*28745*	*90.15%*
17	*78105*	*55543*	*71.11%*	*30670*	*32147*	*104.82%*
18	*81017*	*42334*	*52.25%*	*26801*	*23556*	*87.89%*
19	*76532*	*60104*	*78.54%*	*23274*	*22080*	*94.87%*
20	*84341*	*54129*	*64.18%*	*41696*	*38571*	*92.51%*
21	*66763*	*45721*	*68.48%*	*38697*	*32763*	*84.67%*
22	*81082*	*44953*	*55.44%*	*30756*	*30861*	*100.34%*

Table A.2: Comparison between the number of peaks extracted from the ECG and the number of systolic complexes extracted from the SCG. Close to the number of SCs, the percentage of SCs from SCG with respect to R peaks from ECG is displayed. All data derived after post processing phases. Analysis conducted over 24 hours separating day and night

Subject	**Tag 0** *[%]*	**Tag 1** *[%]*	**Tag 2** *[%]*	**Tag 3** *[%]*	**Tag 4** *[%]*	**Tag 5** *[%]*	**Tag 6** *[%]*	**Tag 7** *[%]*	**Tag 8** *[%]*	**Tag 9** *[%]*
01	*56.53*	*1.17*	*11.02*	*0.03*	*0*	*1.18*	*0*	*0.16*	*7.18*	*22.72*
02	*4.90*	*3.53*	*49.78*	*1.85*	*0.13*	*11.97*	*0.01*	*0.57*	*9.49*	*11.78*
03	*4.07*	*17.05*	*34.84*	*0.52*	*0.30*	*8.96*	*0.04*	*0.50*	*13.95*	*19.77*
04	*37.31*	*1.11*	*12.04*	*0.01*	*0*	*3.83*	*0*	*0.04*	*12.06*	*33.59*
05	*21.37*	*1.94*	*28.08*	*0.02*	*0.01*	*13.32*	*0*	*0.12*	*15.05*	*20.08*
06	*15.68*	*1.92*	*36.46*	*0.56*	*0*	*29.96*	*0.01*	*0.14*	*4.06*	*11.20*
07	*26.46*	*5.48*	*32.57*	*0.26*	*0.05*	*11.54*	*0.01*	*0.47*	*9.88*	*13.27*
08	*14.86*	*3.02*	*41.10*	*0.58*	*0.06*	*11.23*	*0.01*	*0.27*	*10.41*	*18.46*
09	*10.97*	*2.93*	*47.32*	*0.38*	*0.05*	*11.75*	*0*	*0.84*	*7.36*	*18.39*
10	*11.71*	*1.41*	*37.02*	*0.36*	*0.02*	*1.94*	*0*	*0.44*	*9.36*	*37.73*
11	*17.47*	*1.91*	*33.17*	*0.02*	*0.02*	*10.74*	*0*	*0.13*	*10.67*	*25.86*
12	*2.98*	*1.40*	*24.35*	*1.47*	*0.01*	*35.41*	*0.05*	*0.26*	*3.12*	*30.93*
13	*18.35*	*4.28*	*35.22*	*0.62*	*0.17*	*21.47*	*0.02*	*0.97*	*6.12*	*12.28*
14	*2.63*	*9.44*	*33.47*	*0.57*	*0.22*	*7.05*	*0*	*1.11*	*13.05*	*32.47*
15	*2.50*	*6.72*	*44.38*	*0.60*	*0*	*35.65*	*0*	*0.13*	*2.51*	*7.51*

Table A.3: Day beat-to-beat labelling results for subjects in which is possible to identify T peaks. For each participant (row) we tabulate the percentage of beats associated to a particular tag (column). For the further analysis we consider heartbeats corresponding to tag 0 (perfect heartbeat – early and late systole), tag 5 (only early systole), tag 7 (early and late systole, except for RE) and tag 9 (only early systole)

Subject	**Tag 0** *[%]*	**Tag 1** *[%]*	**Tag 2** *[%]*	**Tag 3** *[%]*	**Tag 4** *[%]*	**Tag 5** *[%]*	**Tag 6** *[%]*	**Tag 7** *[%]*	**Tag 8** *[%]*	**Tag 9** *[%]*
01	*59.12*	*0*	*4.70*	*0*	*0*	*0*	*0*	*0.01*	*1.24*	*34.93*
02	*5.36*	*0*	*5.72*	*0*	*0*	*1.27*	*0*	*0*	*1.01*	*86.63*
03	*3.00*	*0*	*9.48*	*0*	*0*	*0.90*	*0*	*0.01*	*30.43*	*56.17*
04	*12.01*	*0*	*6.07*	*0*	*0*	*4.08*	*0*	*0.02*	*12.14*	*65.69*
05	*22.81*	*0*	*13.19*	*0.02*	*0.02*	*21.42*	*0*	*0.03*	*17.70*	*24.82*
06	*58.37*	*0*	*5.55*	*0*	*0*	*0.83*	*0*	*0*	*0.56*	*34.69*
07	*51.10*	*0*	*6.65*	*0*	*0*	*1.08*	*0*	*0.01*	*11.18*	*29.98*
08	*23.84*	*0*	*12.21*	*0*	*0*	*0.60*	*0*	*0.01*	*32.55*	*30.79*
09	*15.19*	*0*	*8.50*	*0.02*	*0*	*4.04*	*0*	*0.09*	*8.96*	*63.19*
10	*14.03*	*0*	*10.03*	*0.04*	*0*	*0.81*	*0*	*0.04*	*5.66*	*69.37*
11	*38.30*	*0*	*5.75*	*0*	*0*	*0.68*	*0*	*0.03*	*5.12*	*50.12*
12	*1.24*	*0*	*7.36*	*0*	*0*	*6.96*	*0*	*0*	*0.51*	*83.94*
13	*47.68*	*0*	*7.71*	*0*	*0.01*	*8.11*	*0*	*0.12*	*6.85*	*29.51*
14	*6.90*	*0*	*17.08*	*0.10*	*0.30*	*8.28*	*0*	*0.12*	*10.46*	*56.75*
15	*19.79*	*0*	*10.63*	*0.21*	*0*	*2.27*	*0*	*0.01*	*20.63*	*19.79*

Table A.4: Night beat-to-beat labelling result for subjects in which is possible to identify T peaks. For each participant (row) we tabulate the percentage of beats associated to a particular tag (column). For the further analysis we consider heartbeats corresponding to tag 0 (perfect heartbeat – early and late systole), tag 5 (only early systole), tag 7 (early and late systole, except for RE) and tag 9 (only early systole)

Subject	**Tag 0** *[%]*	**Tag 1** *[%]*	**Tag 2** *[%]*	**Tag 3** *[%]*	**Tag 4** *[%]*	**Tag 5** *[%]*	**Tag 6** *[%]*	**Tag 7** *[%]*	**Tag 8** *[%]*	**Tag 9** *[%]*
01	*6.14*	*0*	*12.89*	*0.03*	*0*	*51.46*	*0*	*N/A*	*29.49*	*N/A*
02	*28.62*	*0*	*5.83*	*0*	*0.01*	*59.76*	*0*	*N/A*	*5.78*	*N/A*
03	*1.57*	*0*	*6.11*	*0*	*0.01*	*77.91*	*0*	*N/A*	*14.40*	*N/A*
04	*1.89*	*0*	*29.36*	*5.42*	*5.05*	*54.90*	*0.35*	*N/A*	*3.03*	*N/A*
05	*44.94*	*0*	*6.05*	*0*	*0*	*35.30*	*0*	*N/A*	*13.70*	*N/A*
06	*7.92*	*0*	*10.74*	*0.17*	*0.03*	*73.49*	*0.04*	*N/A*	*7.72*	*N/A*
07	*8.24*	*0*	*17.43*	*0*	*0.05*	*46.57*	*0*	*N/A*	*27.70*	*N/A*

Table A.6: Day beat-to-beat labelling results for subjects in which is not possible to identify T peaks. For each participant (row) we tabulate the percentage of beats associated to a particular tag (column). For the further analysis we consider heartbeats corresponding to tag 0 (perfect heartbeat – early and late systole), tag 5 (only early systole), tag 7 (early and late systole, except for RE) and tag 9 (only early systole). Information about tags 7 and 9 are not available

Subject	**Tag 0** *[%]*	**Tag 1** *[%]*	**Tag 2** *[%]*	**Tag 3** *[%]*	**Tag 4** *[%]*	**Tag 5** *[%]*	**Tag 6** *[%]*	**Tag 7** *[%]*	**Tag 8** *[%]*	**Tag 9** *[%]*
01	*0.89*	*5.16*	*57.02*	*2.10*	*0.27*	*32.34*	*0.01*	*N/A*	*2.20*	*N/A*
02	*3.85*	*36.47*	*30.36*	*3.54*	*1.38*	*22.39*	*0.10*	*N/A*	*1.90*	*N/A*
03	*1.04*	*22.99*	*17.72*	*0.06*	*0.03*	*51.63*	*0.01*	*N/A*	*6.53*	*N/A*
04	*0.44*	*62.55*	*15.82*	*3.16*	*1.65*	*14.97*	*0.12*	*N/A*	*1.30*	*N/A*
05	*11.41*	*1.06*	*42.80*	*1.01*	*0.02*	*30.51*	*0*	*N/A*	*13.19*	*N/A*
06	*2.16*	*24.78*	*40.26*	*2.32*	*0.77*	*24.35*	*0.06*	*N/A*	*5.31*	*N/A*
07	*1.26*	*5.54*	*48.12*	*0.34*	*0.09*	*34.73*	*0*	*N/A*	*11.18*	*N/A*

Table A.5: Night beat-to-beat labelling results for subjects in which is not possible to identify T peaks. For each participant (row) we tabulate the percentage of beats associated to a particular tag (column). For the further analysis we consider heartbeats corresponding to tag 0 (perfect heartbeat – early and late systole), tag 5 (only early systole), tag 7 (early and late systole, except for RE) and tag 9 (only early systole). Information about tags 7 and 9 are not available

Subject	24 hours	Day	Night
01	Median: 4 Maximum: 94	Median: 3 Maximum: 94	Median: 20 Maximum: 83
02	Median: 1 Maximum: 116	Median: 1 Maximum: 22	Median: 2 Maximum: 116
03	Median: 2 Maximum: 228	Median: 1 Maximum: 113	Median: 5 Maximum: 228
04	Median: 1 Maximum: 161	Median: 1 Maximum: 78	Median: 22 Maximum: 161
05	Median: 2 Maximum: 70	Median: 1 Maximum: 58	Median: 2 Maximum: 70
06	Median: 3 Maximum: 73	Median: 3 Maximum: 71	Median: 4 Maximum: 73
07	Median: 2 Maximum: 88	Median: 2 Maximum: 75	Median: 3 Maximum: 88
08	Median: 2 Maximum: 111	Median: 2 Maximum: 48	Median: 3 Maximum: 111
09	Median: 2 Maximum: 246	Median: 2 Maximum: 112	Median: 27 Maximum: 246
10	Median: 2 Maximum: 161	Median: 2 Maximum: 161	Median: 4 Maximum: 95
11	Median: 1 Maximum: 121	Median: 1 Maximum: 121	Median: 1 Maximum: 54
12	Median: 2 Maximum: 82	Median: 1 Maximum: 82	Median: 2 Maximum: 54
13	Median: 2 Maximum: 79	Median: 1 Maximum: 79	Median: 3 Maximum: 70
14	Median: 2 Maximum: 97	Median: 1 Maximum: 50	Median: 4 Maximum: 97
15	Median: 1 Maximum: 181	Median: 1 Maximum: 92	Median: 1 Maximum: 181
16	Median: 2 Maximum: 147	Median: 2 Maximum: 118	Median: 4 Maximum: 147
17	Median: 2 Maximum: 218	Median: 1 Maximum: 116	Median: 5 Maximum: 218
18	Median: 1 Maximum: 67	Median: 1 Maximum: 67	Median: 2 Maximum: 36
19	Median: 2 Maximum: 168	Median: 2 Maximum: 145	Median: 22 Maximum: 168

20	Median: 2 Maximum: 118	Median: 2 Maximum: 74	Median: 4 Maximum: 118
21	Median: 2 Maximum: 94	Median: 1 Maximum: 68	Median: 2 Maximum: 94
22	Median: 2 Maximum: 88	Median: 2 Maximum: 88	Median: 2 Maximum: 72

Table A.7: Results of the maximum and median window duration analysable. For each volunteer (each row), median and maximum number of successive heartbeats labelled as tag 0,5,7 or 9 are computed and displayed for the 24 hours recording (second column), daytime (third column) and night-time (fourth column)

A.2 Visual Analysis

Below are the examples obtained from one participating subject (subject 01).
Since the duration of the awakening period was greater than the duration of the sleep period, the day-time's histograms have y-values (Occurrence) much greater than those of the night.

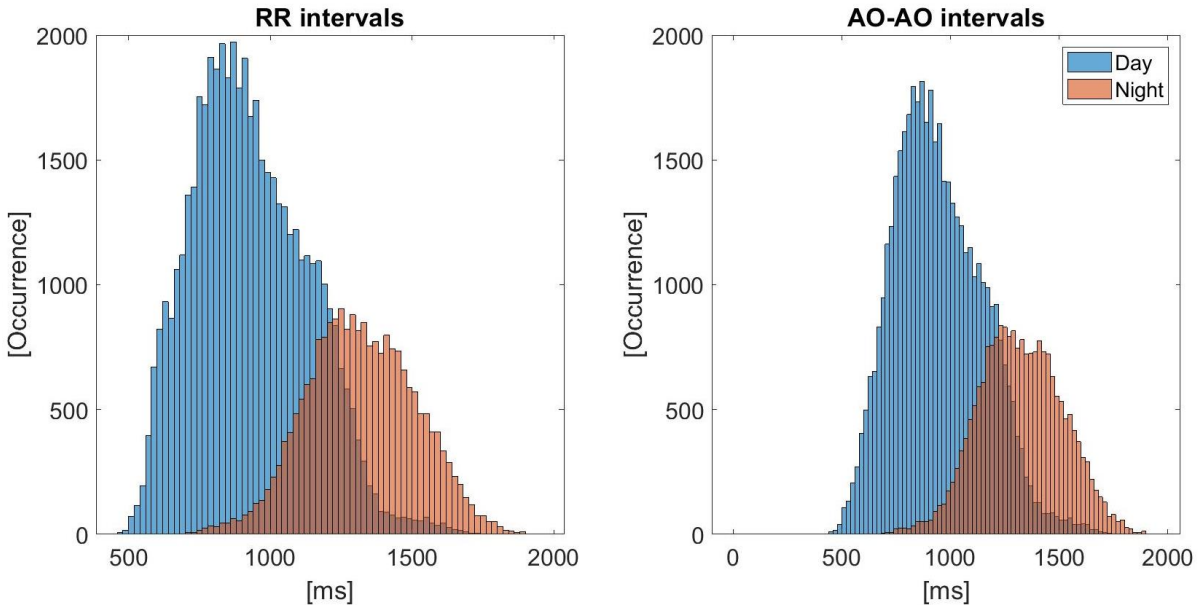

Figure A.1: Histograms of temporal parameters and comparison of values obtained during day (blue) and night (red). The x-axis represents the temporal distance [ms] while the y-axis represents the occurrence (number of times) the that specific value takes place

In *Figure A.1* the left panel represents the day and night distribution of R_iR_{i+1} intervals. while the right panel display the day and night distribution of the AO_iAO_{i+1} intervals. Both parameters show the same distribution across daytime and night-time, with an increase in the length of the cardiac cycle overnight, so that the existence of a circadian pattern is clearly visible by such representation.

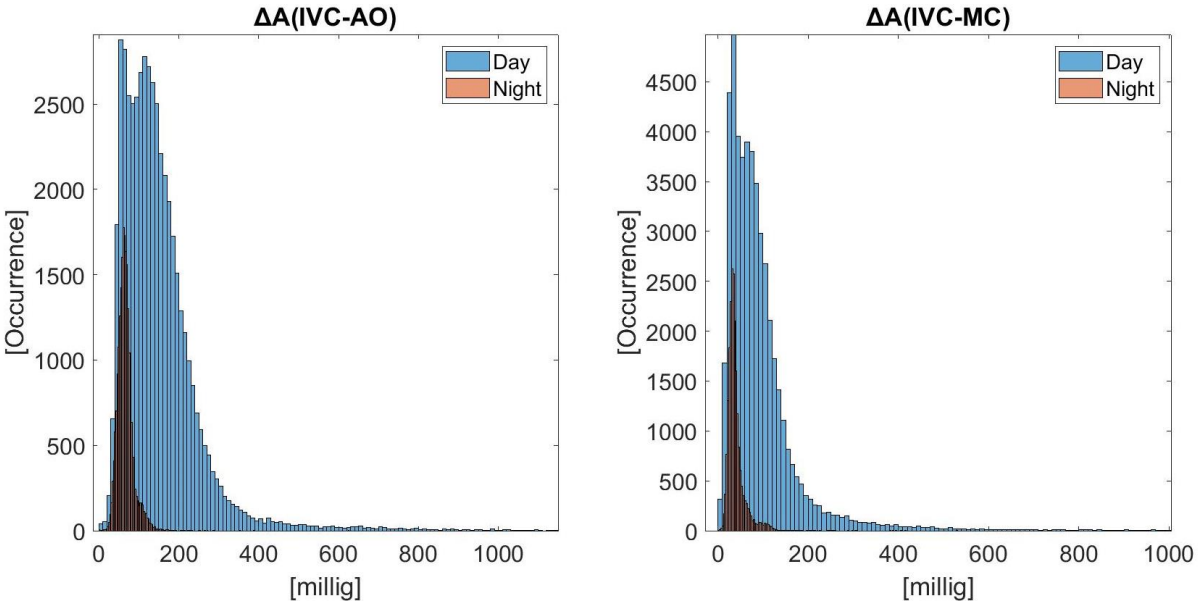

Figure A.2: *Histograms of amplitude parameters and comparison of values obtained during day (blue) and night (red). The x-axis represents the amplitude [millig] while the y-axis represents the occurrence (number of times) the that specific value takes place*

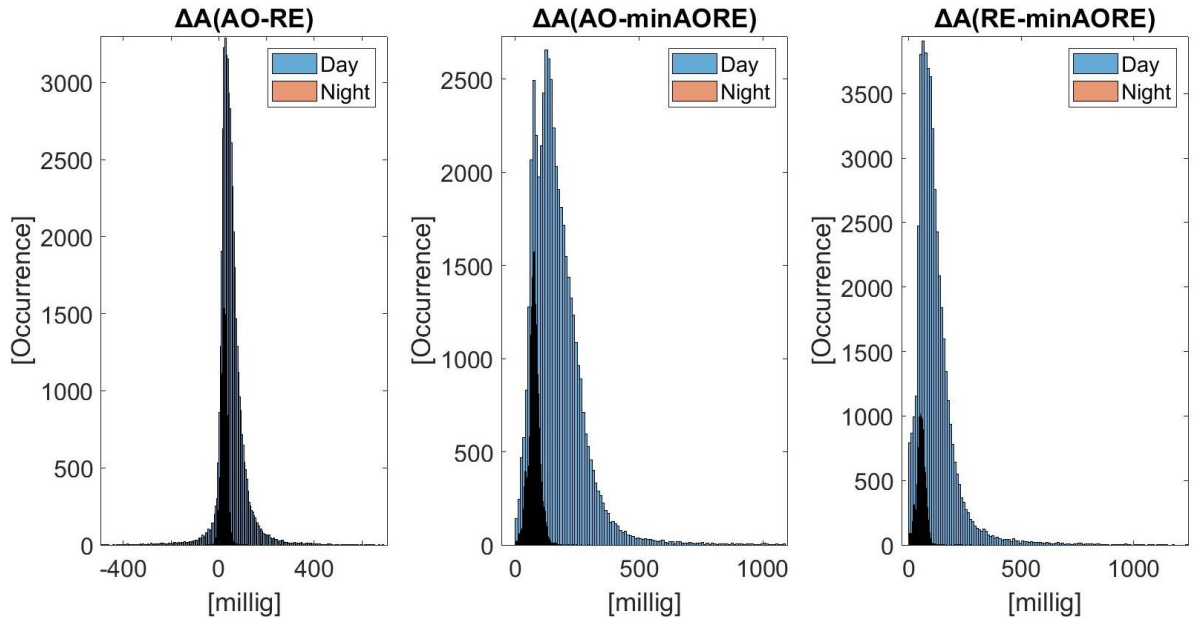

Figure A.3: *Histograms of amplitude parameters and comparison of values obtained during day (blue) and night (red). The x-axis represents the amplitude [milig] while the y-axis represents the occurrence (number of times) the that specific value takes place*

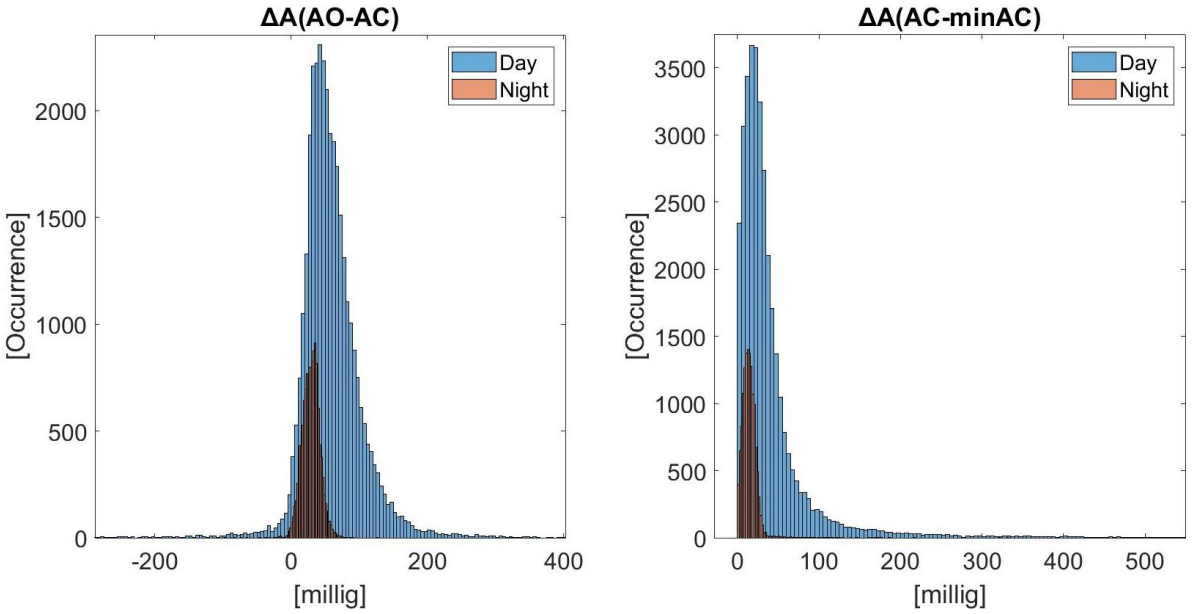

Figure A.4: Histograms of amplitude parameters and comparison of values obtained during day (blue) and night (red). The x-axis represents the amplitude [millig] while the y-axis represents the occurrence (number of times) the that specific value takes place

In

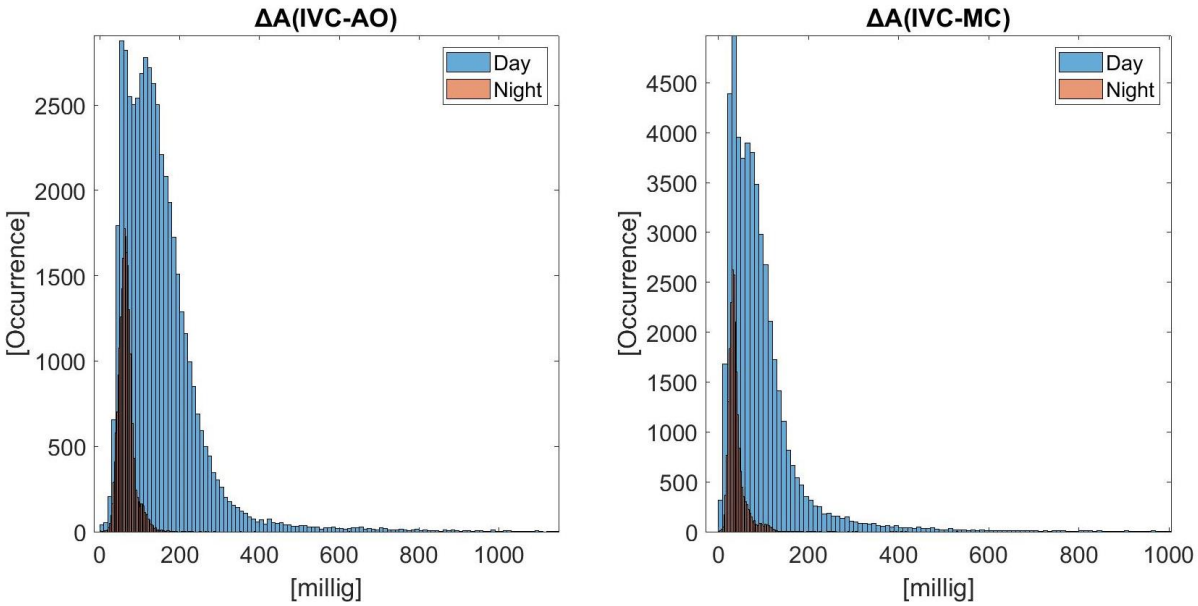

Figure A.2. *Figure A.3* and *Figure A.4* amplitude parameters histograms are shown. Among them, five parameters – ΔA(IVC-AO), ΔA(IVC-MC), ΔA(AO-minAORE). ΔA(RE-minAORE) and the ΔA(AC-minAC) – show a similar pattern: the day distribution shows higher values (expressed in millig) as compared to the night distribution. Moreover, all distributions have values greater than zero because AO has always the highest values and IVC has always the lowest values in terms of amplitude

[millig]. The distributions of ΔA(AO-RE) and ΔA(AO-AC) show also negative values as sometimes AC and RE reach higher values than AO in terms of amplitude [millig].

In *Figure A.5* we can appreciate the histograms relevant to slope parameters with a day distribution with higher values (expressed in millig/ms) with respect to the night distribution.

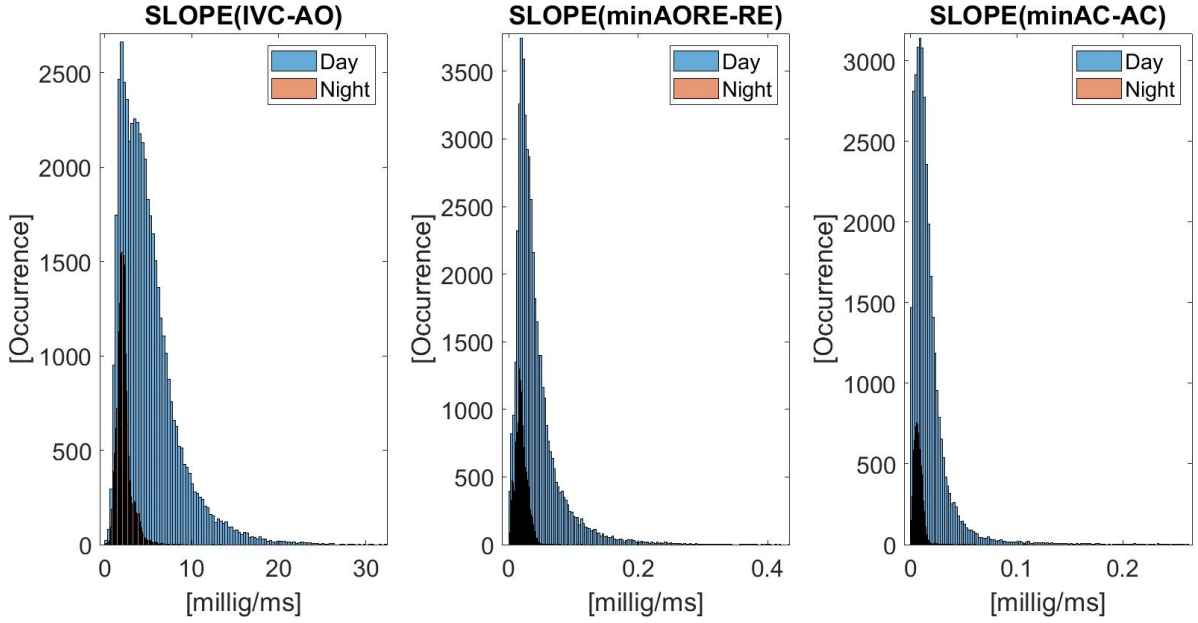

Figure A.5: Histograms of slope parameters and comparison of values obtained during day (blue) and night (red). The x-axis represents the value of the slope while the y-axis represents the occurrence (number of times) the that specific value takes place

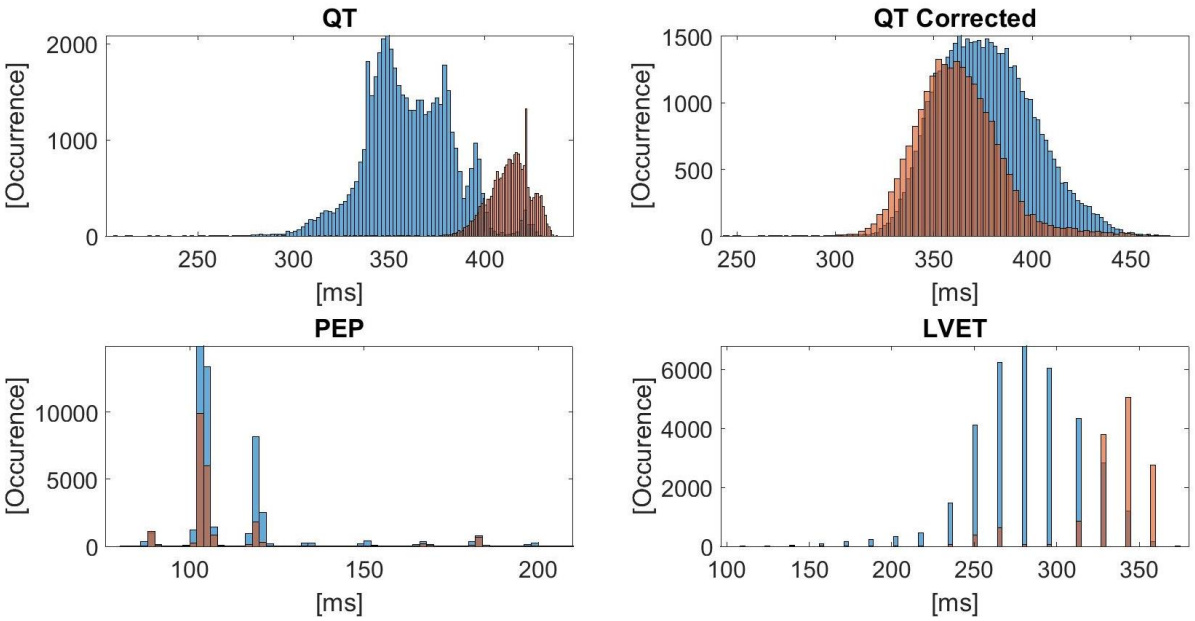

Figure A.6: Histograms of temporal parameters and comparison of values obtained during day (blue) and night (red). The x-axis represents the temporal distance [ms] while the y-axis represents the occurrence (number of times) the that specific value takes place

As regards the temporal parameters, due to the low SCG sampling frequency (64 Hz). only PEP, LVET, QT and QTc intervals show a meaningful distribution, with lower values during the awakening period (*Figure A.6*). As regards the QT interval and its corrected QT form (Bazett's correction), corrected QT shows a clear difference in distribution between day-time and night-time, less evident in the QTc histogram, as expected.

List of Figures

List of Tables